ÉCOLE DE TECHNOLOGIE SUPÉRIEURE
UNIVERSITÉ DU QUÉBEC

MANUSCRIPT-BASED THESIS PRESENTED TO
ÉCOLE DE TECHNOLOGIE SUPÉRIEURE

IN PARTIAL FULFILLMENT OF THE REQUIREMENTS FOR
THE DEGREE OF DOCTOR OF PHILOSOPHY
PH.D.

BY
Mohsen MOKHTABAD AMREI

CHARACTERIZATION OF MICROSTRUCTURE AND TEXTURE OF 13CR4NI MARTENSITIC STAINLESS STEEL WELD BEFORE AND AFTER TEMPERING

MONTREAL, MAY 19, 2016

© Copyright Mohsen Mokhtabad Amrei, 2016 All rights reserved.

© Copyright

Reproduction, saving or sharing of the content of this document, in whole or in part, is prohibited. A reader who wishes to print this document or save it on any medium must first obtain the author's permission.

BOARD OF EXAMINERS THESIS PH.D.

THIS THESIS HAS BEEN EVALUATED

BY THE FOLLOWING BOARD OF EXAMINERS

Mr. Philippe Bocher, Thesis Supervisor
Mechanical Engineering Department at École de technologie supérieure

Mr. Yves Verreman, Thesis Co-supervisor
Mechanical Engineering Department at École Polytechnique de Montreal

Roger Champagne, President of the jury
IT and Software Engineering Department at École de technologie supérieure

Jean-Luc Fihey, Member of the jury
Mechanical Engineering Department at École de technologie supérieure

Denis Thibault, External Member of the jury
Institut de recherche d'Hydro-Québec

Norbert Enzinger, Independent Evaluator
Institute of Materials Science and Welding, Graz University of Technology

THIS THESIS WAS PRESENTED AND DEFENDED

IN THE PRESENCE OF A BOARD OF EXAMINERS AND THE PUBLIC

MONTREAL, MAY 3, 2016

AT ÉCOLE DE TECHNOLOGIE SUPÉRIEURE

FOREWORD

« If your soul's tree yields the fruit of knowledge, you can steer the azure of heaven. »

Nassir Khusraw

ACKNOWLEDGMENTS

I want to thank my dear professor, Philippe Bocher, who patiently taught me so many things and guided me through my studies. Also thanks to Prof. Yves Verreman, Dr. Denis Thibault, Dr. Florent Bridier, Dr. Hossein Monajati, Dr. Majid Hosseini, and Dr. Lionel Germain for their guidance and help. The assistance, ideas, and inspirations given to me by my friend Stephane Godin are also appreciated. Also thanks to Pierre Hovington, Michael Sabourin, Jacques Lanteigne, Carlo Baillargeon, Alexandre Trudel, Alexandre Lapointe, Rene Dubois, and Etienne Dallaire.

Thanks to the jury members for the time they took to read and adjudicate this thesis. Thanks to all of those I have worked with during these years.

Thanks to my parents for placing so much importance on my education, and sacrificing their wishes so I can see mine fulfilled.

Finally, thanks to my wife, Raheleh, who has supported me throughout my studies. I hope I can make it up to you and help you to follow your dreams as well. I love you.

CARACTÉRISATION DE LA MICROSTRUCTURE ET DE LA TEXTURE DES SOUDURES EN ACIER INOXYDABLE MARTENSITIQUE 13CR4NI, AVANT ET APRÈS REVENU

Mohsen MOKHTABAD AMREI

RÉSUMÉ

Les aciers inoxydables martensitiques 13Cr4Ni connus pour leurs performances exceptionnelles dans l'industrie hydroélectrique, où ils sont utilisés principalement dans la construction des différentes composantes des turbines. Compte tenu de la taille et de la géométrie des roues des turbines et des aubes, les procédures de soudage multi-passes sont couramment utilisées dans leur fabrication et leur réparation. Les propriétés mécaniques et la microstructure finales de la soudure sont sensibles aux paramètres du procédé de soudage et à l'historique thermique. Dans le cas de l'acier 13Cr4Ni, les cycles thermiques imposés par l'opération de soudage multi-passes ont des effets significatifs sur la microstructure complexe de la soudure. En outre, les traitements thermiques après soudage sont généralement faits pour réduire l'hétérogénéité de la soudure et améliorer les propriétés mécaniques du matériau par le revenu de la microstructure et aussi par la formation d'une "austénite stable à température ambiante"

Dans la première phase de cette étude, les microstructures et les textures cristallographiques des soudures mono-passe et double-passe cordon de soudage ont été étudiées comme une base pour l'étude de la microstructure plus complexe de la soudure multi-passes. Cette étude a révélé que la dureté maximale est obtenue dans la zone affectée thermiquement du métal de base. En particulier, le cycle thermique de la deuxième passe augmente la dureté de la passe précédente et produit une microstructure martensitique plus fine. Dans les régions de la zone affectée thermiquement, un effet de revenu est rapporté jusqu'à 3 à 6 millimètres de la ligne de fusion. Les particules d'austénite se trouvent aussi dans ces zones et ils sont des indicatifs de la complexité de la microstructure attendue dans les soudures multi-passes.

Dans la deuxième phase de l'étude, la microstructure des soudures multi-passes a été trouvée plus hétérogène que celle des soudures mono-passe et double-passe. Elle est composée de plusieurs régions affectées par les passes de soudure adjacentes. Les résultats montrent que la modification des grains de l'austénite mère est intervenue dans les zones à proximité des passes de soudure précédentes. De plus, des lattes qui ont des interfaces avec angle faible ont été observées à l'intérieur des sous-blocs de martensite en différentes régions. Le profil de dureté de la soudure multi-passes, confirme des effets thermiques superposés des passes adjacentes. Dans certaines régions, un effet de revenu a été observé, alors que dans d'autres un effet de double-trempe a eu lieu.

La dernière phase de cette étude a porté sur les effets de traitements thermiques après soudage sur la formation de l'austénite reformé et des carbures et sur l'évolution de la dureté.

Les effets de la température et du temps de revenu sur la microstructure ont été étudiés. L'étude a révélé que des carbures de taille nanométrique se forment au niveau des interfaces des lattes de martensite et des interfaces de sous-blocs. En outre, il a été déterminé que, pour chaque période de revenu, le pourcentage le plus élevé d'austénite peut être obtenu par un revenu à 610 ° C. De la même façon, le maximum ramollissement est rapporté par un revenu à 610 ° C, pour tous périodes.

Mots-clés: Acier Inoxydable Martensitique, Caractérisation Microstructurale, Soudage à l’arc avec fil fourré, Traitement Thermique, Austénite reformé.

CHARACTERIZATION OF MICROSTRUCTURE AND TEXTURE OF 13CR4NI MARTENSITIC STAINLESS STEEL WELD BEFORE AND AFTER TEMPERING

Mohsen MOKHTABAD AMREI

ABSTRACT

13Cr4Ni martensitic stainless steels are known for their outstanding performances in the hydroelectric industry, where they are mainly used in the construction of turbine components. Considering the size and geometry of turbine runners and blades, multi-pass welding procedures are commonly used in the fabrication and repair of such turbines. The final microstructure and mechanical properties of the weld are sensitive to the welding process parameters and thermal history. In the case of 13Cr4Ni steel, the thermal cycles imposed by the multi-pass welding operation have significant effects on the complex weld microstructure. Additionally, post-weld heat treatments are commonly used to reduce weld heterogeneity and improve the material's mechanical properties by tempering the microstructure and by forming a "room-temperature-stable austenite."

In the first phase of this research, the microstructures and crystallographic textures of as-welded single-pass and double-pass welds were studied as a basis to studying the more complex multi-pass weld microstructure. This study found that the maximum hardness is obtained in high temperature heat affected zone inside the base metal. In particular, the results showed that the heat cycle exposed by the second pass increases the hardness of the previous pass because it produces a finer martensite microstructure. In areas of heat-affected zone, a tempering effect is reported from 3 up to 6 millimeters far from the fusion line. Finding austenite phase in these areas are matter of interest and it can be indicative of the microstructure complexity of multi-pass welds.

In the second phase of research, the microstructure of multi-pass welds was found to be more heterogeneous than that of single- and double-pass welds. Any individual pass in a multi-pass weld consists of several regions formed by adjacent weld passes heat cycle. Results showed that former austenite grains modification occurred in areas close to the subsequent weld passes. Furthermore, low-angle interface laths were observed inside martensite sub-blocks over different regions. The hardness profile of a multi-pass weld was explained by the overlaying heat effects of surrounding passes. In some regions, a tempered matrix was observed, while in other regions a double-quenched microstructure was found.

The final aspect of this study focused on the effects of post-weld heat treatments on reformed austenite and carbide formations, and evolution of hardness. The effects of tempering duration and temperature on microstructure were investigated. The study found that nanometer-sized carbides form at martensite lath interfaces and sub-block boundaries. Additionally, it was determined that for any holding duration, the maximum austenite

percentage is achievable by tempering at 610 °C. Similarly, the maximum softening was reported for tempering at 610 °C, for any given holding period.

Keywords: Martensitic Stainless Steel, Microstructural Characterization, Flux-Cored Arc Welding, Heat Treatment, Reformed Austenite.

TABLE OF CONTENTS

LIST OF TABLES

Page

LIST OF FIGURES

Page

LIST OF ABBREVIATIONS

13Cr4Ni	13%Cr – 4%Ni Martensitic Stainless Steel.
AFNOR	French national organization for standardization (Association française de normalization).
AISI	American Iron and Steel Institute.
ASTM	American Society for Testing and Materials.
AWS	American Welding Society.
CA6NM	Cast 13%Cr – 4%Ni Martensitic Stainless Steel.
CTFA	Aerospace Manufacturing Technology Centre of the National Research Council of Canada (Centre des Technologies de Fabrication en Aérospatiale).
DIN	Deutsches Institut Für Normung E.V. (German Institute for Standardization).
ÉTS	École de technologie supérieure.
EURONORM	Standards of the European Coal and Steel Society.
FCAW	Flux-Cored Arc Welding.
HAZ	Heat Affected Zone.
K–S	The Kurdjumov–Sachs orientation relationship.
PWHT	Post Weld Heat Treatment.
SMAW	Shielded Metal Arc Welding.
TRIP	Transformation Induced Plasticity.
UNS	Unified Numbering System.
HT-HAZ	High-Temperature Heat Affected Zone.
IT-HAZ	Intermediate-Temperature Heat Affected Zone.

LIST OF SYMBOLS AND UNITS OF MEASUREMENTS

A_{C1}	Austenite Transformation Temperature on Heating.
A_S	Austenite Transformation End Temperature on cooling.
bcc	Body-centered cubic crystal structure.
bct	Body-centered tetragonal crystal structure.
C	Carbon Element.
cm	10^{-2} m.
Cr	Chromium Element.
Cr_2O_3	Chromium oxide.
Fe	Iron Element.
hr	Hour.
HV	Vickers hardness unit.
L	Liquid metal.
M	Martensite Phase.
M_F	Martensite Transformation Finish Temperature.
mm	10^{-3} m.
Mn	Manganese Element.
Mo	Molybdenum Element
M_S	Martensite Transformation Start Temperature.
Ni	Nickel Element.
nm	10^{-9} m.
P	Phosphorus Element.
rpm	Revolutions per minute.
S	Sulfur Element.
s	Seconds, unit of time.
Si	Silicon Element.
wt.%	Weight percent.
α	As in α-ferrite, represents the low temperature ferrite phase.
γ	Austenite Phase.
δ, δF	As in δ-ferrite, represents the high temperature ferrite phase.
μm	10^{-6} m.

INTRODUCTION

The life span of hydroelectricity plants, their maintenance, and their electric power production are directly related to the mechanical behavior of their turbines; which is in turn closely related to the turbines' metal microstructures. The hydro-turbines operate at speeds of about 100 rpm up to 1500 rpm depending on the power plant capacity and may continue to work for 70 years. Thus, a typical hydro-turbine should have a life span of about 10^{10} cycles, which indicates the importance of its quality and therefore its microstructural characteristics [1]. In the past, the turbines were used to be made of cast iron. Advances in steel making technology replaced cast iron by mild steel and later by martensitic stainless steels. Despite the fact that the majority of the turbines manufactured in the past 30 years are still made of mild steel, martensitic stainless steels have emerged as a successful substitute of mild steel in plants around the world. Among these martensitic stainless steels is the 13Cr4Ni steel, which shows excellent performance and durability in hydropower industry. A considerable number of new turbines delivered since the mid-80s have been made of 13Cr4Ni steel, either CA6NM steel or other similar grade of steels [1].

CREFARRE (Consortium de Recherche en Fabrication et Réparation des Roues d'Eau, French expression for "Turbine runners manufacturing and repair research consortium"), was founded on manufacturing and repair of turbine runners. This research consortium investigates the challenges that the partners face in hydropower industry. The research roots in the demand of increasing the turbines life and improving their performance. Hydro-Quebec and the turbine manufacturer Alstom Renewable Power Canada are the industrial partners of this consortium that also include École de technologie supérieure (ÉTS), École Polytechnique de Montréal, and Aerospace Manufacturing Technology Centre of the National Research Council of Canada (CTFA). Based on the industry's research needs, research projects have been proposed to universities. Materials characterization and numerical modeling of processes are partly taking place at ÉTS. Alstom and Hydro-Quebec provide access to equipment, materials, and facilities (workshops, laboratories, equipment)

and jointly with the universities, they manage the research. The present study, “Characterization of microstructure and texture of 13Cr4Ni martensitic stainless steel multi-pass weld before and after tempering” is one of the PhD project in the CREFARRE program.

Multi-pass welding procedures were being used for manufacturing of turbines by ALSTOM Power for Hydro-Québec. These welding procedures are being followed by post-assembly heat treatments in order to increase the ductility of the martensitic steel and to reduce the residual stresses caused by the welding. Indeed, studying the effects of multi-pass welding procedure and subsequent heat treatments on microstructure is the core of this study.

This study starts with investigating the as-welded microstructure. This is an essential component of the study either to investigate the initial weld microstructure as the smallest constituent of the joint or to understand the effects of multi-pass thermal cycles. The significance of as-welded microstructure becomes more if the occasional repairs required at plant site are considered, where performing heat treatments are relatively difficult or in cases not convenient. Eventually, the study focuses on the evolution of microstructure and hardness during multi-pass welding and after tempering.

The thesis starts with a concise literature review in the first chapter, and then in the second chapter, it focuses on the microstructure of single- and double-pass welds in the as-welded state and tries to study and isolate the effects of the subsequent pass. In the third chapter, the as-welded microstructure of multi-pass welds has been studied and the effects of adjacent passes were documented. In the fourth chapter, the effects of different heat treatments on microstructure and hardness are examined in the context of a multi-pass weld, with particular attention given to the reverse transformation of martensite to austenite. The second, third and fourth chapters are presented in the form of articles and they are published in referred journals. Eventually the thesis finishes with the discussions chapter in order to integrate the project’s findings.

The originality of the present study lies in the investigation of the complex microstructure of a 13Cr4Ni steel weld, and the significance of fabrication process on its mechanical properties. The 13Cr4Ni steel can undergo a diffusional martensite-to-austenite transformation, which occurs at around 600 °C. The result is a stable austenite phase that forms between martensite laths and remarkably alters the mechanical behavior of the steel. These austenite particles are mechanically unstable and they are able to transform back to martensite under mechanical load (transformation induced plasticity, TRIP effect). The TRIP effect improves the resilience and mechanical properties of the 13Cr4Ni steel [2]. As this transformation can be triggered either by the heat cycle of an adjacent pass or by a deliberate heat treatment, it proves the importance of understanding the effects of welding procedures. The present study focuses on the effects of weld procedure heat cycles and accompanying heat treatments on microstructure, which has not been performed previously with such precisions and details.

CHAPTER 1

LITERATURE REVIEW

The present study arose out of a perceived need to understand the relationship between the microstructure characteristics and mechanical properties of steel-welded joint and to document the influence of the multi-pass welding process on these characteristics. This project necessitates a review of advanced information on the microstructural features of the steel multi-pass weld under consideration: the 13%Cr-4%Ni steel (13Cr4Ni).

The literature review presented in this chapter starts with a general overview of 13Cr4Ni martensitic stainless steel classification and characteristics. 13Cr4Ni weld metallurgy are then discussed, followed by a review of the specific 13Cr4Ni steel weld features. In the final section of the chapter, some specific austenite revealing techniques used in this study are introduced.

1.1. 13Cr4Ni Metallurgy

A review of 13Cr4Ni steel metallurgy is presented in this section and the microstructural characteristics of the steel are outlined.

1.1.1. General

The 13Cr4Ni alloy was developed in the 1960s as part of a research project that sought to develop new types of stainless steel suitable for hydroelectric turbine rotors [3]. Conventional martensitic stainless steels were previously used for this purpose, but they carried a high risk of hot cracking and required numerous precautions be followed carefully during the welding procedure. To decrease the risk of hot cracking during welding, low carbon content martensitic stainless steels were used, while nickel was added to the

composition of the steel to maintain its martensitic structure, producing a steel containing 13% Cr and 4% Ni [4].

Although 13Cr4Ni steel is known to have a fully martensitic microstructure, the actual steel making process may create a complex microstructure consisting of martensite, δ-ferrite, and austenite. Previous research has shown that the makeup of the final microstructure is related to the composition, solidification, and heat treatment history of the steel [5-7]. In order to understand the mechanisms leading to this complexity, a concise review of the steel microstructure formation is offered below.

1.1.2. 13Cr4Ni Classification

The 13Cr4Ni steel chemical composition range is shown in Table 1.1 and its common specifications under different standards are listed in Table 1.2. The steel is a member of the martensitic stainless steel family and is available in both cast and wrought forms. Martensitic stainless steels are essentially alloys of iron, carbon, chromium and nickel that transform into a body-centered tetragonal crystal structure at low temperatures. They are known to be corrosion resistant, ferromagnetic, and heat-treatment hardenable [8].

Table 1.1 – Chemical composition ranges of 13Cr4Ni steel Adapted from ASTM International A743M-03.

Element	**Cr**	**Ni**	**C**	**Mo**	**Si**	**S**	**P**
Nominal wt.%	11.5-14	3.5-4.5	0.06 max	0.4-1.0	1.0 max	0.04 max	0.04 max

Table 1.2 – Standards and related specifications of 13Cr4Ni steel.

Standard	Specification	Cast or Wrought
EURONORM	1.4313-X4 Cr Ni Mo 13-4	Wrought
AFNOR	Z4CN13.4	Wrought
DIN	X5 Cr Ni 13-4,W.Nr. 1.4313	Wrought
AISI	Type 4l5	Wrought
UNS	S41500	Wrought-Electrode
ASTM	CA6NM	Cast
AISI-AWS	Type 410NiMo	Wrought-Electrode
UNS	J91540	Cast

1.1.3. Effect of Alloying Elements on Microstructure of Martensitic Steels

1.1.3.1. General Effects of Alloying Elements

Alloying elements can be categorized in two types based on their effects on phase stability they provide. The addition of chromium and certain alloying elements known as "alpha gene" elements promotes the formation and stabilization of ferrite phase (α, alpha). Other elements, including carbon, manganese and nickel, promote austenite stability (γ, gamma); these elements are known as "gamma-gene" elements and they expand the austenite stable region of phase diagram of steel, resulting in increased stability of austenite in iron-chromium alloying systems at low temperatures. However, in martensitic steels, it is important that the amount of gamma-gene elements remains relatively low to force the austenite phase to stay unstable and undergo martensitic transformation at low temperatures. In contrast, high amounts of gamma-gene elements may cause the material to retain some austenite after the martensitic transformation [9]. A brief review of major alloying elements of the steel is presented below.

- **Effect of Chromium on Microstructure**

Chromium promotes the formation and stability of the ferrite phase [10]. Probably the most interesting and famous effect of this element on steel is the improvement in steel's ability to resist staining and corrosion. In addition to increasing the hardenability of steels, it can also

increase their toughness and fatigue resistance [11, 12]. In order to have a martensitic stainless steel, chromium percentage should not be less than 10.5% to keep the chromium oxides stable at steel surface to maintain stainless properties. The upper limit for chromium percentage is the ferrite phase formation in order to keep the martensitic transformation possible.

- **Effect of Nickel on Microstructure**

Nickel, which serves as an austenite-stabilizing element, is important in the development of martensitic steels. Adding this element to the steel allows for a higher chromium percentage in the austenite phase, which in turn increases the steel's corrosion resistance. Furthermore, the stability of austenite phase is essential to undergo further martensitic transformation. Nickel also lowers the martensitic transformation temperature (M_s) by stabilizing the austenite phase during cooling of the steel.
Unfortunately, the addition of nickel decreases the solubility of carbon atoms in the ferrite phase, causing the formation of chromium carbides and contributing to a depletion of carbon atoms (and eventually chromium). The formation of these carbides has been found to correlate with a softening of the microstructure and a significant decrease in the corrosion resistance of the steel [13].

Finally, nickel diffuses to the austenite phase during tempering. The enrichment caused by this diffusion results in further increased stability of the austenite region of microstructure [2, 14].

- **Effect of Carbon on Microstructure**

Carbon is also a gamma-gene element. The main effect of adding carbon to stainless steel is thus similar to the effect obtained by adding nickel: an increase in the austenite stability and a decrease in the M_s temperature. However, the hardness of martensite is directly related to the

concentration of carbon it contains. Thus, to preserve weldability and toughness of the steel, it is essential to maintain the carbon content as low as possible by adding other gamma-gene elements [15]. Keeping the carbon content low also minimizes the formation of chromium carbides and helps control chromium depletion [12].

- **Effect of Molybdenum on Microstructure**

Similar to chromium, molybdenum is an alpha gene element that promotes the formation of ferrite. Molybdenum tends to shrink the stable region for austenite (gamma loop), thus raising the austenite transformation end temperature (A_s). The main role of this element is to increase the mechanical properties of the steel; again, however, caution must be taken, since the presence of molybdenum causes precipitation hardening through the formation of carbides [12].

1.1.3.2. Effects of Alloying Elements on 13Cr4Ni Microstructure

Diagrams, such as the Schaeffler diagram, have been used to summarize the effects of alloying elements on steel microstructures after solidification or welding. The dot in Figure 1.1 shows the position of a typical 13Cr4Ni steel plotted on a Schaeffler diagram in comparison to other steel groups. However, it has been found that these diagrams are not precise for low-carbon martensitic stainless steels [4]. The position of the 13Cr4Ni alloy in this diagram shows that a fully martensitic steel is expected. However, the formation of some ferrite particles can occur, as micro-segregations may arise during solidification [12].

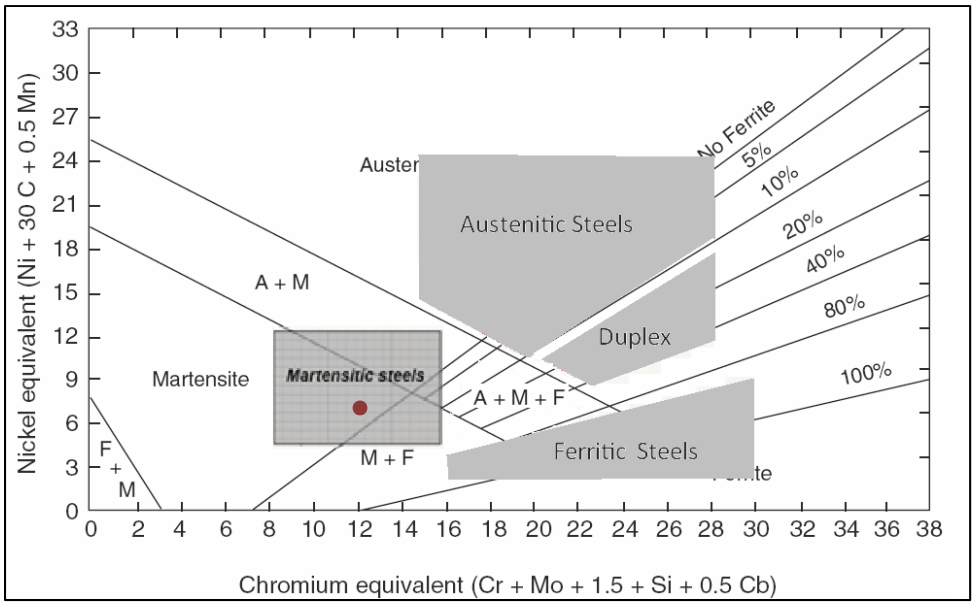

Figure 1.1 – Composition ranges of stainless steels plotted on a Schaeffler diagram. The dot shows the position of a typical 13Cr4Ni steel. Taken from Lippold (2005,32).

1.1.4. Transformation during cooling of 13Cr4Ni Martensitic Stainless Steels

1.1.4.1. Solidification and cooling of 13Cr4Ni

The 13Cr4Ni martensitic stainless steel starts to solidify to δ-ferrite at about 1500 ˚C. The δ-ferrite phase has a body-centered cubic (bcc) crystal structure which grows in a <001> crystal directions aligned with the direction of heat flow along the solidification front [11]. The δ-ferrite phase begins to transform into austenite between 1300 ˚C and 1400 ˚C, depending on the composition of the steel. Research has shown that this transformation occurs in a way that the {110} planes in the former δ-ferrite are parallel to the {111} planes in the austenite [9]. The ferrite-to-austenite transformation finishes at high temperatures (lower than 1400 ˚C, depending on the composition of the steel), giving a fully austenitic phase [10, 12].

Figure 1.2 presents the Fe-Cr-Ni phase diagram, Adapted for transformation temperatures and phases of 13Cr4Ni steel. This diagram shows that 13Cr4Ni starts to solidify into δ-ferrite at about 1470 °C and it becomes fully δ-ferrite at 1450 °C in equilibrium conditions. This δ-ferrite then transforms to austenite at 1300 °C, leading to a fully austenitic phase at temperatures lower than 1230 °C.

Austenite transformation to ferrite happens at temperatures below 720 °C as illustrated in Figure 1.2. However, the formation of the ferrite phase is very slow and it can be understood by considering an isothermal transformation diagram of the steel.

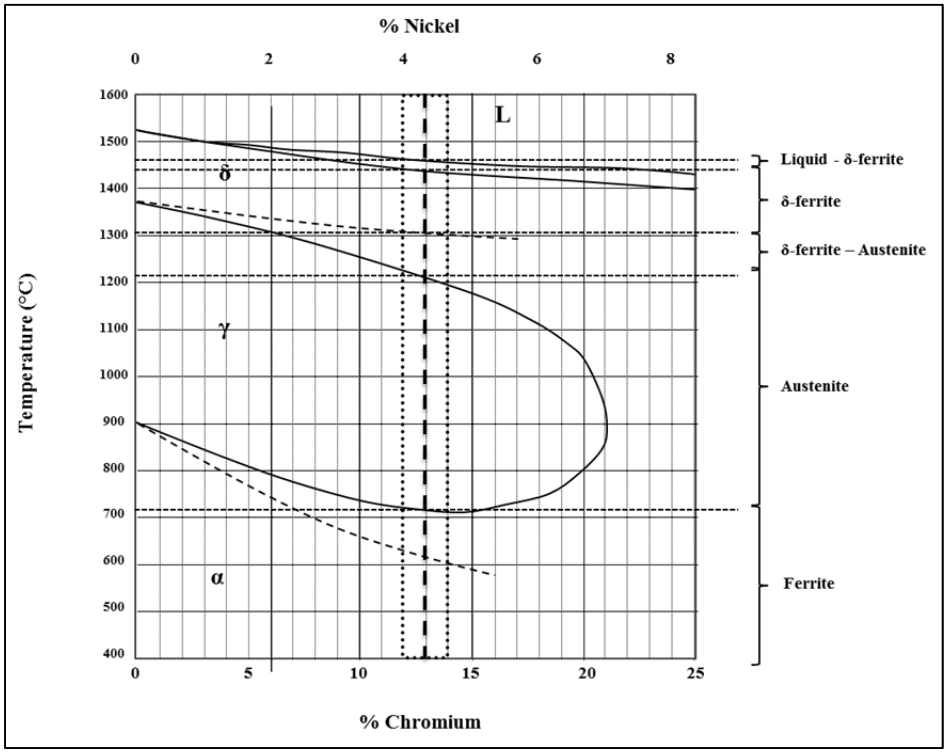

Figure 1.2 – 13Cr4Ni phase diagram showing the phase transformations in equilibrium condition. The dotted curve above and below austenite region show the transformation temperatures on heating which are useful to explain transformations during heat treatments. Adapted from Folkhard (1988,11).

Figure 1.3 shows the continuous cooling transformation diagram of 13Cr4Ni steel. The diagram reveals that there is no α-ferrite transformation for any common cooling rate, even when the steel is held at temperatures close to A_{C1} for weeks. Eventually, the martensitic transformation will overrun any other transformation.

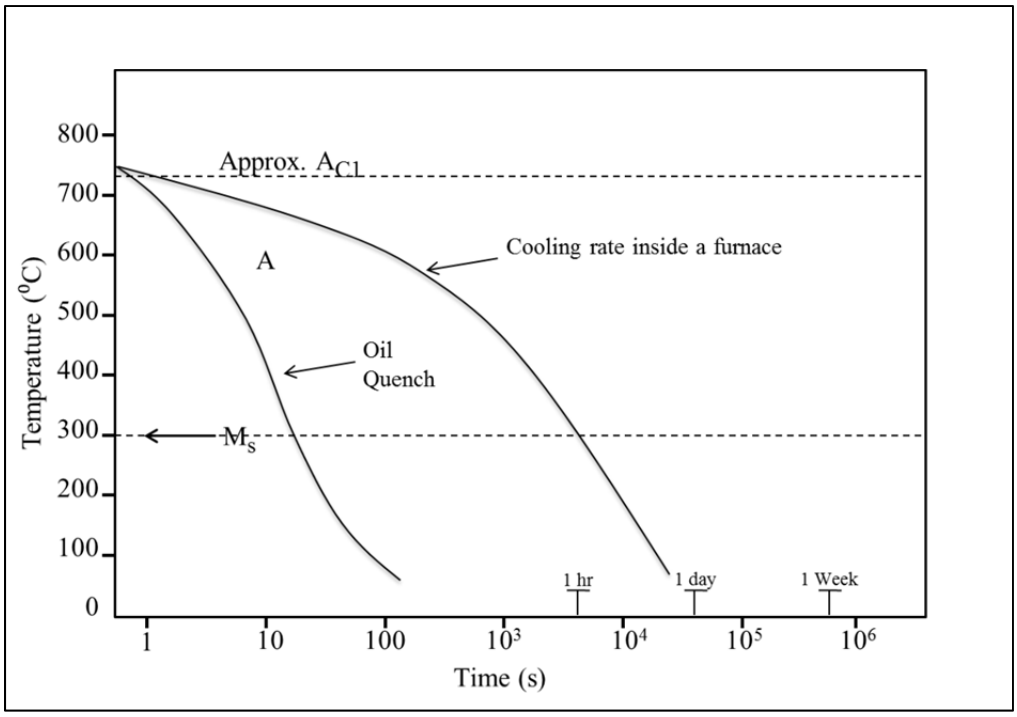

Figure 1.3 – Schematic and approximate isothermal transformation diagram for 13Cr4Ni stainless steel. No transformation happens in common holding times. The curves of typical cooling rates by quenching in oil and in a furnace are also shown in the diagram (diagram adapted from (Lippold (2005, 61) for a CA6NM steel).

1.1.4.2. 13Cr4Ni Martensitic Transformation

The martensitic transformation is the inevitable transformation of 13Cr4Ni steel microstructure at low temperatures. This transformation happens without any long-range diffusion of atoms; instead, a homogeneous and military movement of many atoms results in a change in the crystal structure and transforms it into a body-centered tetragonal (bct) crystal [11]. The movement of atoms in such a transformation is usually in the orders of interatomic

distances, with the atoms maintaining their places, relative to one another. The movement of large numbers of atoms explains why this transformation is often referred to as a "military transformation."

1.1.4.3. Martensite Transformation Start Temperature

Almost all alloying elements (with a few exceptions, like cobalt) tend to lower the starting temperature for the martensite transformation (M_S). Among these elements, carbon has the most significant influence. A number of equations have been developed to predict the martensite transformation start temperature in stainless steels. The following formula (Equation (1.1)) is specifically recommended for martensitic stainless steels by using weight percentage of alloying elements [16].

$$M_s\,(°C) = 540\,(°C) - (497C + 6.3Mn + 36.3Ni + 10.8Cr + 46.6Mo)\,(°C) \qquad (1.1)$$

This formula shows that, in most martensitic stainless steels containing less than 0.25 wt% of carbon, the M_S value will be relatively high, typically in the range of 200–400 °C. The M_S temperature of 13Cr4Ni was calculated at about 300 °C by Thibault et al. [17]; since the completion temperature for the martensite transformation (M_F) is normally about 100 °C below M_S, the transformation is expected to be finished at room temperature. However, in steels containing 4% Ni or more, the M_F temperature can be below room temperature, allowing some austenite to be retained in the microstructure [12].

1.1.5. 13Cr4Ni Martensite Characteristics

1.1.5.1. 13Cr4Ni Martensitic Microstructure

13Cr4Ni microstructure characteristics is a produce of its martensite transformation nature. A martensitic transformation takes place with definite orientation relationships on specific habit planes. This transformation produces lattice imperfections and surface reliefs. The nucleation mechanism of martensitic transformation has been found to affect the material's final morphology. It has been found that simple dislocations are more preferable martensite nucleation sites than surface and grain boundaries. As a result, martensite tends to nucleate from everywhere within the austenite grain volume rather than just at surface or grain boundaries [11]. This leads to a relatively uniform matrix mostly characterized by the nature of the transformation rather than the former microstructure. As a result, 13Cr4Ni mechanical properties are strongly related to its transformation characteristics.

The martensitic transformation of the 13Cr4Ni alloy can be well described by the fact that the original austenite phase with habit planes at {111} is related to {011} planes of martensite. This relation is known as the Kurdjumov–Sachs relationships [9]:

$$(111)\gamma // (011)_M \tag{1.2}$$

$$[10\bar{1}]\gamma // [\bar{1}1\bar{1}]_M \tag{1.3}$$

The 13Cr4Ni steel has a lath-shaped martensite microstructure, which is the very characteristic of a low carbon martensite. This type of microstructure is one of the two basic forms of martensitic microstructures: lath-shaped or plate-shaped. The carbon content of the steel determines which form will be predominant (Figure 1.4). The carbon content of the 13Cr4Ni steel is less than 0.06%; therefore, its microstructure is lath-shaped [11].

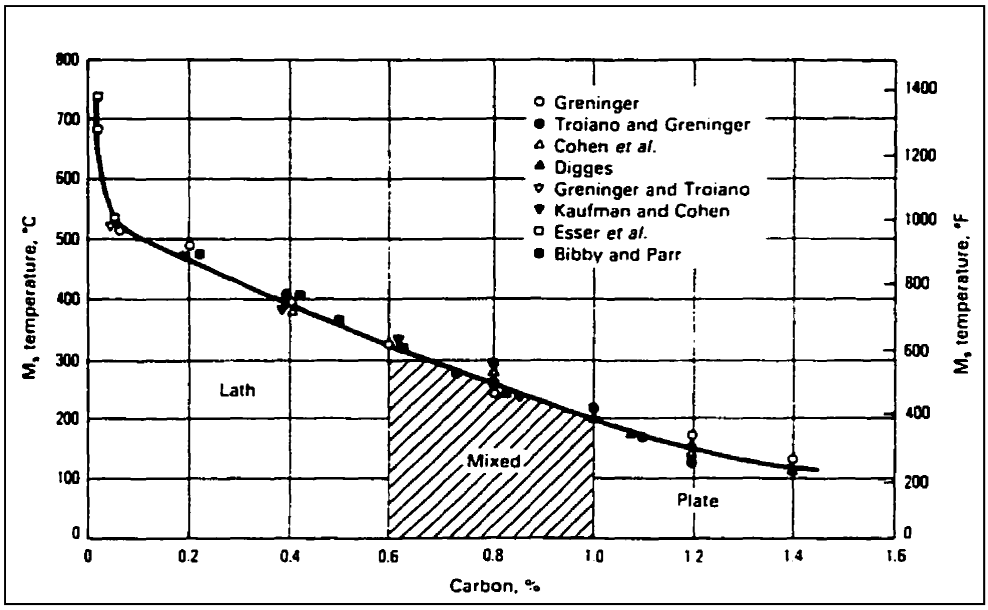

Figure 1.4 – M_S temperature and martensite morphology as a function of carbon content TakenG. Krauss (1980, 52).

Lath martensite consists of packets, blocks, sub-blocks, and laths. The pre-transformation austenite grain, also known as the "parent austenite grain," is divided into packets (Figure 1.5(a)). Each martensite packet is further divided into plate-like blocks that have the same habit plane. The blocks have sizes in the order of 50 microns and consist of laths with similar crystal orientations [18-20].

Recent research has identified new components, called "sub-blocks," within the martensite blocks. Sub-blocks correspond to a single variant characterized by the Kurdjumov–Sachs (K–S) orientation relationship with the parent austenite grain. It has been proposed that these sub-blocks, measured about 10 microns wide, are connected to each other along a habit plane with a {111} orientation. This means that sub-blocks form low-angle boundaries (Figure 1.5 (b)) [18-20]. However, studies have found that the sub-block boundaries act as barriers to dislocation movements and eventually increase the steel strength [18].

Laths are the smallest martensite features found inside sub-blocks and they are about 500 nm thick (Figure 1.5 (b)). Although these crystals appear lath-shaped in cross section, the actual shape is a needle. These needle-like crystals are parallel to the <110> direction of former austenite [9]. The complex morphology of lath martensite affects the toughness and strength of high-strength steel; the complexity of lath martensite morphology derives primarily from the lath characteristics, but also can be affected by other phases formation and prior heat treatments [9].

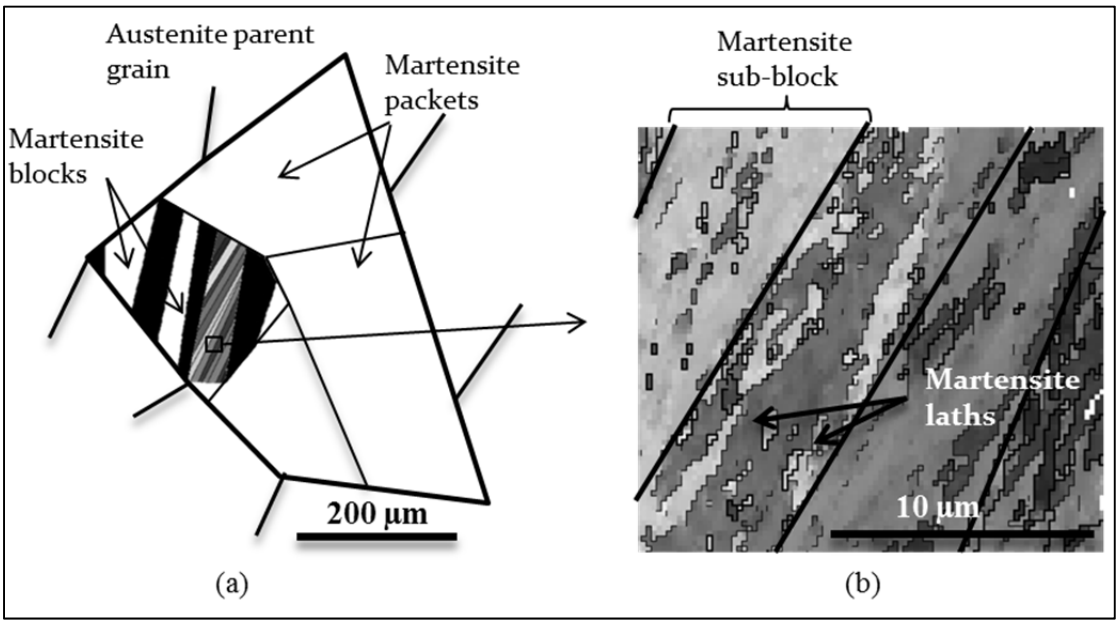

Figure 1.5 – Schematic presentation of packets, blocks, sub-blocks, and laths of martensitic stainless steels microstructure (Adapted from Morito et al. (2003) [19]).

1.1.5.2. Retained Austenite

Some austenite can be retained in the microstructure of highly alloyed steels, particularly those containing 4% Ni or more, where the martensitic transformation may finish below room temperature [21]. This retention has the potential to increase the toughness of the steel. “Retained” (or “remained”) austenite is found in martensite sub-blocks and laths interfaces [12]. Retention is particularly common between the last remaining martensite plates in the

transformation, where high elastic stress may be responsible for a halt in martensite growth [7, 11]. Researches have found that increased carbon content can lead to higher elastic stress and thus to a higher percentage of retained austenite [7, 11, 22]. Others found that austenite entrapment can also take place due to the clustering of solid solution atoms, particularly nickel atoms. Clustering of alloying elements can lower the temperature required for martensitic transformation in small regions and thus halt the transformation [7, 11]. So austenite retention should be considered as a common circumstance of martensitic transformation especially among high alloy martensitic steels.

The volume fraction of retained austenite (and its stability against transformation) has a strong effect on the strength and fatigue properties of TRIP and martensitic stainless steels [23-25]. Retained austenite percentage can be revealed on an X-ray diffraction-pattern. Based on the intensity of the retained austenite peaks, researchers have measured the amount of the retained austenite. It has been found that with increasing volume percentage of retained austenite, the toughness and elongation of the steel increase [26, 27]. Retained austenite has also been shown to serve as a crack arrester or blunter, due to its higher toughness in comparison to martensite. The martensite transformation itself absorbs a considerable amount of energy, which stops crack growth. Indeed higher austenite values is desirable [24-28].

1.2. Welding Aspects of 13Cr4Ni Martensitic Stainless Steels

1.2.1. Welding Metallurgy of Martensitic Stainless Steels

Welding is often considered as a rapid solidification; in case of martensitic steels, the presence of surrounding metal acts as a heat sink and guarantees the occurrence of final martensitic transformation. The transformations undergone during the cooling down of liquid metal are presented by the following sequence which has been also schematically presented in Figure 1.6 in the weld solidification front.

– $L \rightarrow L + \delta F \rightarrow \delta F \rightarrow \delta F + \gamma \rightarrow \gamma \rightarrow M$

These steps show the solidification path for the steel: L stands for liquid, while δF, γ and M stand for δ-ferrite, austenite, and martensite respectively.

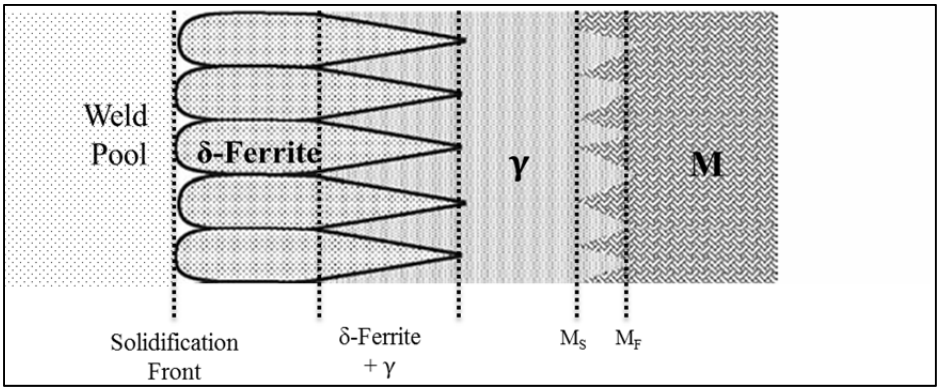

Figure 1.6 – Transformation behavior of a fully martensitic fusion zone. Dashed lines present the transformation temperature and the solidification front. (Adapted from Lippold (2005, 64) [12]).

1.2.2. δ-ferrite Formation

In martensitic stainless steels under normal cooling conditions, the austenite phase will transform to martensite at low temperatures; however, in some martensitic stainless steels, traces of δ-ferrite are retained in the martensite matrix [12]. The presence of δ-ferrite in the microstructure of martensitic stainless steels is undesirable as the hardness of ferrite in low-carbon ferritic and martensitic stainless steels is low (between 150 and 200 HV [29] which is more than 150 Vickers units lower than the fresh martensite with a typical hardness higher than 300 HV). Steel in this case exhibits reduced yield and tensile strength compared to a fully martensitic steel [16, 30]. In addition, a microstructure of more than 10% ferrite can result in a 50% reduction in impact energy [31, 32].

The retention of ferrite comes from segregation of alloying elements and its presence in the martensitic microstructure is a function of the balance between ferrite-promoting and austenite-promoting elements together with the solidification conditions [12, 33-37].

The conditions in the weld pool and along the solidification front are not necessarily thermodynamically in equilibrium. Alloying elements can build up ahead of the solidification front leading to segregation. Severe segregation of alloying elements may cause some ferrite to solidify as a eutectic ferrite at the end of the transformation. These ferrite phases are rich in ferrite-promoting elements like Cr and Mo. On cooling, each region of the weld metal follows its own phase diagram path; the enriched δ-ferrite follows the phase diagram of ferritic steel (remaining ferrite), while the other δ-ferrites follow the steel-phase diagram to transform into austenite and eventually martensite at room temperature (Figure 1.7). The stable ferrite stays trapped between metal dendrites along the grain and sub-grain boundaries. The final weld microstructure will consist of a mixture of martensite and δ-ferrite particles.

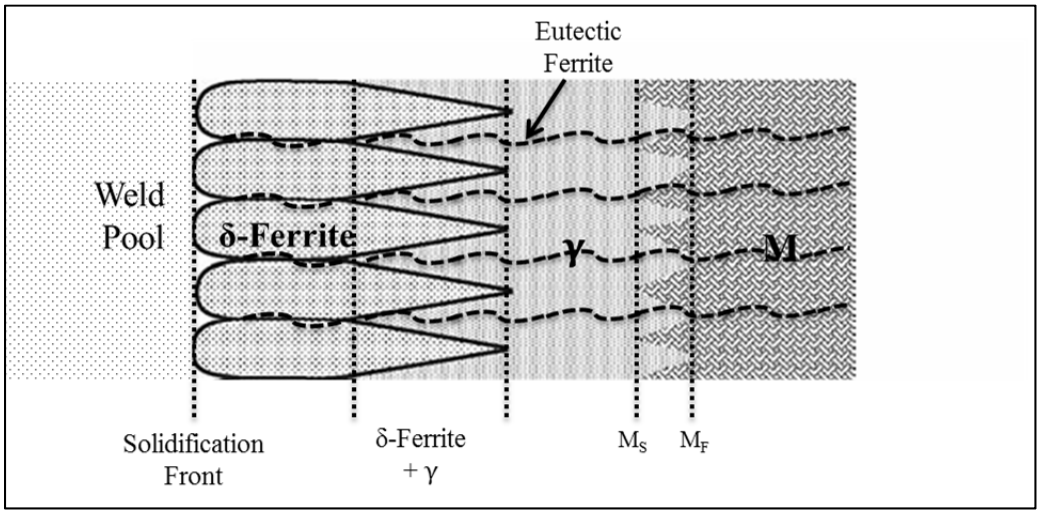

Figure 1.7 – Transformation behavior of a fusion zone in martensitic stainless steel containing eutectic ferrite (Adapted from Lippold (2005, 64) [12]).

1.2.3. Heat Affected Zones

During welding, the base metal regions surrounding the weld metal experience thermal cycles created by the weld heat. These regions are called HAZ (Heat Affected Zones). The metallurgical changes in these regions undergo are closely related to the thermal cycles imposed to them. Even if the time of exposure could play a role, the specific changes undergone by a particular region can be approximately predicted based on the maximum imposed temperature. Studies characterizing 13Cr4Ni steel HAZs have identified a number of distinct zones, delimitated based on metallography, hardness values, and expected phase transformation [37-39]. These zones include:

1- Partially melted zone containing δ-ferrite.

2- Zone totally transformed to δ-ferrite (corresponds to region heated up to stable δ-ferrite).

3- Dual-phase zone heated up to the temperature of the ferrite-austenite region.

4- Zone heated up to the temperature of the austenite area [39]:

- 4A- Region where a complete recrystallization happens, including grain growth and carbide dissolution.
- 4B- Region where a partial recrystallization and dissolution of carbides happens.

  4C- Region where dissolution of carbides is negligible and no grain size change is expected.

5- Zone corresponding to the partially austenitized region during heating. This region includes the areas close enough to the fusion line which heats up to A_{C1}[1]. Although this region is not in the austenite stable region of the phase diagram, some austenite reforms here as the more stable phase over martensite:

---

[1] Austenite transformation temperature on heating. The A_{C1} is for an ideal steel alloy on heating. Real alloys with segregations don't have a precise transformation temperature [12].

- 5A- Region where the austenite produced during heating fully transforms back to fresh martensite on cooling. It is probable that a diffusionless transformation to austenite has happened during heating [39, 40].
- 5B- Region where austenite produced during heating is stable and does not transform to martensite on cooling.

6- Tempered region; no phase transformation occurs during heating, but some degree of tempering happens [41].

In a multi-pass weld case, the HAZs are more important as each pass produces new HAZ over its surrounding which could be either over the base metal or on the other passes. The effects of HAZs could add up over each other and increase the complexity of thermal history imposed to the weld regions.

Many metallurgical aspects are used in order to distinguish HAZs regions [39]. For example, if the hardness is considered (Figure 1.8), the approximate locations of some regions can be found but hardness measurements are not precise enough to distinguish all regions [41].

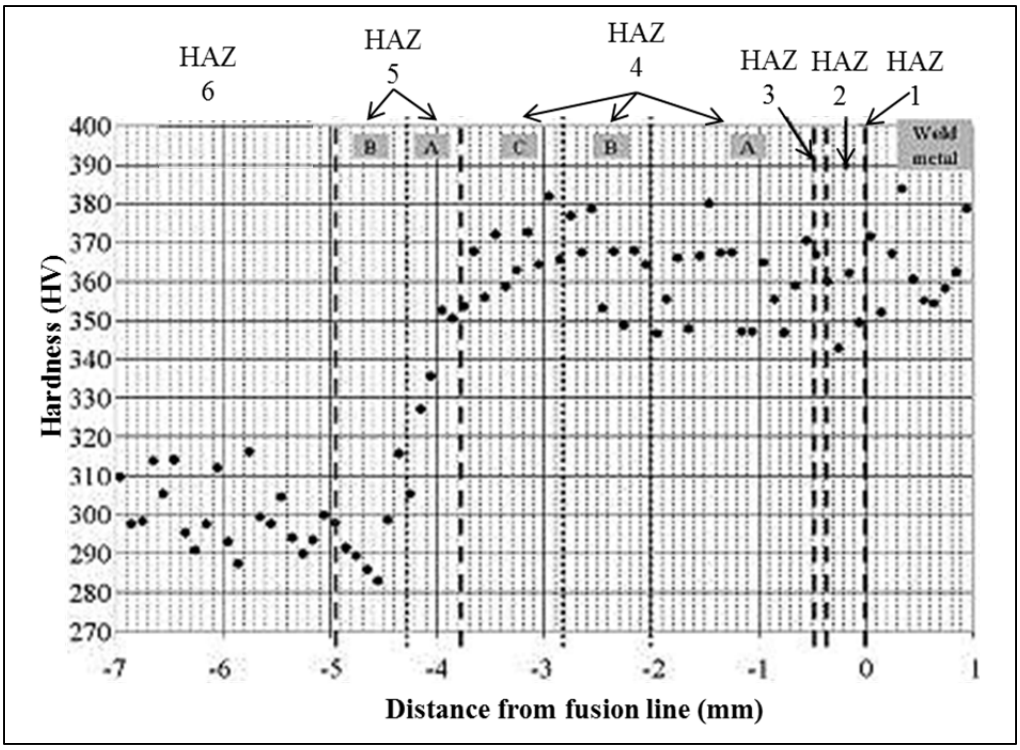

Figure 1.8 – Hardness of different regions of 13Cr4Ni weld HAZ (Adapted from Thibault et al. (2009) [39]).

1.2.4. Multi-Pass Welding

Multi-pass welding is a common practice for welding thick components. Each pass heat cycle produces thermal effects on previous passes and surrounding base metal. In case of the steel of the current study which is very sensitive to heat treatment, the accumulative effects of these heat cycles produce various properties and microstructure in each pass; ranging from a tempered to an annealing-quenched microstructure. Although the tempering are desirable, annealing and quenching are troublesome. Grain coarsening, carbide and ferrite formation has been repeatedly reported in multi-pass weld microstructure of the steel [37]. Thus, multi-pass welding procedures are usually followed by heat treatments to diminish these unwanted effects.

1.2.5. Post-Weld Heat Treatment

Post-Weld Heat Treatment (PWHT) is usually required for martensitic stainless steels. The PWHT has two main purposes: to temper the martensite matrix and to release weld residual stresses. The temperature range used for tempering martensitic stainless steels is normally from 480 °C to 750 °C; however, heat treatments at low temperatures (~200 °C) have been carried out. PWHT can also be dene to reform austenite phase, which has significant effects on fatigue resistance and impact properties [2, 7, 42-44]. For example, PWHT can lower the hardness of the HAZ and also lower the susceptibility to cold cracking [17].

Although an annealing heat treatment is relatively expensive, it can be done on the entire weld structure to fully optimize properties of the weld metal, following by quenching and tempering. The annealing heat treatment austenitizes the entire structure and dissolves most of the δ-ferrite remaining in the weld metal and HAZ, yielding a uniform fresh martensitic microstructure after quenching. Various tempering heat treatments can then be used to achieve the desired properties [45-48]. However, annealing the whole structure is not usually practical; instead, partial tempering or local heating of the joint is carried out prior to welding and between passes [49].

Tempering temperature and holding time have effects on many aspects of the weld microstructure, including tempering of martensite, amount and stability of reformed austenite, formation or dissolution of carbides, and recovery or recrystallization of microstructure. Tempering temperature is more influential for temperature-dependent features; conversely, holding time is more influential for the features that are diffusion-assisted microstructures [7, 13, 50, 51]. The importance of a proper heat treatment temperature and holding time can be understood when strengthening mechanisms are involved. These mechanisms are accompanied by a significant loss of toughness, which can be restored with a proper heat treatment [52].

1.2.5.1. Reformed Austenite

Based on recent studies, a remarkable combination of mechanical properties can be obtained in high-strength, low-carbon martensitic steels by proper tempering at temperatures close to "austenite formation temperature during heating". These tempering heat treatments form a stable austenite called "reformed" austenite, which is dispersed along the martensite lath boundaries or the austenite parent-grain boundaries [51, 53]. Reformed austenite is responsible for the high toughness, low temperature-impact toughness, and high fatigue strength of these low-carbon martensitic steels. The formation and evolution of reformed austenite by tempering heat treatments is the key to improve mechanical properties of weldments. The reformed austenite undergoes martensitic transformation which blunt crack tips or absorbs deformation energy which leads to higher toughness, higher fatigue strength and more elongation [6, 24, 47, 54].

1.2.5.2. Effect of Tempering Temperature

Many researchers have studied the effects of tempering temperature on reformed austenite formation and martensite hardness. However, the details of austenite reformation remain a matter of debate considering the complexity of its nature; including steel composition, microstructure, and prior heat treatment history.

Figure 1.9 schematically summarizes the reformed austenite percentage formed at different heat treatment temperatures from different studies. It has been found that for the 13Cr4Ni family the very first sign of austenite formation can be detected at temperatures about 100 °C below A_{C1} (Although the use of A_{C1} for a mixed microstructure is not accurate, it provides a mean to understand the behavior of the phases) . The formation of austenite is attributed to the clustering of nickel, chromium, and manganese at lattice imperfections, lath interfaces, and grain boundaries [55]. The peak of reformed austenite is reported to be around A_{C1}, but it is also very dependent on the microstructure characteristics of the steel [7, 13, 54, 56, 57].

Although the amount of reformed austenite is expected to increase as the temperature rises beyond the peak (based on the phase diagram of steel; see Figure 1.2), studies measuring reformed austenite have found that this amount decreases; eventually, at temperatures of 100 ^{o}C or more higher than the peak of austenite, no more reformed austenite is reported. This finding can be explained by the fact that higher tempering temperatures provide similar diffusion possibilities for Fe, Cr, and Ni atoms and help to homogenize the microstructure, so the austenite produced at high temperature is not stable at low temperatures, despite the high-temperature higher percentage [7, 13, 54, 56, 57].

Similarly, Figure 1.10 schematically summarizes the relation between austenite percentages and hardness of the steel. Researches show that the hardness decreases as the austenite percentage increases, with the lowest hardness values corresponding to the highest austenite percentage. Eventually, hardness increases again with the formation of fresh martensite. Although a link is obvious between austenite percentage and hardness, it should be considered that austenite phase is not the only factor that controls the steel hardness. Beside reformed austenite, a number of other factors have been found to contribute to martensite hardness, including the intensity of tempering, carbides formation, and fresh martensite formation [7, 13, 54, 56, 57].

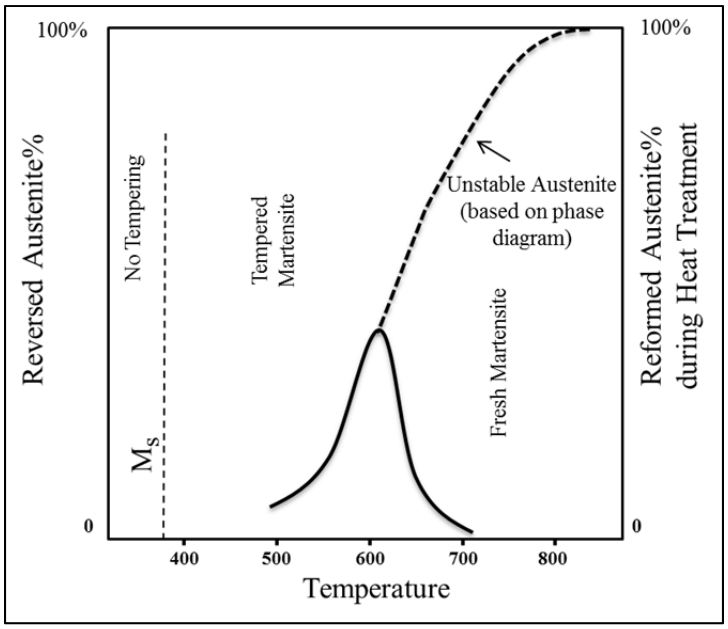

Figure 1.9 – Schematic presentation of the effect of heat treatment temperature on austenite formation of 13Cr4Ni (Adapted from Song et al. (2011) [7, 13, 54, 56, 57]).

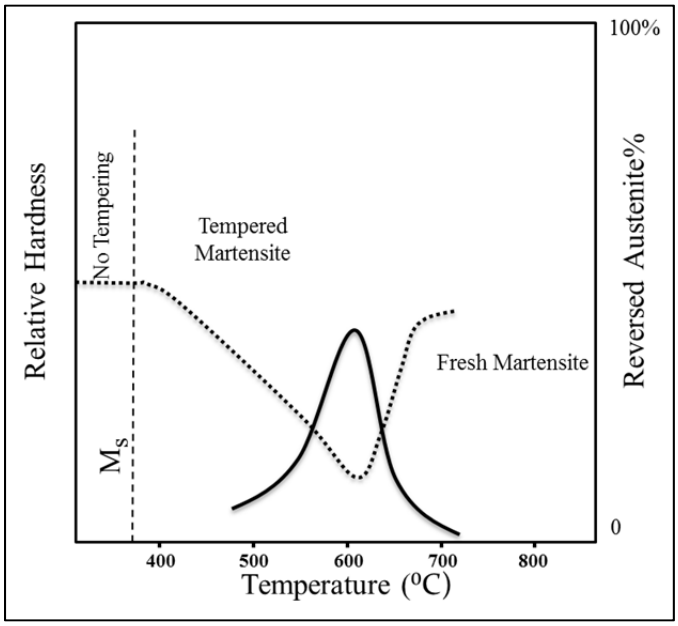

Figure 1.10 – Schematic presentation of the effect of heat treatment temperature on the relative hardness of 13Cr4Ni. Dotted line represents the relative hardness (Adapted from Song et al. (2011) [7, 13, 54, 56, 57]).

1.2.5.3. Effect of Holding Time

Studies show that the tempering holding time also affects the amount of reformed austenite in the final product. For example, for a 13Cr4Ni steel, tempering at 600 °C for 3 hours formed 11.5% austenite, while tempering for 12 hours produced 14% of austenite [54]; a steel containing 13% Cr-6% Ni showed the same trend [58].

Figure 1.11 schematically represents the holding time effects on the reformed austenite percentage and the hardness. Higher austenite percentages form over a longer holding time at temperatures lower than the peak of austenite; this effect is attributed to the fact that higher percentages of gamma-gene elements can be achieved during a longer holding time. A longer holding time provides more time for gammagene elements to diffuse to the interfaces, eventually leading to higher austenite percentages. At temperatures higher than peak, longer holding time means enhancing the heat treatment capacity in homogenizing the microstructure rather than selective diffusion of gammagene elements. The resulting uniformity in microstructure decreases the chemical stability of austenite at low temperatures, leading to more fresh-martensite with less reformed austenite [7, 56, 59]. The same argument is useful to explain the effects of holding time on hardness; at temperatures lower than the peak, longer holding time means higher austenite percentages and higher degrees of tempering which leads to lower hardness. At temperatures much higher than the peak, longer period means less reformed austenite and more fresh martensite which results in higher hardness values [13, 54, 58].

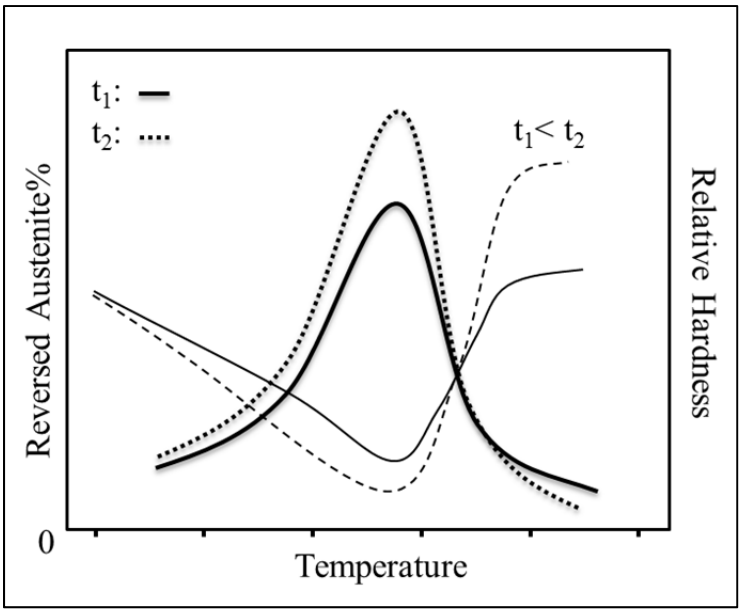

Figure 1.11 – Schematic representation of the effects of holding time on austenite percentage and hardness of 13Cr4Ni steel. Thicker lines correspond to austenite values and thinner lines to relative hardness values (Adapted from Song et al. (2010) [13, 54, 58]).

1.2.5.4. Carbide Formation

Research has shown that $Cr_{23}C_6$ carbide forms at the 13Cr4Ni steel martensite packet interfaces and lath boundaries [12-13]. Although, the precipitation of carbides was found to increase hardness and brittleness of the steel microstructure, their formation causes a depletion of matrix carbon content, thereby increasing the martensitic transformation temperature (M_S) and resulting in the production of a softer martensite matrix [13]. These opposite roles of carbide show the importance of carbide formation study on the mechanical properties of the steel.

Furthermore, formation of carbides depletes carbon and chromium atoms from their surrounding areas, resulting in higher concentrations of nickel atoms in areas close to carbides. It has been found that the high concentration of nickel atoms promotes reformed

austenite formation in areas close to carbides, which can be used also to explain the companionship of carbides and reformed austenite [7].

1.2.5.5. Widmanstätten Austenite

Widmanstätten austenite can be found in some stainless steels, especially in low carbon martensitic steels weld microstructure. Similar to Widmanstätten ferrite in carbon steels, Widmanstätten austenite forms parallel narrow wedges extending from a grain boundary, or from δ-ferrite regions (Figure 1.12). The Widmanstätten austenite structure is more common in austenitic stainless steels [35, 36].

The Widmanstätten structure depends on its formation mechanism. The Widmanstätten structure in carbon steel forms when carbon atoms are displaced during austenite formation; the rate of austenite growth is controlled by the rate of carbon diffusion. In austenitic stainless steels, the Widmanstätten austenite structure originates by a reconstructive transformation [36, 60] in which the position of the atoms in the crystal in the new phase is different from their position in the previous phase, causing the entire crystal structure of the new phase to be reconstructed. In low-carbon martensitic stainless steel, the reported morphology and coarseness of the Widmanstätten austenite indicates the formation through a reconstructive transformation similar to austenitic stainless steels [37]. As the martensite transformation eventually happens at low temperatures, only some traces of these pre-existing structures may be found in the martensitic stainless steel microstructure.

The formation of Widmanstätten austenite accompanies a sharp surface relief similar in appearance to martensite laths. The driving force for the interphase boundary migration producing the γ-fragments (Widmanstätten austenite) is thought to arise from the partial supersaturation of alloying elements in the initially formed laths. This can be explained in terms of a shear-assisted diffusional transformation model where the lattice change occurs via a diffusional individual atomic jumps and the resulting elastic strain is relaxed by lattice

shear. The partial supersaturation of alloying elements may keep this austenite even stable at room temperature [61].

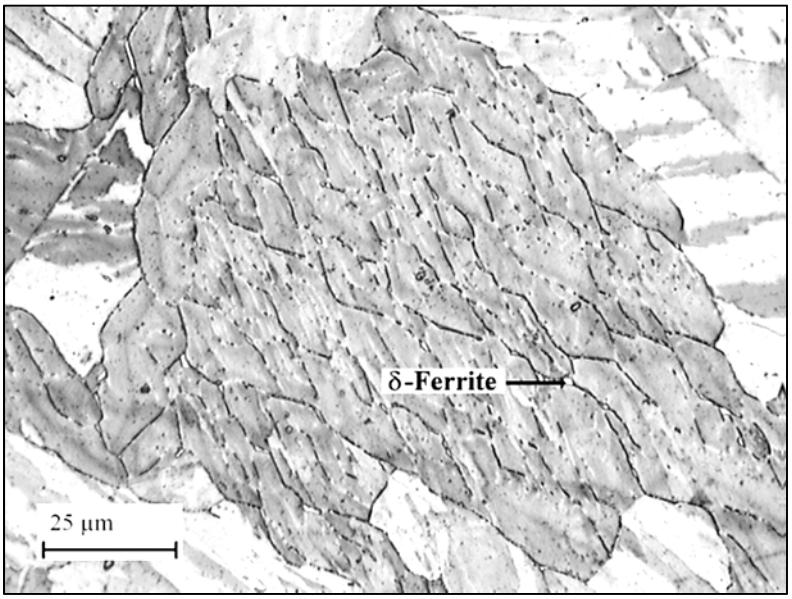

Figure 1.12 – The Widmanstätten austenite structures in the weld are of a 12%Cr martensitic stainless steel (KL 12CR) etched sample. Taken from Carrouge (2002,86) [37].

1.3. Austenite Revealing Techniques

Austenite phase is an important aspect of 13Cr4Ni martensitic stainless steels, either as the origin of its final martensite phase or as the reformed austenite after tempering. Research showed that austenite characteristics affect the microstructure and mechanical properties of the final martensitic stainless steel [62]. Many techniques are available to reveal and study the characteristics of austenite phase in both cases. The following sections introduce briefly the austenite grain recalculation and austenite revealing electropolishing techniques. The former is used to reveal austenite parents grains and texture from the martensite phase, and the latter is the technique to reveal austenite particles formed by tempering the steel.

1.3.1. Austenite Grain Recalculation

Austenite grain recalculation provides means to study the former austenite phase before undergoing martensitic transformation. Unfortunately, it is rarely possible to characterize austenite microstructure at high temperatures, and it is also hard to trace it at room temperature, since it fades inside the martensite matrix. However, many methods have been developed to characterize austenite microstructure by its remaining traces or its effects on subsequent martensite phase [63]. The most common ones are based on metallographic techniques that reveal the austenite grain boundaries but they are often hard to interpret and use [64].

Recently, reconstruction methods have been proposed and developed by using Electron Backscattered Diffraction analysis (EBSD) that recalculate the parent austenite grains from the martensite orientation maps. Some of these methods involve manual grouping of variants while others involve automated reconstruction [63, 65]. Although some of these reconstruction methods are promising in the case of steels, the research in this field is very active and on-going [63, 66-68].

One of the most common and reliable methods is based on regrouping of recalculated former austenite regions. In order to distinguish the martensite variants related to the same parents identified on the orientation map, orientation and topological criteria are used: the variants must be close neighbors and reconstructed regions should share a unique parent orientation. Thus, two main steps are involved in calculating the austenite phase map: first, adjacent variants are collected on the martensite map to form primary clusters of a parent orientation; second, the orientationally related clusters are added to a calculated parent orientation [63, 67].

When a very strict orientation relation holds between the austenite and martensite phases, each martensite variant may be related to 24 possible parents [9]. Thus, the parent austenite is

the unique shared element between all sets of solutions. In reality in a grain region, these calculations are complicated by large deviations and misorientations around each theoretical variant and by the close orientations of some potential parents (solutions) providing similar solutions [63, 67].

1.3.2. Austenite Revealing Electropolishing Technique

Electropolishing technique is very useful to reveal austenite particles formed by tempering. The selective corrosion of phases with this technique provides the opportunity to study austenite phase while other metallography techniques may transform the austenite or they are unable to reveal austenite on martensitic stainless steels. Electropolishing technique also provides a polished surface and can remove traces of deformation formed by prior surface preparations [69].

The electropolishing process includes smoothing and brightening of the metal surface. By running the electrolytic cell consisting of a pre-ground sample, electrolytic solution and a cathode, the sample is treated by the solution with a proper combination of parameters [70]. The metal surface becomes the anode of the cell and a thin viscous liquid layer is formed by the reaction between the metal and the electrolyte. This layer of solution, called the "polishing film," controls the steady flow of ions to the metal surface. More rapid ionic and molecular movement through the thinner polishing film at peaks may also be responsible for smoothing action [70].

Different types of current–voltage relationships are used in electrolytes for different metals. Figure 1.13 shows a common relationship; this pattern can be useful for determining electropolishing parameters. Five distinct regions are shown on the cell-voltage curve. In region A-B, current density increases with potential, some metal dissolves, and the surface has a dull, etched appearance. Region B-C shows an unstable condition, and region C-D indicates a stable regime in which equilibrium is reached and smooth polishing occurs.

During this stage, current density stays constant, causing a constant flow of anions from the electrolyte to the surface. Thus, the best polishing conditions occur along C-D. In region D-E, gas bubbles form as the polishing film breaks, causing severe pitting. Region E-F is a final rapid polishing stage with evolution of gas [71].

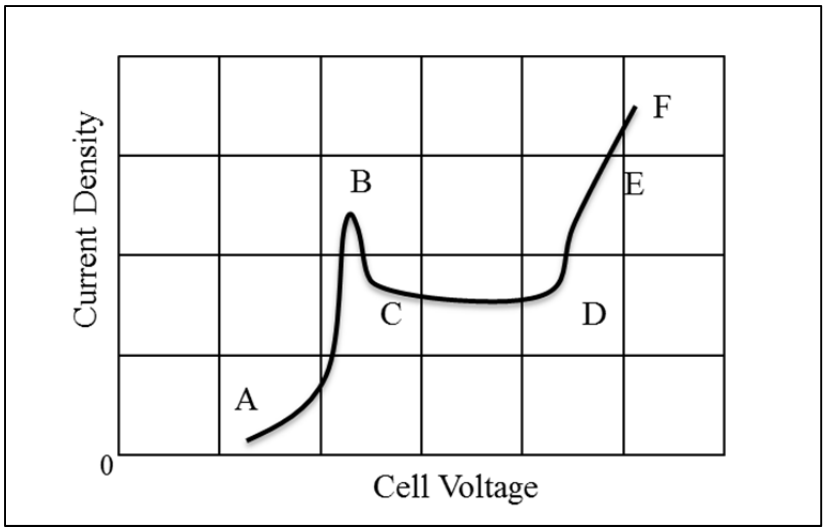

Figure 1.13 – Schematic variations of cell voltage as a function of current density for electropolishing using a potentiometric circuit (Adapted ASM Handbook(2004,285) [71]).

Many different electrolytes have been suggested for electropolishing stainless steels [71]. The most famous type is a solution of ClO_4^- ions with water, an alcohol and an organic solvent. A very common solution for 13Cr4Ni is a combination of per-chloric acid, water, alcohol, and butyl cellusolve [3, 14, 37, 39, 51, 72, 73].

1.4. Conclusions

Although characterizing as-welded structures and studying heat treatment effects are not new topics, they are very active fields of research that tie directly into efforts at improving the mechanical properties - and eventually the life span - of hydro-turbine structures. The present chapter has focused on reviewing the most important aspects of past researches; a review of literature concerning the metallurgical aspects of weld microstructure.

The chapter has introduced the 13Cr4Ni steel microstructural characteristics and it has demonstrated various factors that can have significant influences on these characteristics. It can be acknowledged that a large number of studies have examined characteristics of the steel phases and microstructure. They revealed that although the 13Cr4Ni steel can be simply categorized under martensitic stainless steels, its microstructure features are not very simple to predict. Additionally, most of the studies about the steel were focusing on cast or wrought forms of the steel and a study of multipass welded microstructure was missing among them. The literature review has also revealed that a multipass procedure can have complex influences on microstructure of the steel. For example, the literature review showed that the heat-affected zones in welded joints of 13Cr4Ni stainless steel require special attentions. These regions consist of sub-regions with distinct microstructures according to metallurgical transformations undergone during welding. They may present different microstructures and morphologies of δ-ferrite, austenite and martensite.

A second facet of the review sought to understand the effects of a post-weld heat treatment on microstructure evolutions; this review section covered topics such as tempering of martensite, formation of reformed austenite, and the evolution of microstructure in heat-affected zones. It has been shown that heat treatments alter the microstructure of the steel.

This project was defined in three parts to investigate the actual challenges faced by industries. The approach to the project problematic was determined to be the characterization of the multipass welded 13Cr4Ni steel provided by parameters and specifications of the manufacturer. The first step was defined to study a single and a double-pass weld. This part helps to investigate the as-welded state of a single weld, its microstructural features and its heat-affected zones. Subsequently, the double-pass weld helps to understand the effects of a second weld pass on the as-welded microstructure of the first pass.

After obtaining adequate understanding of a single pass microstructure and interactions between two passes, the next step is to investigate the actual as-welded multipass

microstructure. This includes evaluations of the heat-affected zones, microstructure variations, hardness evolutions and weld defects with the help of knowledge obtained from previous step. The last step is to investigate the effects of tempering on a multipass weld microstructure. This part is considered as a summary of the study, which expected to help form a better understanding of the complex nature of 13Cr4Ni multipass welded joint.

The following chapters present articles published on the topics of study mentioned in the introduction to this thesis.

CHAPTER 2

ARTICLE NO. 1
MICROSTRUCTURE CHARACTERIZATION OF SINGLE AND MULTI-PASS 13CR4NI STEEL WELDED JOINTS

Mohsen Mokhtabad Amrei[1], Yves Verreman[2], Florent Bridier[1], Denis Thibault[3], Philippe Bocher[1]

[1]École de Technologie Supérieure, Montréal, Québec, Canada.
[2]École Polytechnique de Montréal, Montréal, Québec, Canada.
[3]Institut de recherche d'Hydro-Québec, Canada.

Keywords: Martensitic stainless steels; Flux-Cored Arc Welding(FCAW); 13Cr4NiMo steels; As-Welded Microstructure; Hardness; Martensite; δ-ferrite; Heat Affected Zone; Reversed[2] austenite; Tempering;

Published in Metallography, Microstructure, and Analysis, June 2015, Volume 4, Issue 3, pp 207-218.

Abstract

13Cr4Ni martensitic stainless steels are frequently used in hydroelectric industries. Considering the size and geometry of the turbine runners manufactured in hydroelectric industries, multi-pass welding procedures are common methods for fabrication and repair. In this research, the microstructures and crystallographic textures of single-pass and double-pass welds have been studied as a first approach to understand a multi-pass weld. The highest hardness has been measured in high temperature heat affected zone inside the base metal. Attentions should be given to toughness properties of this region. Similarly it has been found that the heat of the second pass increases the hardness of the previous pass and it produces a finer martensite microstructure. In areas of heat affected zone, 3-6 millimeters far from the

[2] "Reformed austenite" has been replaced reversed austenite in the current theses as reversed austenite mostly presents the austenite phase formed by a military reverse transformation of austenite to martensite.

fusion line, a tempering-like effect is reported; traces of austenite have also been found in these areas documenting the complexity of the microstructure found in the multi-pass welds.

2.1. **Introduction**

Low carbon martensitic stainless steels such as 13Cr4Ni steels are widely used in hydroelectric, power generation, offshore and petrochemical industries, where high strength, toughness, and wear resistance of components are mandatory. Due to the size of the parts to be manufactured, welding processes are used for fabrication and repair despite the possible mismatch in mechanical properties of the body and the welded area [12]. To minimize the mismatch 410NiMo flux-cored filler wire is used to produce weld metals with sufficient toughness as it has the same composition and its carbon content is lower than conventional martensitic stainless steels [15].

During solidification, 13Cr4Ni steel solidifies to δ-ferrite and starts to transform into austenite at around 1300 ˚C. In thermodynamically equilibrium conditions this transformation ends around 1200 ˚C [10]. However, due to the actual high cooling rates of the welding procedures, small amounts of δ-ferrite can remain in the final microstructure at room temperature because of micro-segregation of alloying elements, during solidification [12]. At lower temperatures, the austenite transforms to martensite with small amounts of retained austenite between martensite laths [6, 21, 72, 74]. Thus, after cooling down to room temperature, the microstructure is martensitic with potentially small amounts of δ-ferrite and austenite.

Welded parts of 13Cr4Ni are usually subjected to post weld heat treatments (PWHT) which consist of a single or a double stage tempering heat treatment. The goal of these heat treatments is to temper the fresh martensite formed during cooling. It has been shown that a proper PWHT can transform some martensite back to austenite in large amounts (up to 25%) which influences mechanical properties [3]. However, this study focuses on non-heat treated weld conditions to better understand their microstructure formation and characteristics. In

particular, the work will focus on an adjacent weld pass which produces a local heat treatment in the already solidified regions.

2.2. Experimental Conditions

Flux-Cored Arc Welding (FCAW) process was used to deposit the weld beads on a steel substrate. Single-pass and double-pass welds were performed on a CA6NM plate using 13Cr4Ni flux-cored welding electrodes (E410NiMoT1-4) with a robotic welding machine and according to AWS A.5.22. Welding parameters are given in Table 2.1. Figure 2.1 shows the schematic cross sections of the single-pass and double-pass samples. The nominal composition of weld plate and the welding electrode are shown in Table 2.2.

Table 2.1 – Welding parameters.

Method	Pre-heat temp. (˚C)	Interpass Temp. (˚C)	Voltage (V)	Current (A)	Torch Speed (mm/s)	Filler deposit rate (kg/h)	Heat Input (J/mm)	Welding Position	Gas
FCAW	180	200	21.1	209	4.5	3.9	980	1G	Argon-25% CO2

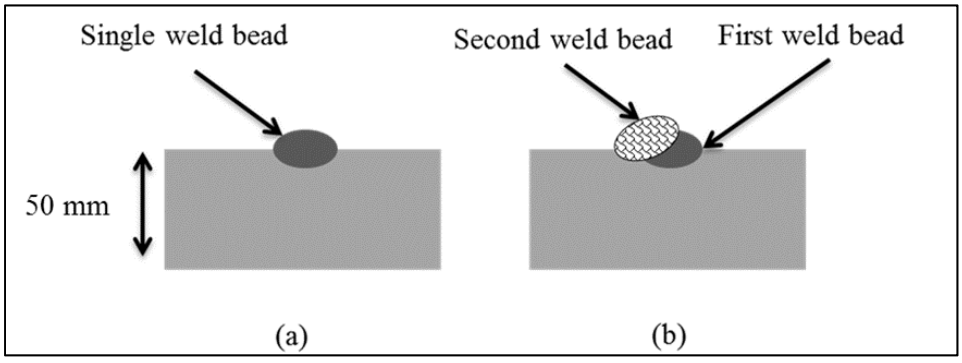

Figure 2.1 – Schematic cross sections of (a) single-pass sample and (b) double-pass sample.

Table 2.2 – Nominal composition of base metal and welding electrode (wt%).

Grade	Dimension	C	Mn	P	S	Si	Cr	Ni	Mo	Cu
CA6NM	5 cm THK.	<0.06	<0.5	<0.04	<0.03	<0.1	11.5-14	3.5-4.5	0.4-1.0	<0.05
E410NiMoT1	1.6 mm Dia.	0.021	0.36	0.008	0.011	0.37	12.46	4.39	0.56	0.03

Table 2.3 – Chemical compositions of base metal and weld metal samples (wt%)

Name	C	Mn	P	S	Si	Cr	Ni	Mo	Al	N
CA6NM	0.043	0.713	0.0267	0.0049	0.43	12.5	4.17	0.467	0.019	-
Weld metal	0.022	0.377	0.0099	0.0094	0.44	11.6	4.5	0.529	0.0136	0.00284

The actual chemical composition of the weld metal and base metal were measured by the Glow Discharge Atomic Emission Spectrometers (except for C, N, O, and S that were measured by combustion/fusion determination methods). Microstructure, chemical composition, hardness and austenite percentage were determined in the as-welded conditions. Samples were polished and electro-polished with a solution of 65ml $HClO_4$, 550 ml ethanol, 70ml butyl-cellusolve, and 70ml H_2O at 25°C, 25V for 20s to reveal austenite particles. The volume fractions of the austenite in samples were measured by X-ray diffraction from a Rietveld analysis diffractometer at Institute de Recherche d'Hydro-Québec (IRÉQ) [75]. Hardness evaluations have been done in as-welded samples using a micro-hardness testing machine with a load of 200g and a loading time of 10.2s. A Scanning Electron Microscope (SEM) operated at 20kV was used to observe the microstructures of the samples. Electron Backscatter diffraction (EBSD) maps were used to study the grains orientations of weld metal with Tango orientation map display and manipulation software.

2.3. Chemical Compositions

The chemical compositions of base metal and weld metal are given in Table 2.3. In the weld zone, compositions are close to the nominal composition of the consumable electrode. The

low carbon content of the filler electrodes produced a low carbon weld metal of about ~0.023wt.% of carbon. Low carbon content produces high ductility of the weld metal and increases the fracture properties of the joint [15].

The chromium and nickel equivalent (Cr_{eq} and Ni_{eq}) can be calculated from the following Schaeffler formulae [12]:

$$Cr_{Eq} = Cr + Mo + 1.5\times Si + 0.5\times Nb \quad (2.1)$$

$$Ni_{Eq} = Ni + 30\times C + 0.5\times Mn \quad (2.2)$$

The values for the weld metal of this study are Cr_{eq}=12.79 and a Ni_{eq}=5.36.

Based on the Schaeffler diagram a fully martensitic microstructure is expected as shown in Figure 2.2. In fact, it stays very close to martensite-δ-ferrite and martensite-austenite regions. However, the Schaeffler diagram cannot predict the existence of delta-ferrite if segregation takes place [76], nor that of retained austenite if chemical diffusion takes place during long temperature exposure when some austenite is present in the microstructure [22].

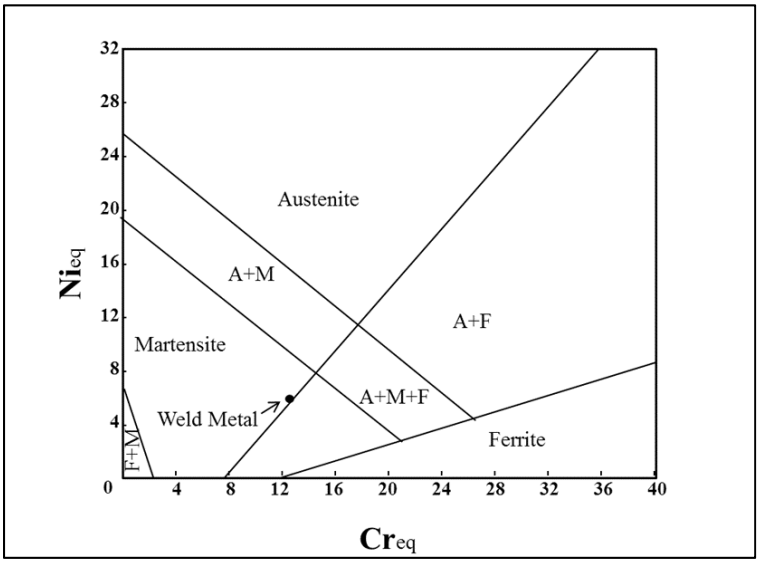

Figure 2.2– Schaeffler diagram and microstructure prediction of the weld metal. Taken from Lippold (2005,32).

2.4. Microstructure of the Base Metal after Welding

The base metal displays similar features for single and double-pass welded samples. In the next sections, only the single-pass sample will be presented and discussed, but similar observations have been made on the double-pass sample.

The microstructure of a single-pass weld sample is shown in Figure 2.3. Four distinctive zones can be seen in the microstructure: base metal, heat affected zone (HAZ), high temperature HAZ (HT-HAZ) and weld metal. As described by Carrouge, the thermal cycle of the weld produces more zones based on the steel phase diagram [37], however they cannot be differentiated in Figure 2.3.

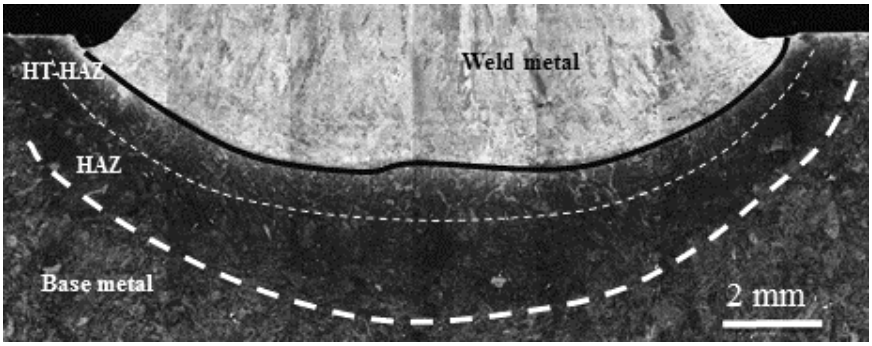

Figure 2.3 – Microstructure of a single-pass weld.

Base metal had a low resistance to the etchant as compared to the weld metal. A darker aspect is obtained due to the presence of carbides. The microstructure of base metal in regions unaffected by heat cycle consists of fine tempered martensite laths, as shown in Figure 2.4. δ-ferrite phase appears in between martensite laths as bright white regions [77]. These regions can also be clearly found using band contrast images form EBSD measurements (Figure 2.5) as in the etched image, δ-ferrite appears as white particles. Image analysis showed 1.3 % of δ-ferrite phase with average area size of 233 μm^2 and average size of 22.6 micrometers. These ferrite grains are remnants from the casting procedure.

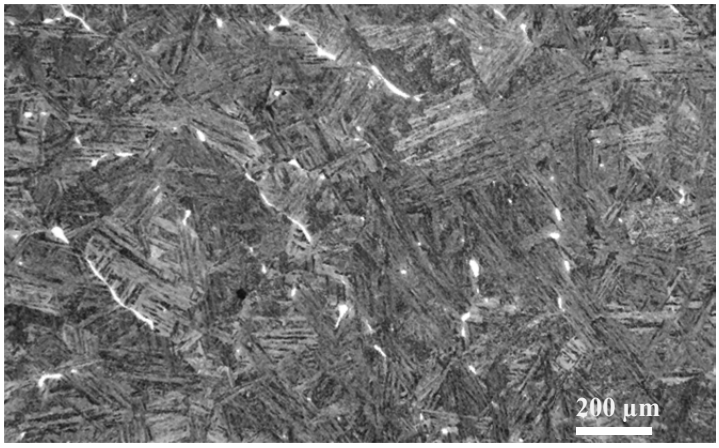

Figure 2.4 – Microstructure of the CA6NM steel (base metal consisting of tempered martensitic matrix and δ-ferrite particles, etched by Villella's reagent).

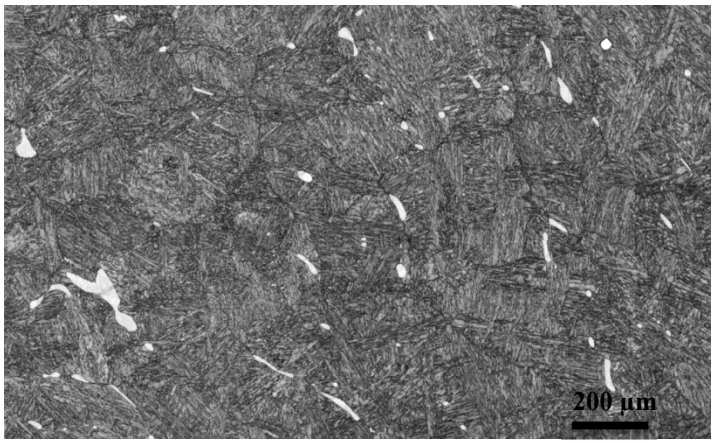

Figure 2.5 – EBSD band contrast image of the CA6NM steel (base metal) microstructure.

The HAZ region in the base metal is the darkest area around weld. It etches easily as carbides formation could happen due to weld thermal cycle [40]. Apart from becoming darker than the base metal when etched, there is no other detectable microstructure difference which can differentiate HAZ from base metal. Then it is difficult to define precisely the border between the unaffected base metal and HAZ. The HAZ seems 3 mm thick in Figure 2.3, but it will be shown later that this distance is in fact about 6 mm based on hardness measurements.

The region of the first 500 micrometers adjacent to the weld metal is called high temperature HAZ (HT-HAZ) (Figure 2.3). It was exposed during welding to temperatures greater or equal to the δ-ferrite transformation temperature. Between 300 and 500 micrometers from the fusion line, parent austenite grain boundaries can be seen in the microstructure as they are underlined by chromium-rich bright regions (Figure 2.6). These boundaries are more resistant to etching than martensite. Closer to the fusion line, a region about 300 μm in width displays the traces of dendritic type microstructure. Black micro segregations can be found, marking the previous ferrite dendritic structures (Figure 2.7). These structures document the fact that weld heat generated a semi-liquid region where the former ferritic structure of solidification was able to be reformed. The fusion line precise location was determined by the presence of plenty of micro-inclusions in the weld metal side as shown in the upper part of Figure 2.7.

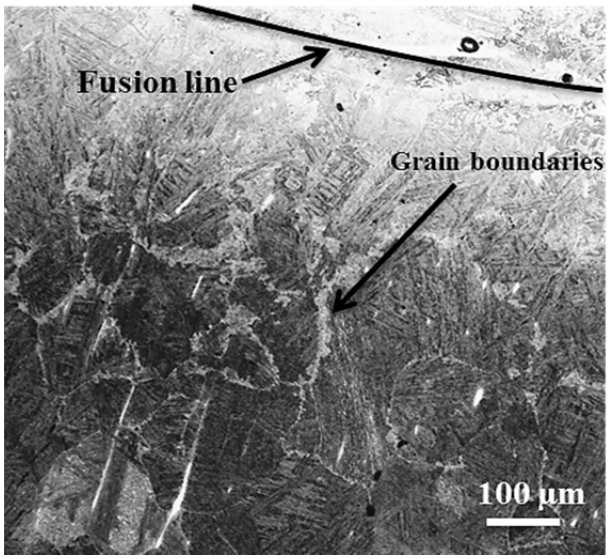

Figure 2.6 – Optical image of parent austenite grain boundaries underlined by bright phase in HT-HAZ (between 300 and 500 micrometers from the fusion line).

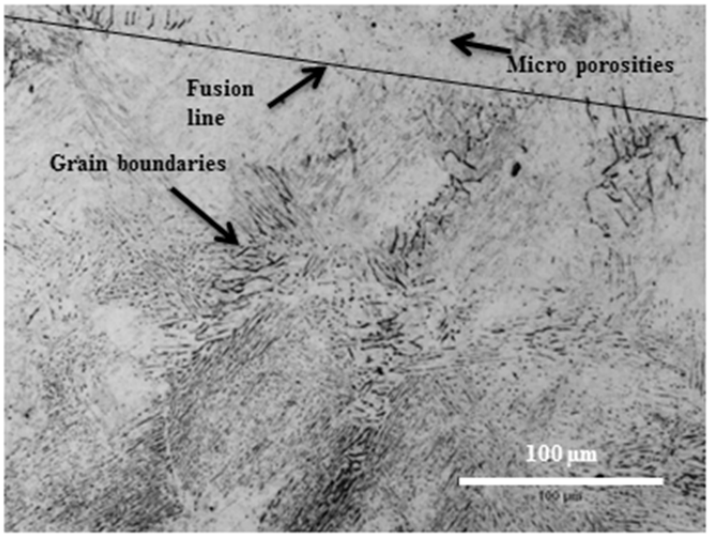

Figure 2.7 – Optical image of grain boundaries in HT-HAZ. Grain boundaries reformed δ-ferrite segregations in areas close to the fusion line.

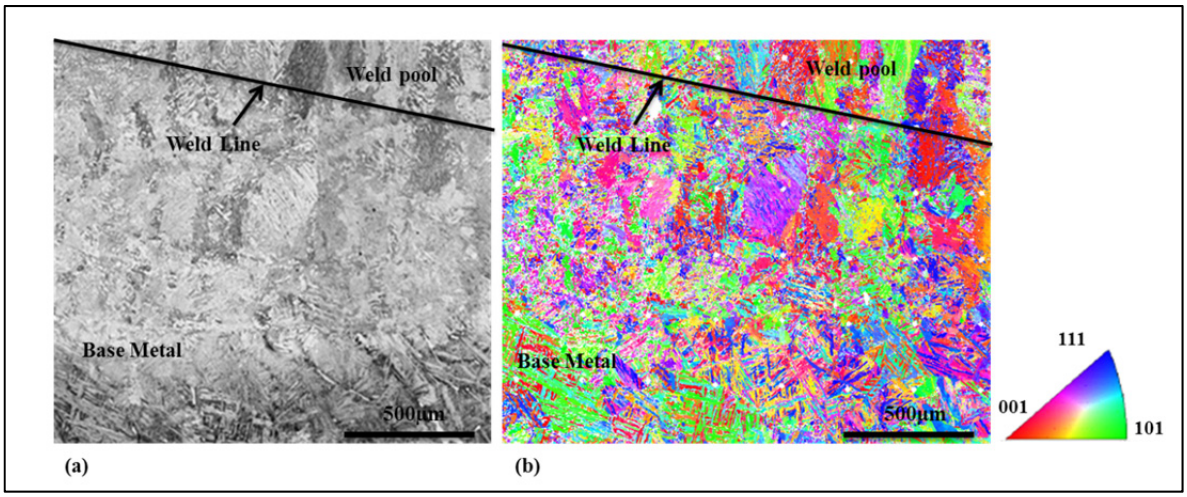

Figure 2.8 – (a) -Microstructure of a HAZ region etched by Kalling's no.2 reagent. (b) EBSD map of the same region. The welding direction is perpendicular to the image.

After a Kalling's etch together with EBSD maps of the HAZ, fine martensite microstructure was found in the HT-HAZ (Figure 2.8). This shows that the heat of the single pass produces a fine and fresh martensite microstructure in areas close to the fusion line. As one moves far from the fusion line, the martensite packets and laths appear more clearly suggesting that the

temperature in these areas was just high enough to produce a partially fresh martensite microstructure.

2.5. Microstructure of the Single-pass Weld Metal

In the single-pass weld metal sample, the microstructure can mostly be considered as fully martensitic. Although there are some evidence of inhomogeneities at the microscopic scale, such as former Widmanstätten austenite structures and δ-ferrite dendrites segregations traces, no austenite has been found using XRD measurements or electropolishing technique.

After a Kalling's etching, about 5 mm long columnar dendrites were found in the single-pass weld (Figure 2.9). The grains display a general direction which suggests directional solidification perpendicular to the solid metal toward the top of the weld. EBSD maps were taken from the same location where Kalling's reagent had actually revealed crystalline orientation contrasts. Figure 2.10 documents an example of a good correspondence between EBSD orientation maps and etched microstructures.

The contrast resulting from the Kalling's etch is related to the various crystallographic orientations of the martensitic laths. These variations lead to different chemical activities in response to the chemical reagent and produce contrast in the metallography imaging. The large columnar microstructure observed macroscopically is actually the effect of a severe variant selection as most of the martensitic laths present in a grain have the same grey level, i.e., the same orientation. According to the various EBSD and Kalling's etch images obtained in the present work, only few martensite orientations are formed from the austenite grain. Moreover, as martensite laths do not pass from an austenite parent grain to another, the columnar microstructure represents the austenite grain when very few variant selection is taking place [11]. Actually, the columnar-like martensite microstructure shows that severe variant selection has also been taking place during δ to γ transformation.

Figure 2.9 – Optical image of weld columnar growth in the single-pass weld metal.

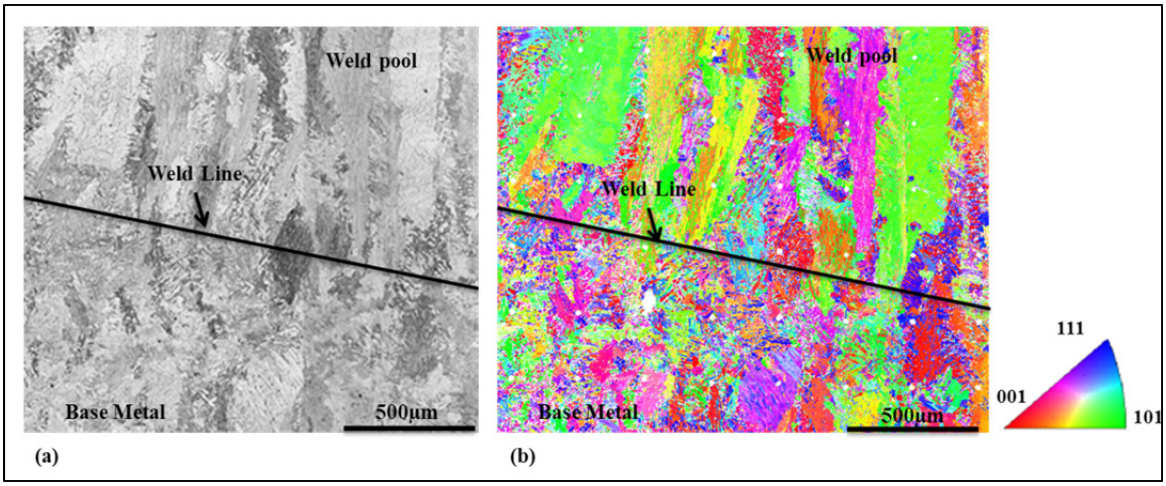

Figure 2.10 – Microstructure of the single-pass weld. (a) Etched by Kalling's no.2 reagent. (b) EBSD map of the same region of weld presented in (a). The welding direction is perpendicular to the image.

Former Widmanstätten austenite phase was found all over the weld inside columnar dendrites as shown in Figure 2.11. Widmanstätten austenite was formed during the cooling of the ferrite phase and leaves traces like narrow wedges starting from former δ-ferrite grain boundaries [37].

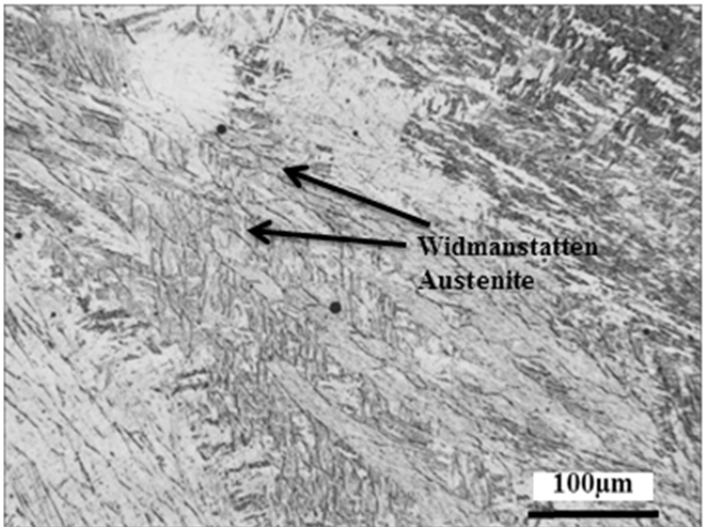

Figure 2.11 – Microstructure of the single-pass weld with traces of former Widmanstätten austenite microstructure (Optical image of the etched sample).

The traces of former δ-ferrite dendrites are found close to the fusion line and at some places in the weld pool. These former δ-ferrite dendrites are revealed by the presence of canyon-shape structures resulting from the segregations of gammagene elements as seen in Figure 2.12. This figure shows an example found in the middle of the weld pool as revealed by Kalling's reagent. Stronger segregation marks are found close to the fusion line. These δ-ferrite dendrites usually stretch parallel to the fusion line as they are oriented by the flow of the molten metal.

Figure 2.13(a) illustrates such a case using an SEM image. Actually, the negative of this image better displays the shape of the dendritic structure as illustrated in Figure 2.13(b). These regions, about 300 micrometer large, are chromium-rich and have a relatively low content of iron as found by EDX (Figure 2.13). The composition measurements have shown that these are alphagene regions in the weld and that the composition of the weld is not homogeneous. They could result from solidification segregations and δ-ferrite particles from the base metal, or most probably from welding consumables partially dissolved in the weld pool.

2.6. Microstructure of the Double-pass Weld Sample

The double-pass weld sample consists of two adjacent weld passes onto the plate (see Figure 2.1). The microstructure of the second pass is very similar to that of the single-pass specimen and will not be discussed in detail. Similarly, the base metal will not be discussed.

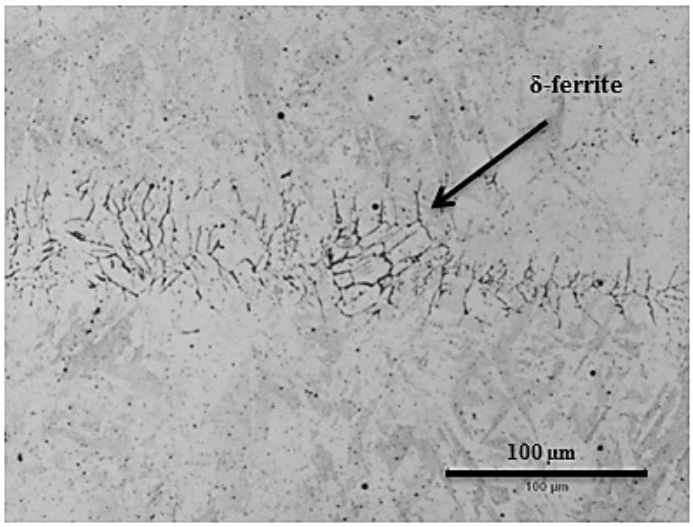

Figure 2.12 – δ-ferrite traces in the martensitic matrix of single-pass weld revealed by Kalling's etchant.

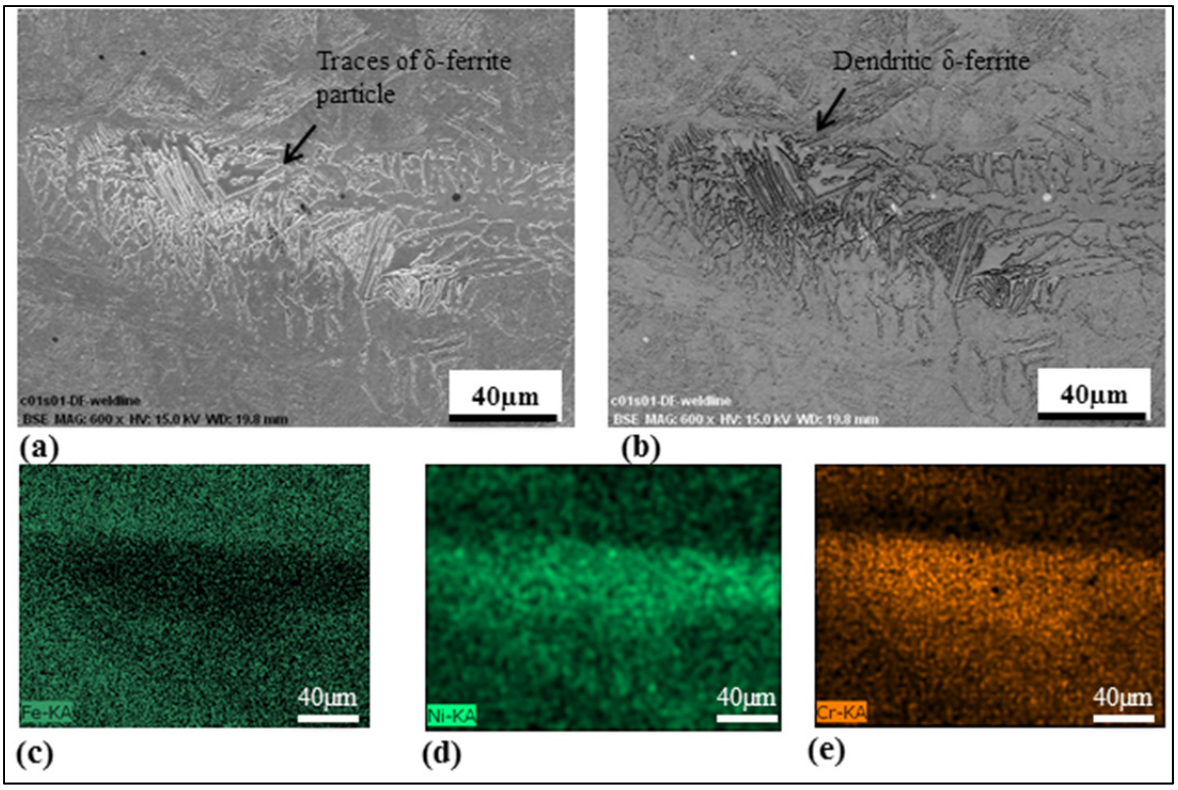

Figure 2.13 – SEM image and EDX maps of traces of former δ-ferrite phase close to the fusion line. (a) SEM image of microstructure. (b) Negative image of (a) showing the dendritic structure of ferrites. (c), (d), and (e) EDX spectroscopy of iron, nickel, and chromium in the same area of image (a).

The first pass is affected by the heat of the second pass and could actually be considered as the HAZ of the second pass. In this case, the HAZ forms over the fresh martensite microstructure of the first pass and it has a hardness about 340 HV. As a consequence, this HAZ is quite different from the HAZ formed in the base metal that was originally tempered martensite having hardness around 290 HV. Therefore three distinctive regions can be observed on the optical image of first pass; HT-HAZ, intermediate temperature-HAZ (IT-HAZ), and Tempered region (Figure 2.14). It is worth mentioning that the position of the second pass fusion line could not be determined precisely. In fact, the criterion used to define

the position of the first pass fusion line was the different natures of porosities[3] on both sides of the fusion line (small porosities in the weld metal, large ones in the base metal). As these defects are similar on both sides of the second pass fusion line, only the onset of columnar grains can be used as a criterion to define the second pass fusion line and it makes the precision for the position of the second pass fusion line in the range of hundreds of micrometers.

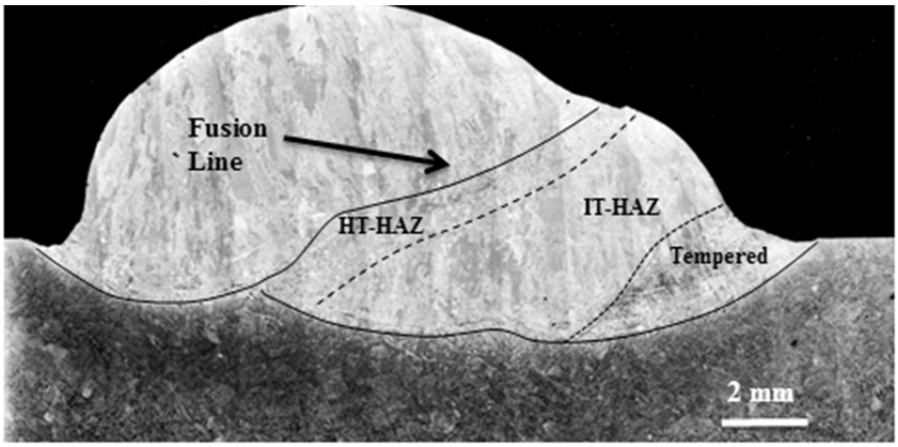

Figure 2.14 – Different regions in the first pass of a double-pass weld, based on microstructure observations.

The HT-HAZ has a fine martensite microstructure as revealed by the EBSD map shown in Figure 2.15 (a) and (b). The martensite laths of the first pass have been broken down into a finer microstructure. The thermal cycle of the second pass decreases the size of martensite laths in HT-HAZ and more variants are formed.

The IT-HAZ displays a microstructure similar to the initial single-pass microstructure, i.e. large martensite laths and columnar morphology stretching toward the top of the weld pass (compare to the lower part of the Figure 2.16). The heat of the second pass did not

[3] Later in the research, it has been observed that porosities are actually the voids of removed oxides.

significantly affect the martensite structure, suggesting that similar variant selections are taking place in this region as in the single-pass.

Tempered-HAZ is located 3 mm away from the second pass and it is darker in the image, as seen in Figure 2.14. This darker aspect is due to the formation of chromium and molybdenum carbides induced [4]by the second pass [7, 37]. Some probable traces of reformed austenite have been found in this area in accordance with the results of XRD measurements showing about 2 percent of austenite phase in the sample. They are seen as white filaments in images as illustrated in Figure 2.17. No trace of austenite has been found in any other region of the weld. These austenite particles suggest that the second pass increased the temperature high enough and for a sufficiently long period of time to allow gammagene element diffusion to martensite boundaries and (re)form austenite. The local enrichment of gammagene elements in the microstructure generates regions with low M_S values, allowing the locally formed austenite to be stable at room temperature [39].

[4] Formed by the second pass heat cycle.

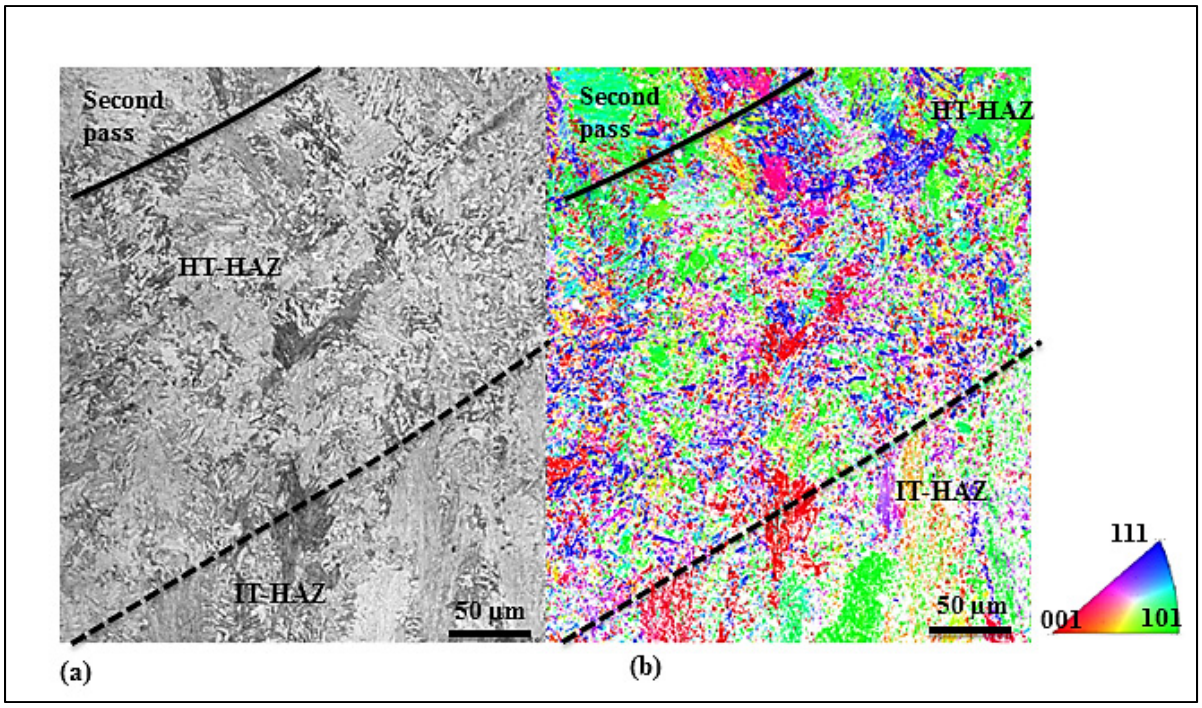

Figure 2.15 – Microstructure of HT-HAZ of double-pass sample. (a) Etched by Kalling's no2. (b) EBSD map of the same region of weld presented in (a).

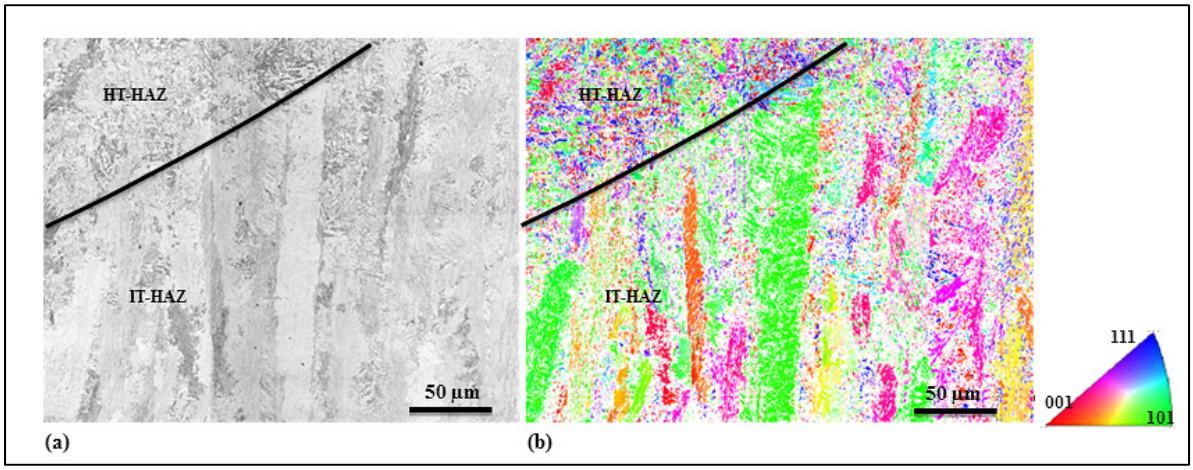

Figure 2.16 – Microstructure of IT-HAZ of double-pass sample. (a) Etched by Kalling's no2. (b) EBSD map of the same region of weld presented in (a).

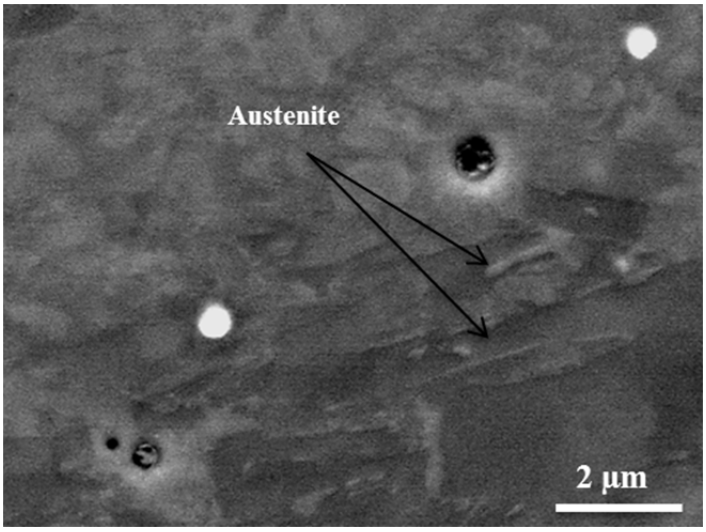

Figure 2.17 – FE-SEM image of austenite particles found in the tempered HAZ inside first weld due to the thermal cycle generated by the second pass.

2.7. Hardness Maps

In order to characterize the local properties of the weld and relate them to the microstructure variations identified in the previous sections, hardness maps have been measured on the single-pass and double-pass samples.

The hardness map of single-pass weld is shown in Figure 2.18. The weld metal has almost a uniform hardness with a mean hardness value of 350±7 HV (the ± sign shows the standard deviation and it serves the same purpose for the rest of the text). The HAZ of the single-pass measured by hardness goes more than 6 mm deep into the base metal. A hardness higher than the mean hardness of the weld metal was used as a criterion to define the HT-HAZ. A region about 1 mm deep with hardness up to 370±13 HV was found. This corresponds to the region with fine microstructure and the hardness measured is typical of fresh martensite in 13Cr4Ni steels.

The boundary of the HAZ could be recognized as the area where the hardness values of HAZ decrease to the base metal hardness value which is about 290 HV. An area of lower hardness values was found before the HAZ boundary at 3 mm away from the fusion line. This area has hardness values only 10 HV below the typical hardness of the base metal, but it illustrate the effect of the thermal cycle of the weld, which was sufficient to produce changes similar to a tempering heat treatment. The thermal cycle of the weld can not only over-temper the martensite of the base metal, but can also form reversed austenite, resulting in low hardness values [3, 7, 51]. The hardness map of double-pass weld is shown in Figure 2.19. The hardness map of the second pass is similar to the single-pass sample, but with slightly higher values. As it is estimated by image analysis of the weld sample cross section, 25% of the actual composition of the first pass comes from the base metal and then, the composition of the first pass is different from the expected nominal composition of the electrode. This leads to higher Mn content and lower N and S percentages, and showing lower hardness values [12]. Even if the second pass dissolves a significant amount of the first pass (about 20% of dilution for the second pass is measured), the overall composition of the second weld is closer to the nominal electrode so that lower hardness is obtained. Actually, one can expect that the nominal composition will be obtained after several welded passes. The consequence of these composition variations is that lower hardness values could be expected in the weld passes closer to the base metal; however as explained in the following section, there are other phenomena which can affect the above statement.

On the other hand, the HAZ introduced by the second pass in the first pass spreads over a 3 mm length with a mean hardness of 355±8 HV which is 5HV higher than the original hardness of the single-pass weld. The heat affected distance is similar to the one induced by the single pass in the base metal, but the effect on the hardness level is different. The hardness values in the heat affected region of single-pass are rather homogenously distributed and it is not possible to distinguish the presence of a HT-HAZ. The HT-HAZ can actually be only found based on a microstructure observation (This is related to fine martensite formation in HT-HAZ explained at Figure 2.15 and Figure 2.16). After this 355 HV region,

there is an area of lower hardness (320±8 HV) which corresponds to the expected tempered region suggested by the microstructure examination (This is related to the darker region with evidence of reformed austenite illustrated in the Figure 2.14).

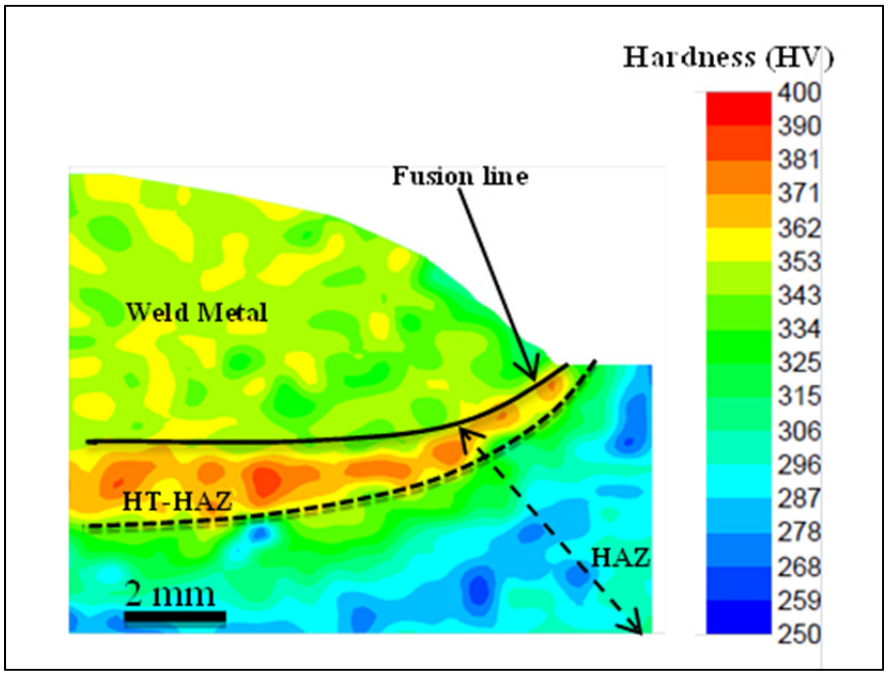

Figure 2.18 – 2D Hardness map (HV) of the single-pass weld shown in Figure 2.1. (2000 measurement points for a resolution of 150 micrometer along horizontal and vertical directions).

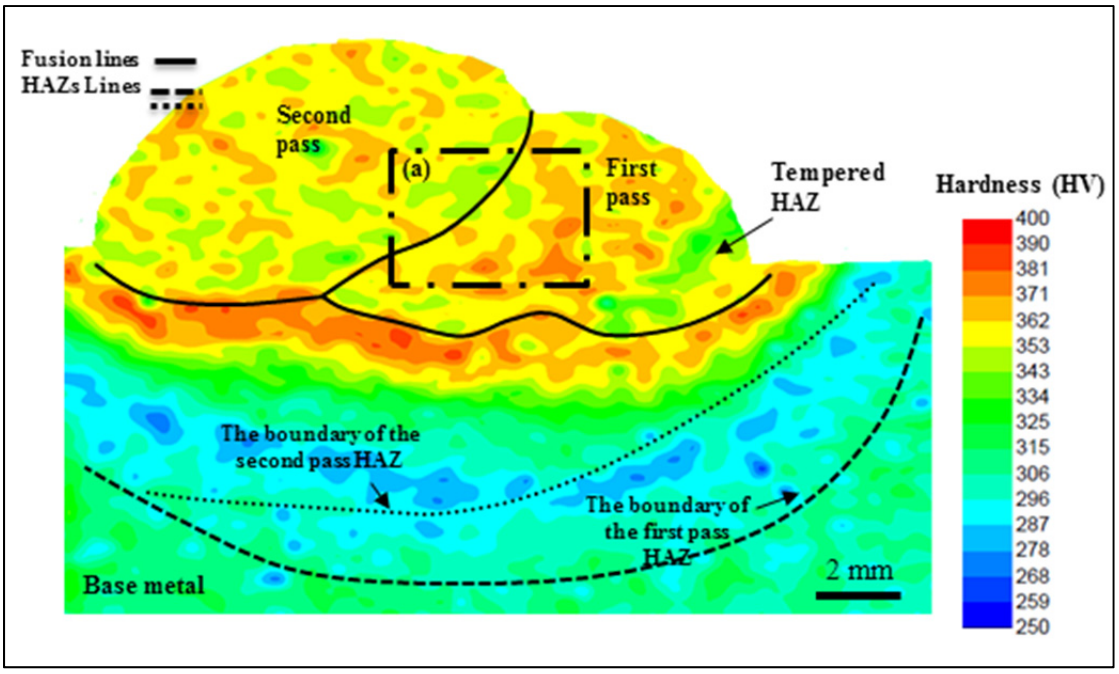

Figure 2.19 – Hardness map of double-pass weld sample showing the different regions (Same resolution as Figure 2.18).

The effects of the second pass on the first pass and its HAZ have been documented by making hardness measurements along two lines; one being taken in the single-pass sample and the other one in the same region in the double-pass sample (Figure 2.20).

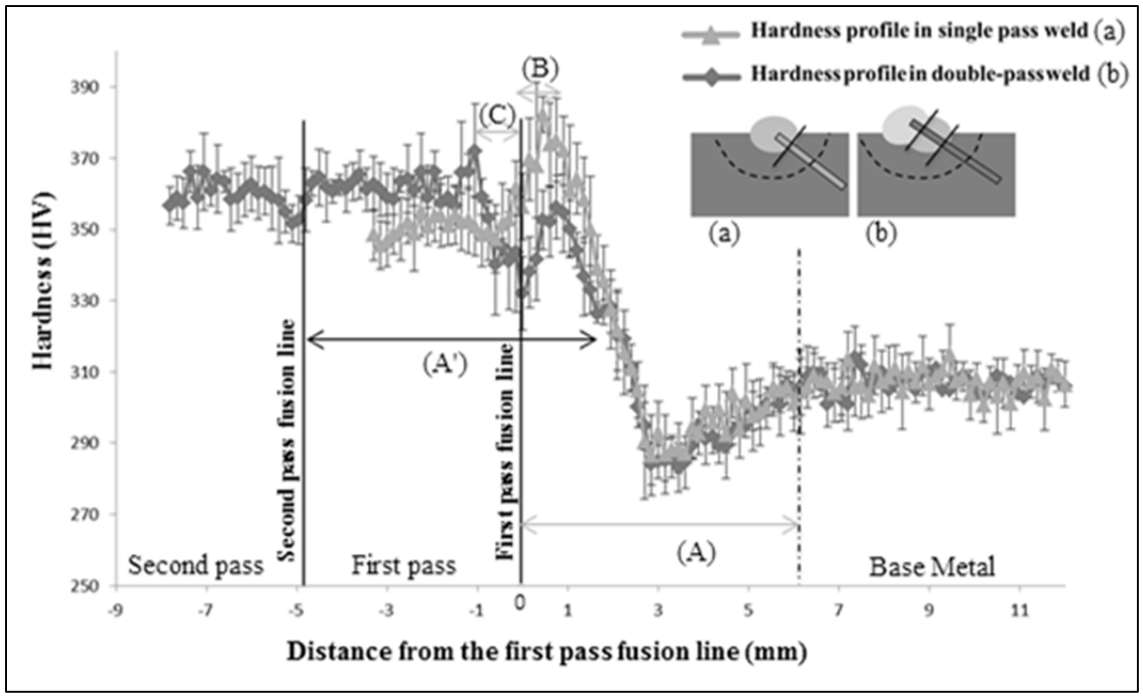

Figure 2.20 – Linear hardness measurements from the first pass fusion line. The upper-right insert shows the schematic positions of the regions used for these measurements in (a) the single-pass sample and (b) in the double-pass sample.

No effect on the hardness is seen beyond 6-7 mm from the fusion line (the HAZ of the first pass corresponds to Zone (A) in Figure 2.20). The first pass thermal cycle tempers the martensite present in the base metal at distances between 3 and 6 mm. Microstructural evaluations showed that austenite particles were reformed in these regions where the A_{C1} temperature of the base metal was reached. By moving towards to the fusion line, the temperature reached by the weld thermal cycle is higher. The temperature increases until it becomes enough to transform some martensite back into austenite for a sufficient time to chemically stabilize it by gammagene elements diffusion.

The HAZ hardness increases at a distance less than 3 mm from the fusion line. In this region, the amount of reformed austenite is so high that no gammagene element enrichment is possible and fresh martensite is found at room temperature. Fresh martensite is responsible for the high hardness in this region. On the metallography sections (Figure 2.10) it can be

seen that the initial lath structure of the base metal martensite is replaced by an austenite parent grain-like structure.

The hardness reaches a maximum of 380±11 HV at about 500 μm from the fusion line. This peak of hardness corresponds to the location where the temperature was high enough to transform all martensite back into austenite which led the microstructure to be fresh martensite after cooling.

Lower hardness was measured between the hardness peak and the fusion line (See zone (B) in Figure 2.20). This corresponds to the region where δ-ferrite traces were found (Figure 2.7). The very high temperature in this zone transforms some austenite into δ-ferrite, producing a slightly softer matrix. Retained ferrite is expected to be softer than fresh martensite, resulting in lower hardness.

In the weld, the hardness decrease continues for the first 1 mm (See zone (C) in Figure 2.20). In this zone too, traces of δ-ferrite were found (Figure 2.12 and Figure 2.13). These traces are δ-ferrite phases of the base metal which consumed partially in the semi-solid region of the weld metal and they had not enough time to mix thoroughly with the weld metal. These unmixed phases generate complex microstructures with a local composition that is an intermediate composition between the base metal and the weld metal. The rest of the weld at the left presents a relatively homogeneous hardness of about 350 HV which is a typical hardness of fresh martensite microstructure.

As for the effect of the double-pass weld, one can see that the heat effect of the second pass does not extend beyond 6-7 mm from its fusion line (Zone A' in Figure 2.20). This is coherent with what was observed for a single-pass HAZ. A drop in hardness occurred at 3 mm to 6 mm away from the second pass fusion line. This drop is the tempering effect of the second pass similar to what has been found in the same distance from the fusion line of the first pass. The hardness of the first pass was increased of about 10 HV after receiving heat from the second pass in areas 3 mm from the fusion line and closer. In these areas, some

fresh martensitic microstructure forms over the fresh martensitic microstructure of the first pass with a similar circumstance/mechanism to what has been reported in the single-pass in the first 3 mm. This double-quenched martensite forms finer martensitic packets within the grains and more carbides [78]; then it is expected to be harder than a one-time fresh martensite.

A small drop in hardness was seen close to the second pass fusion line. However, as explained earlier, the location of the second pass fusion line could not be precisely specified based on metallographic observation. One can assume that this drop is found before the fusion line due to the formation of δ-ferrite in the double-quenched martensite matrix. The present authors propose to use this hardness drop as a more precise criterion to determine the second fusion line. This hardness drop can only be seen on precise hardness profiles and was not captured on the 2D hardness maps shown in Figure 2.19 unless a more suitable color scale is used. An adapted color scale for frame (a) in Figure 2.19 ranging from 330 to 390 HV can reveal the fusion line as displayed in Figure 2.21.

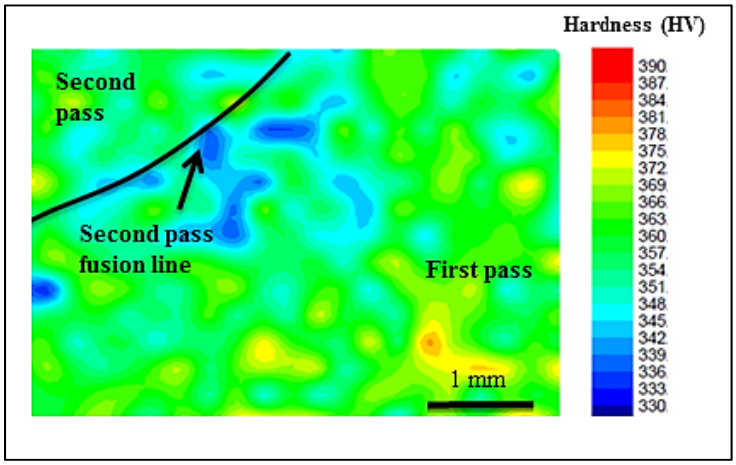

Figure 2.21 – Part of the hardness map of double-pass weld sample close to the second fusion line.

The linear hardness profiles in Figure 2.20 show that the second pass hardness is higher than the hardness of the as-welded single-pass. The lower Mn content and the higher N percentages in the second pass could explain this difference. It can be predicted that a multi-

pass procedure may improve the hardness uniformity of the welded joint if extending similar effects of the second pass to several passes.

If the decrease of the maximum hardness peak value is related to tempering effects induced by the second pass, the hardness increase on the first 3 mm of the HAZ of the second pass can be a consequence of the double quenching of the microstructure in this region. Double-quenching is known to increase martensite dislocation density, promote carbides coarsening, and increase crystallography variant selections, which eventually produces harder martensite [78, 79]. The region that was originally fresh martensite as a part of the first pass weld metal is re-austenitized by the second heating / quenching sequence induced by the second pass. The second pass rises up the temperature higher than Ac_1 at distances closer than 3 mm from the second pass fusion line resulting in a significant increase in hardness.

The present work showed that the second pass seems to homogenize the hardness of the built-up structure with a smoother transition between the base metal and the weld passes. However, one can wonder how additional passes could affect the microstructure and hardness distribution which will be presented by authors in a different article and further research will be made in this direction.

2.8. Conclusions

The heat cycle of the weld produces heat affected regions 6 millimeter deep in to the base metal. The closest region to the weld line exhibits the hardness peak at its 500 micrometers from the fusion line. Traces of dendritic δ-ferrite were found, confirming that high temperatures were achieved during the weld deposition close to fusion line. Farther in the base metal, the heat cycle produces a microstructure which is mixture of fresh martensite and tempered martensite from 500 micrometer to 3 mm. The regions farther than 3 mm from the fusion line exhibit the low hardness of the base metal tempered martensite.

In 13Cr4Ni weld metal, columnar grains microstructure filled with fine martensite laths were observed. It has been observed that most of this columnar macrostructure from the first pass

does not change by the heat cycle of the second pass. This finding has been confirmed by the images produced form etched samples with Kalling's no.2 reagent revealed the same features as the maps from the EBSD. It has been shown that the heat of the second pass increases the mean hardness of the first pass but tempers the regions farther than 3 mm from its weld line resulting in softening of the previous pass HAZ. In some regions of the HAZ, the thermal cycle exposed by the second pass transforms the fresh martensite microstructure into austenite. The results showed that a multi-pass weld procedure produces a relatively more uniform hardness profile in the welded joint compared to a single pass procedure.

Acknowledgements

The authors would like to acknowledge Natural Sciences and Engineering Research Council of Canada (NSERC), Institut de Recherche d'Hydro-Québec (IREQ), Alstom Power, and École de Technologie Supérieure (ÉTS) for the technical and financial support. The authors are grateful to IREQ laboratory for the Rietveld analyses and metallography studies and to Dr. Pierre Hovington for the SEM studies.

CHAPTER 3

ARTICLE NO. 2
Microstructure Characterization and Hardness Distribution of 13Cr4Ni Multipass Weld Metal

Mohsen Mokhtabad Amrei[1], Hossein Monajati[1], Denis Thibault[2], Yves Verreman[3], Lionel Germain[4,5], Philippe Bocher[1]

[1]École de Technologie Supérieure, Montréal, Canada.
[2]Institut de recherche d'Hydro-Québec, Montréal, Canada.
[3]École Polytechnique de Montréal, Canada.
[4]Université de Lorraine, Laboratoire d'Étude des Microstructures et de Mécanique des Matériaux (LEM3), UMR 7239, Metz, F-57045, France
[5]Université de Lorraine, Labex DAMAS, Metz, F-57045, France

Published in Materials Characterization, Volume 111, January 2016, Pages 128–136.

Abstract

Multipass welding is a common method for fabrication and repairs of large industrial steel parts. In the hydroelectric industry these parts are commonly made with 13Cr4Ni steels that present outstanding performances. In this research, the microstructures and crystallographic textures of a multipass weld have been studied. The microstructure was found to be complex and heterogeneous, consisting of several regions affected by adjacent weld passes. The study showed that austenite parent grains modification happened in areas close to the subsequent weld passes. However, parallel and low angle interface laths were observed inside martensite sub-blocks over different regions. The hardness profile was explained by overlaying the simple three regions heat affected zone. In some regions a tempering heat treatment effect was observed while in some other regions a double-quenching has happened.

Keywords: 13Cr4NiMo martensitic stainless steels; Multipass weld microstructure; Heat Affected Zone; Reformed austenite; Tempering;

3.1. Introduction

13Cr4Ni belongs to the low carbon martensitic stainless steels. They have lots of applications in hydroelectric, power generation, offshore and petrochemical industries. Multipass welding processes are common for the fabrication and repair of this steel as the carbon content is low enough to avoid loss of toughness and compressive residual stresses built in the weld after each pass [12, 39, 80]. Generally, the composition of the electrode is similar to the base metal in order to produce weld metals with similar properties [15]. 410NiMo filler metal family is the best choice among available electrodes.

13Cr4Ni steel solidifies to δ-ferrite, then starts to transforms into austenite at around 1300 ˚C and ends, in a thermodynamically equilibrium conditions, at around 1200 ˚C [10, 12]. At temperatures lower than 1200 ˚C austenite decomposes and if a thermodynamically equilibrium is achieved; ferrite and carbides are expected to be the stable phases at room temperature. However in cooling conditions which are typical of production, the very slow rate of ferrite-carbides formation maintains the austenite existence at low temperature and then austenite is subjected to the martensitic transformation.

The fully martensitic microstructure expected after cooling to room temperature, may be very complex. Alloying elements segregation in-between dendrites at the final stages of solidification can stabilize δ-ferrite phase which can remain in the microstructure even at room temperature [12]. Furthermore, the transformation of austenite to martensite can be incomplete and small amounts of retained austenite may remain between martensite laths [6, 21, 72, 74].

The microstructure of a multipass weld is even more complex as the thermal cycles of subsequent passes act as several quick heat treatments which can affect the microstructure. As a result, some carbides and austenite can be formed or modified locally. It has been shown that the reformed austenite can be stable at room temperature and it improves

toughness and fatigue properties. However, in cases of receiving excessive heat from adjacent weld passes, the reformed austenite transforms back to fresh martensite on cooling and it significantly reduces the impact properties [40, 51, 54, 55, 81].

The focus of this study is on the heterogeneous nature of as-welded multipass microstructures such as various heat-affected regions inside weld beads and hardness distributions in order to better understand microstructure features characteristics, formations, and evolutions. Previously, and as a first step toward the goals of the current study, a comprehensive study on a single pass weld microstructure has already been conducted [82].

3.2. Materials and Characterization Methods

A 50 mm thick weld metal was deposited on a 50 mm thick CA6NM substrate (25 cm× 50 cm) using 13Cr4Ni flux-cored welding electrodes (E410NiMo) and a Scompi robotic welding machine [83] according to AWS A5.22 in order to reproduce the industrial condition. The welding parameters are presented in Table 3.1. The nominal and measured compositions of substrate and the welding electrode are shown in Table 3.2. The deposited weld metal was the result of 10 layers of 40 adjacent and parallel weld passes, for a total of approximately 400 passes as shown schematically in Figure 3.1. Each pass was deposited in the longitudinal (X) direction beside previous pass and over the layer beneath. The welding direction was always positive X. In producing each complete layer (about 40 passes), the torch moved along the Y direction, +Y and –Y in subsequent layers. Samples used in this study have been taken from the middle of the weld.

Table 3.1 – Welding parameters.

Method	Interpass Temp. (˚C)	Pre-heat temp. (˚C)	Voltage (V)	Current (A)	Torch Speed (mm/s)	Filler deposit rate (kg/h)	Heat Input (J/mm)	Welding Position	Gas
Flux-Core Arc Welded (FCAW)	200	180	21.1	209	4.5	3.9	980	1G	Argon-25% CO2

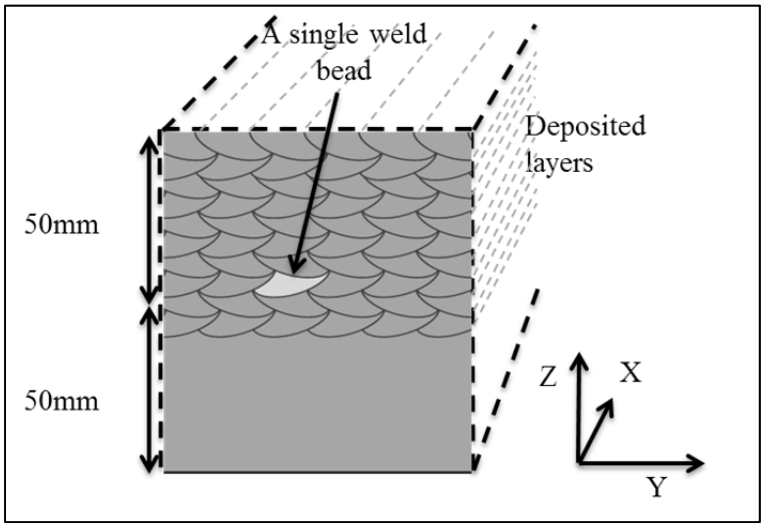

Figure 3.1 – Schematic cross-section of the weld layers.

Table 3.2 – Nominal and measured composition of substrate metal and welding electrode (wt%).

Grade	Cr	Ni	Mo	Si	Mn	C	P	S	Cu	N
CA6NM (ASTM)	11.5-14	3.5-4.5	0.4-1.0	<0.1	<0.5	<0.06	<0.04	<0.03	<0.05	-
CA6NM (As measured)	12.5	4.17	0.467	0.43	0.7	0.04	0.027	0.005	0.02	-
E410NiMo (ASTM)	12.46	4.39	0.56	0.37	0.36	0.021	0.008	0.011	0.03	-
E410NiMo (As measured)	11.6	4.5	0.529	0.44	0.38	0.023	0.01	0.01	0.014	0.003

Microstructure, chemical composition, and hardness were determined in the as-welded condition. The actual chemical composition of the weld metal and base metal were measured

by a Glow Discharge Atomic Emission Spectrometer on an average surface of 4 mm^2. The elements C, N, O, and S were measured by combustion/fusion determination methods. A spectrometer operated at 15 kV with the working distance of 15 mm was used to perform chemical composition analysis of the weld layer regions, phases and inclusion particles using ESPRIT analytical software (Bruker Corporation, Germany). To reveal microstructure and austenite particles, samples were polished mechanically and then electro-polished with a solution of 65 ml $HClO_4$, 550 ml ethanol, 70 ml butyl-cellusolve, and 70 ml H_2O using an electropolishing device at 25 °C, 25 V for 20 s. The austenite volume fractions in samples were measured by X-ray diffraction from a Rietveld analysis with a X-ray diffractometer machine [75]. Hardness evaluations on large maps have been done using an automatic micro-hardness testing machine with a load of 300 g and a loading time of 10.2 s. A Scanning Electron Microscope (SEM) operated at 5 kV to 20 kV was used to observe the samples microstructures. Electron Backscattered Diffraction (EBSD) technique was used to determine the grains orientations in the weld metal. The integration time was 5 ms and 2×2 binning was used for the acquisition and grain orientation maps were made using Tango software. Then, austenite grains reconstructions were done on EBSD maps using specific reconstruction technique [84]. Optical and SEM images were used to quantify determine dilutions and inclusions distributions in weld layers. For this, ImageJ software using threshold filtering methods was applied [77].

3.3. Results and Discussions

3.3.1. Chemical Composition

The measured chemical compositions of the base metal and weld metal given in Table 3.2 show that there are some chemical differences between the base metal and the weld metal, however they can be both considered as 13Cr4Ni steels. The chemical composition of layers presented in Figure 3.2 shows a slight composition gradient in the first weld layers. Base metal had slightly higher chromium content as compared to the weld electrode composition

which dilutes gradually layer by layer moving away from the base metal. The opposite happens for the nickel content as it was slightly lower in the base metal. The chemical compositions of layers become almost the same after layer 3 and there are no obvious variations if heterogeneity and measurement errors are taken into account. The variations in chemical compositions can be explained by the heterogeneous nature of the weld metal along with the relatively small size of measured spots (about 1 μm^2).

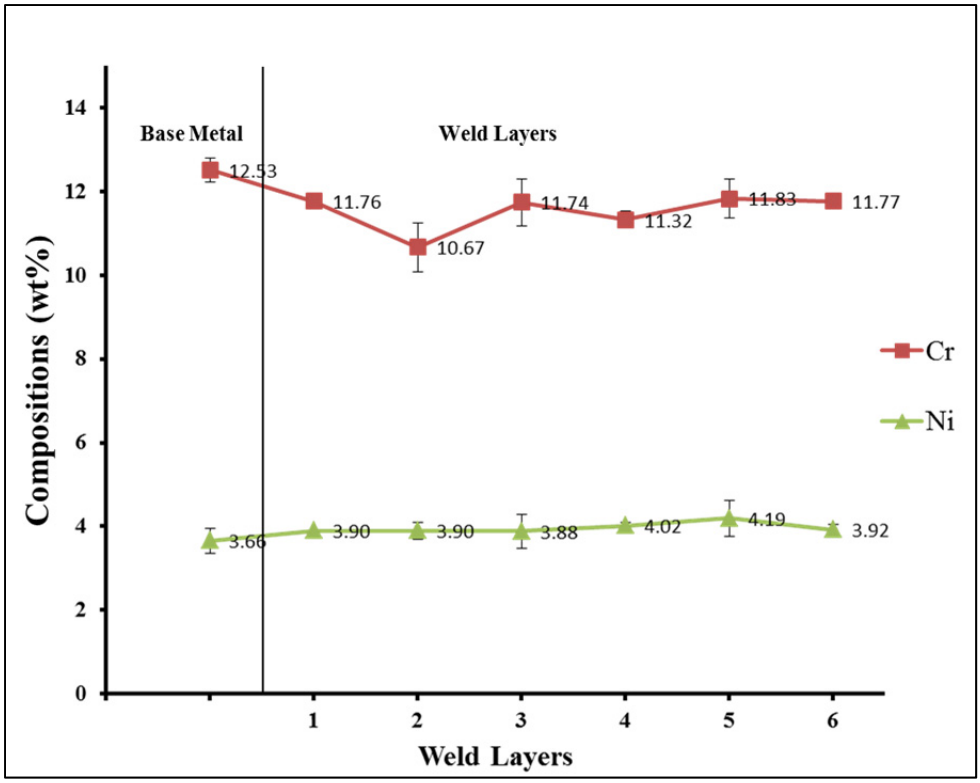

Figure 3.2 – Chromium and nickel contents of the base metal and the successive weld layers measured on average surfaces of 1 μm^2.

3.3.2. Microstructure of the As-Welded Multipass Sample

The microstructure of a multipass weld taken from the center of the deposited weld metal is presented in Figure 3.3(a). Individual beads could be recognized in the microstructure. Regions with column-shaped packets microstructure and fine martensite microstructures can

be distinguished. The fine martensite regions helps to delimitate the individual beads as presented in Figure 3.3(b).

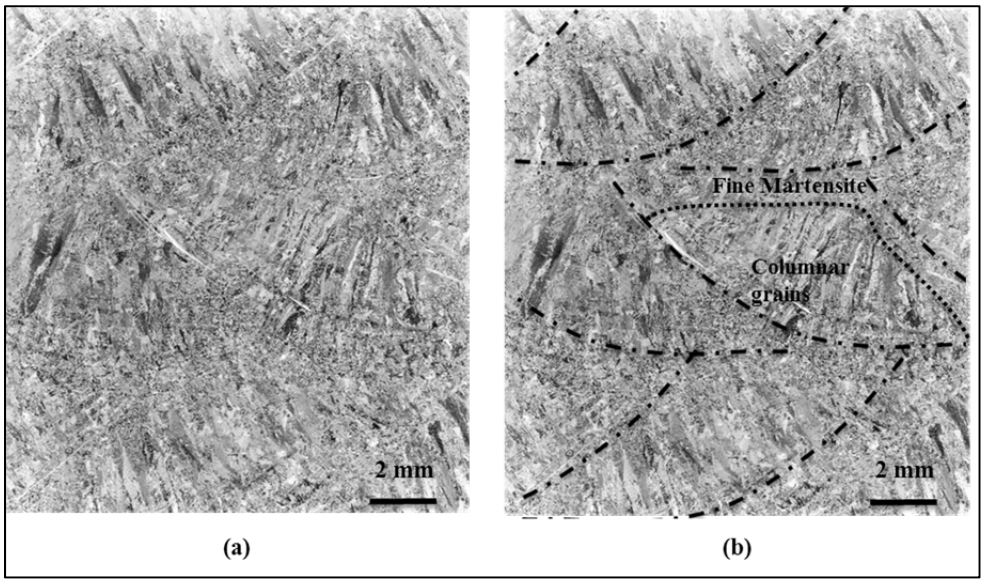

Figure 3.3 – (a) Microstructure of a multipass weld sample etched by Kalling's no.2 reagent (Transverse cross-section perpendicular to the weld plate which corresponds to the Z-Y plane in Figure 3.1). In (b), the dashed lines represent the weld bead boundaries in (a); the dotted line separating the column-shaped and fine martensite is drawn based on microstructure observations.

The column-shaped microstructure can be seen as features extending from the fusion line of a weld pass towards the subsequent passes. These columns are following the heat flow direction toward the surface of each bead. It is most likely that these are former austenite columnar grains traces formed from δ-ferrite solidification structure and the grains structures were not significantly modified by the martensitic transformations during cooling ($\gamma \rightarrow M$). Even in some regions in which the heat of subsequent passes has raised the temperature to austenite region, the microstructure remains as columns on cooling as it transforms back to fresh martensite again. The fresh martensite which has been formed over a formerly fresh martensite of the as-welded metal, is called double-quenched martensite and it is expected to be slightly harder than the weld fresh martensite due to higher dislocations density and additional precipitation of carbides [78]. This part of columnar region in which double-

quenched martensite can form is called intermediate temperature HAZ (IT-HAZ). Away from the fusion lines where the temperature raise is about “martensite to austenite transformation temperature on heating” (A_{C1}), the increase in temperature is just enough to produce some austenite particles and to temper the fresh martensite matrix [39]. This part of columnar region is called Tempered region. Although the tempered martensite shows lower hardness values, it is difficult to distinguish the corresponding region in an etched sample.

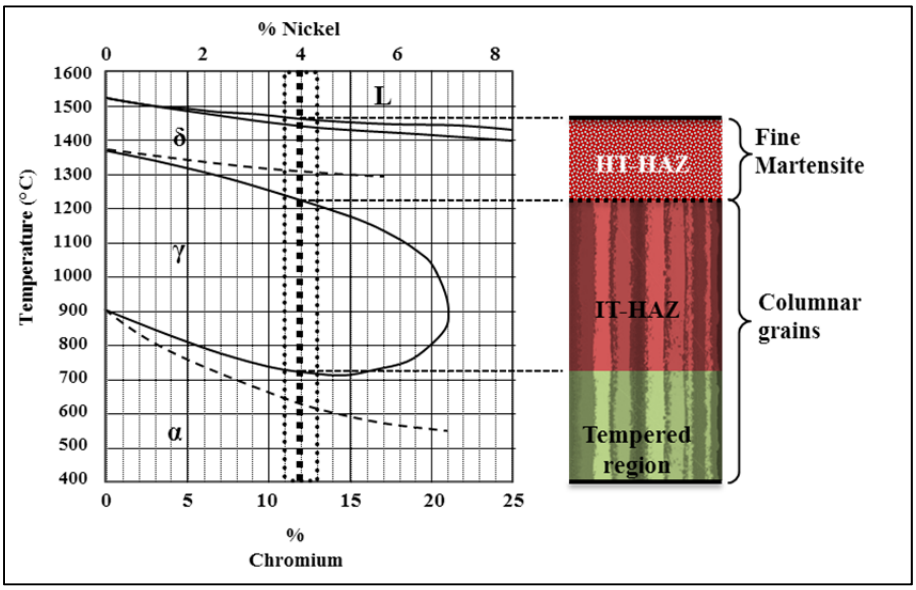

Figure 3.4 – Phase diagram showing the phase’s domain and their corresponding HAZ inside a single weld bead (phase diagram adapted from Folkhard (1989,11) [10]). Phase diagram dashed lines are transformation lines showing possible transformations on heating. The scheme on the right corresponds to the regions observed in a weld bead thermally affected by an adjacent single bead [82].

The fine martensite zones can be considered as areas in which the subsequent or adjacent passes was close enough to rise the temperature up to ferrite stable region. Heating above 1300 °C (approximately) has changed the formerly column-shaped microstructure of packets and then it has generated smaller martensite blocks and sub-blocks after cooling to room temperature. This area was called the high temperature HAZ (HT-HAZ) [37].

Figure 3.4 shows the schematic correlation of microstructure and phase diagram on heating. The simplified three-layered HAZ can be seen as HT, IT, and Tempered on this diagram corresponding to the heat effects of only one subsequent pass and the related phase transformations.

A longitudinal cross-section (Z-X plane in) of the multipass weld sample is presented in Figure 3.5. Column-shaped packets of martensite could be seen together with a fine grain martensite zone similar to what has been shown on the transverse cross-section figure (see Figure 3.3). Having column-shaped grains in both longitudinal and transversal cross-sections is the evidence for columnar dendritic solidification in weld. The fine martensite region (HT-HAZ) width is also determined to be about 500 μm for the welding conditions of current study.

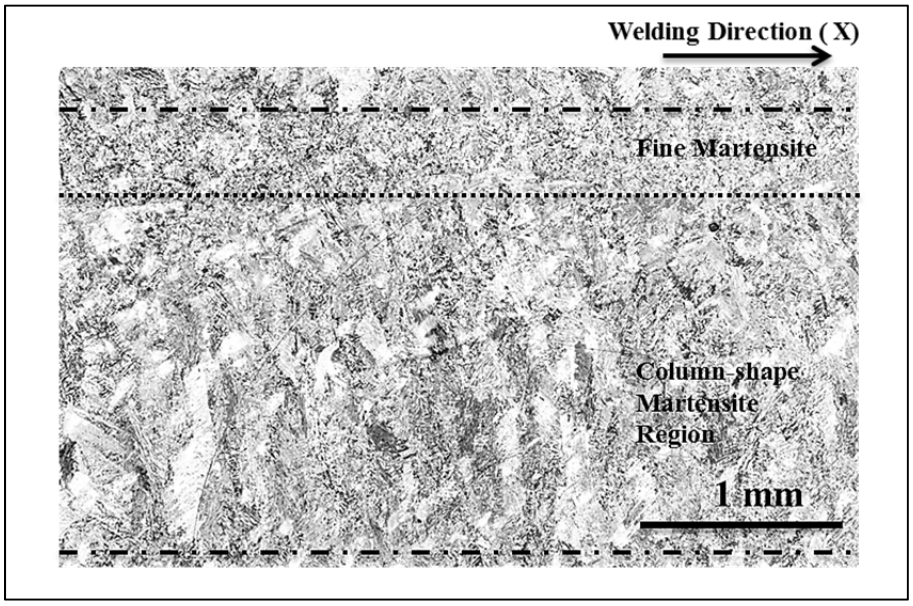

Figure 3.5 – Microstructure of a bead in multipass weld sample etched by Kalling's no.2 reagent (longitudinal cross-section, perpendicular to weld plate). Dashed lines are showing the approximate weld bead boundaries. Dotted lines are separating the fine martensite and columnar region inside the weld bead.

3.3.3. EBSD Analysis of Multipass Weld Sample

The column-shaped packets and fine microstructures can be clearly revealed under EBSD. For instance, by comparing the image of etched sample with its EBSD map (Figure 3.6(a) and (b)), it becomes clear that in the columnar zone, each column corresponds to a region with parallel packets and blocks of similar orientations. This confirms the assumption that a strong variant selection has been taken place in these regions during the solidification and subsequent phase transformations. Even becoming exposed to the later passes thermal cycle did not change the packets and blocks variant selection in this region.

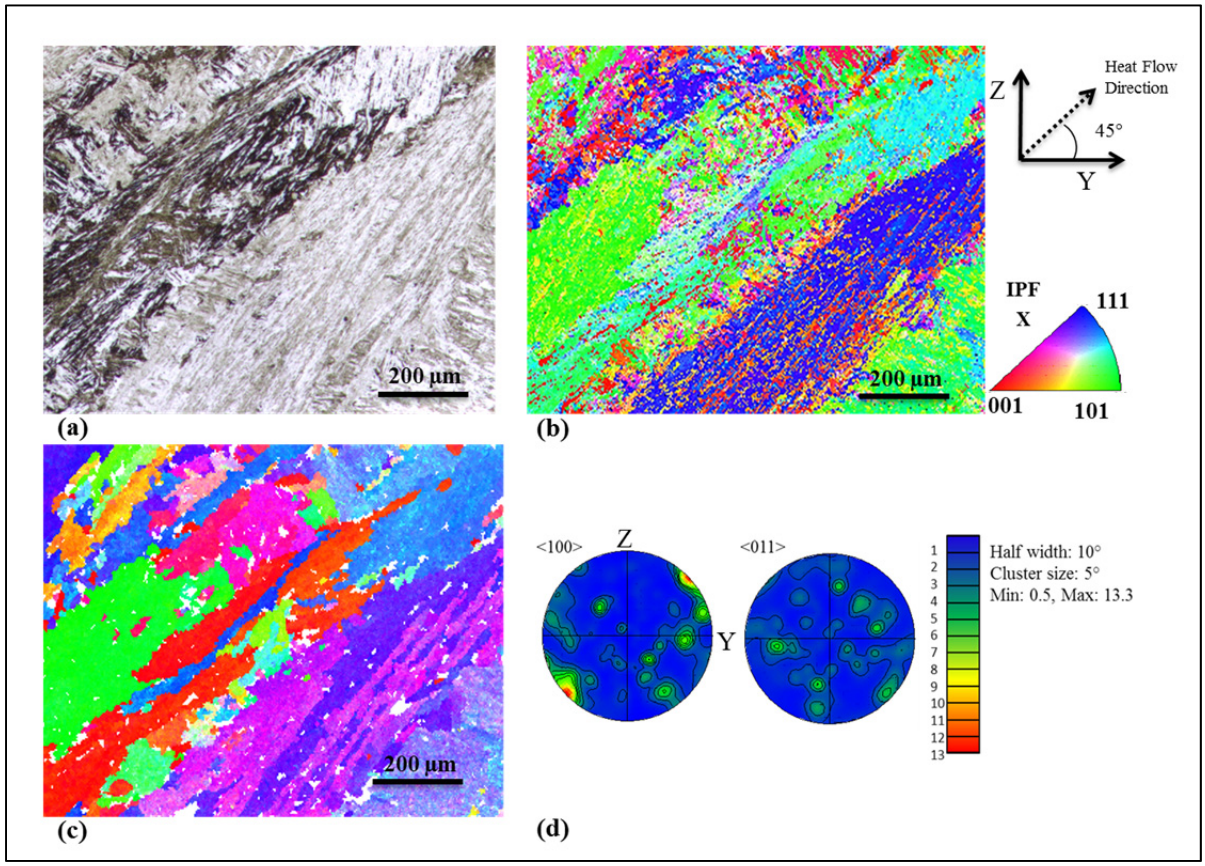

Figure 3.6 – Multipass weld microstructure in columnar zone. (a) Etched by Kalling's no.2 reagent. (b) EBSD map according to the colored inverse pole figure on X direction (Figure 3.1). (c) Austenite parent grain reconstruction of the EBSD map. (d) Pole figures of column-shaped martensite zone in <100> and <011> directions. The welding direction (X) is perpendicular to the images.

The austenite grains reconstruction presented in Figure 3.6(c) shows that austenite parent grains kept the expected columnar microstructure and martensite packets formed inside columnar austenite grains. The austenite grains in this region are several millimeters long in the cooling direction and about 200 μm wide. The persistence of solidification microstructure confirms that the crystallographic texture transformations from δ-ferrite to austenite and eventually to martensite were happened with strong variant selections.

Pole figures of the columnar area are presented in Figure 3.6(d). Although the presence of some packets along heat flow direction created high intensities in the figures, no strong texture is observed.

A high magnification SEM and EBSD analysis can reveal the detailed microstructure of columnar area (Figure 3.7). This type of microstructure can be found everywhere in the columnar region. The EBSD map shows that sub-blocks are consisted of many parallel laths of low-angle interfaces and some high-angle boundaries. The widths of the laths were measured about few hundreds of nm. These laths are revealing the complexity of the column-shaped martensite packets microstructure at high magnification.

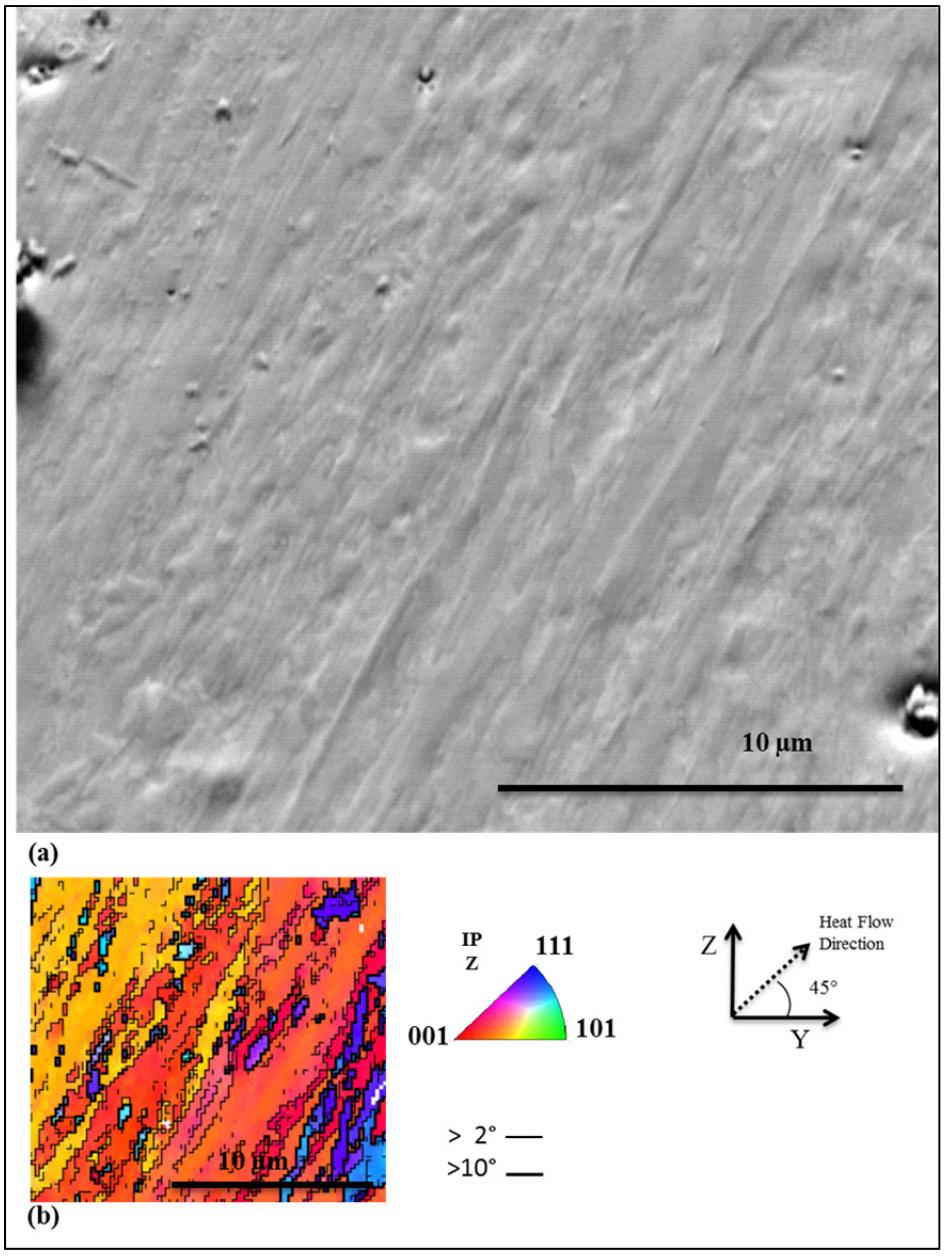

Figure 3.7 – (a) A typical Secondary Electron image (SE-SEM) in tilted conditions and at high magnification of the columnar area). (b) EBSD map of the area shown on (a).

For the fine martensite regions (HT-HAZ), the EBSD map shows a fine microstructure similar to the one revealed on the etched sample. The optical microstructure and EBSD map of the laths are presented in Figure 3.8(a) and (b)). The austenite parent grains reconstruction

was also performed in the fine martensite zone (Figure 3.8(c)). Grain reconstruction showed austenite grain modification to about 40 µm. Studies suggested that the thermal cycle of adjacent pass was high enough to trigger recovery and recrystallization stages but the grain growth reported in these studies [37] cannot be confirmed. Another hypothesis is that the transformation of austenite to delta-ferrite, and then again to austenite produced smaller austenite grains. The reason can be the fact that more nucleation sites are present compared to the initial cooling of the weld metal. Thus, the former solidification microstructure disappears and a finer martensite is produced. Pole figures of this area confirm the absence of an as-welded texture (Figure 3.8(d)).

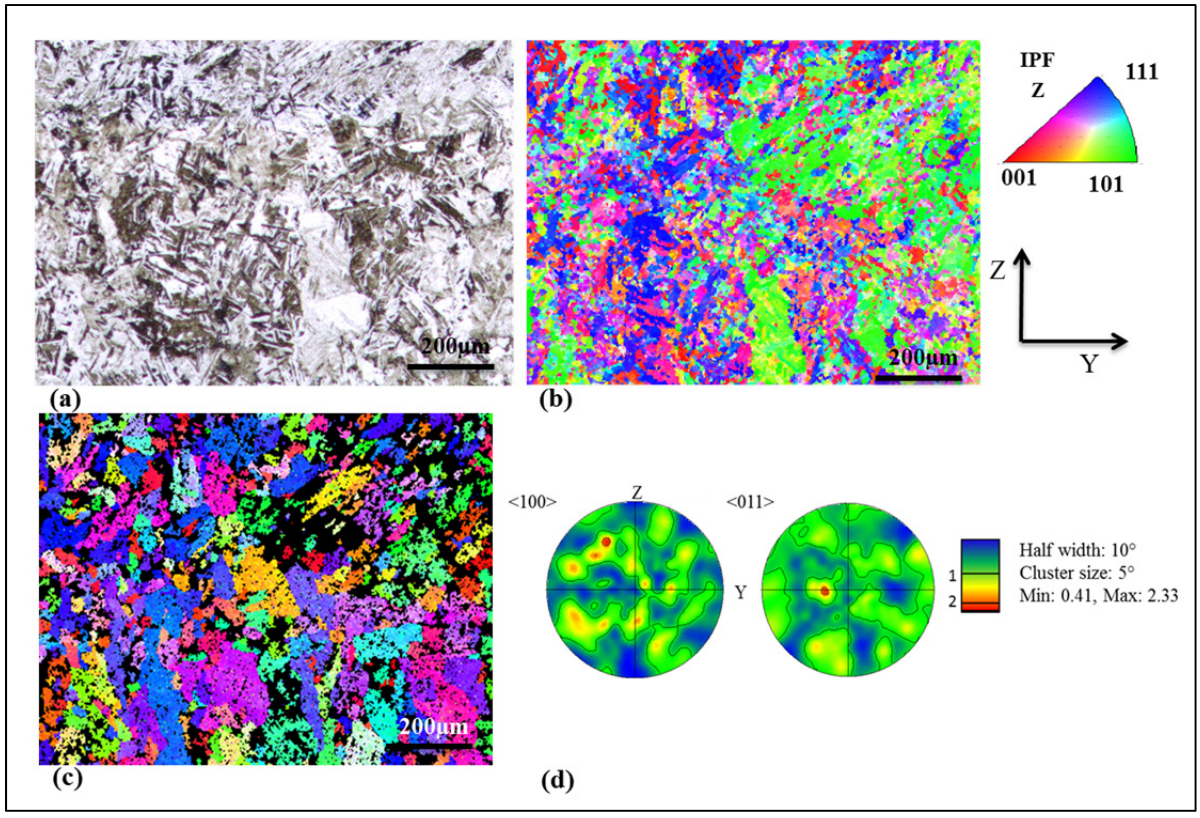

Figure 3.8 – Microstructure of fine martensite zone. (a) Optical microscopy image after etching by Kalling's no.2 reagent. (b) EBSD map according to the colors invers pole figure legend of Y-Z plane (see) of the same region presented in (a). (c) Austenite parent grain reconstruction of the EBSD map. (d) Pole figures of fine martensite region in <100> and <011> directions. The welding direction (X) is perpendicular to the images.

SEM imaging and EBSD analysis of a fine grain microstructure at high magnification is presented in Figure 3.9. Small sub-blocks were observed in SEM image with carbides precipitated at sub-block boundaries. The EBSD map shows that the sub-blocks are still consisted of parallel laths similar to columnar region. The widths of these laths also observed to be about few hundred nm. In fact in fine grain region, the heat cycle of adjacent pass breaks down the columnar microstructure into smaller sub-blocks. However, parallel interfaces are still present inside these sub-blocks.

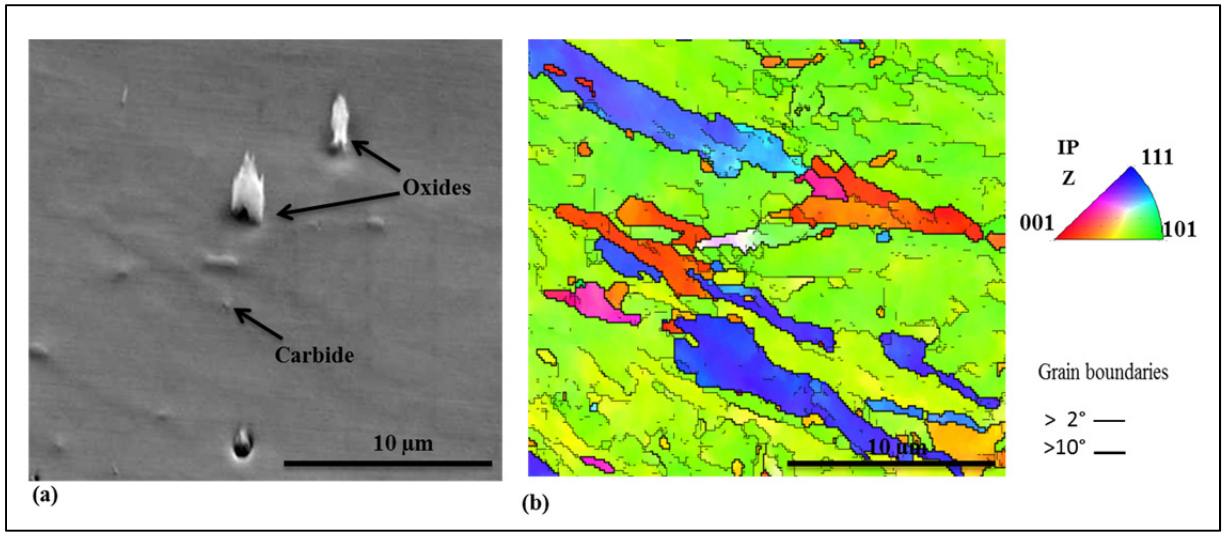

Figure 3.9 – (a) high magnification SEM image of fine martensite region (tilted view). (c) EBSD map of the area shown on (a).

3.3.4. Inhomogeneity in the Weld

Heterogeneities at microscopic scale were found in the microstructure of the multipass weld; δ-ferrite traces, Widmanstätten austenite traces, oxides inclusions, carbides, and austenite particles were found in between martensitic laths. Identifying these heterogeneities helps to better understand the weld complex nature.

δ-ferrite traces have been found in the weld as microstructures parallel to the weld lines (Figure 3.10(a)). It has been shown that their formation is due to solidification segregation close to electrode un-dissolved particles enriched in high ferrite-stabilizing alloying elements

[82]. They are formed during the last stage of solidification and their presence is a sign of inadequate mixing in the weld pool or an insufficient heat input.

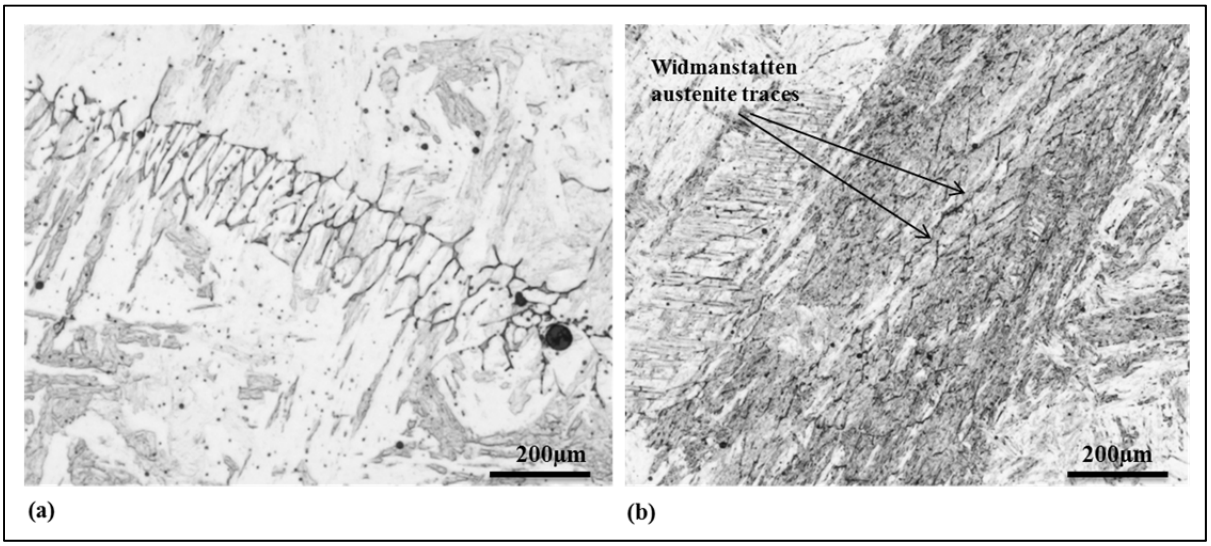

Figure 3.10 – (a) δ-ferrite traces in the martensitic matrix of the multipass weld revealed by Kalling's etchant. (b) Microstructure of the multipass weld with the former Widmanstätten austenite traces that remained inside a martensite grain in the IT-HAZ regions.

Widmanstätten austenite traces are another type of inhomogeneity in the weld which have been found inside martensite columnar laths as shown in (Figure 3.10(b)). Widmanstätten austenite has been formed during the cooling of the ferrite phase and left traces like narrow wedges starting from the boundaries of former δ-ferrite columnar grains [37]. Widmanstätten austenite then left heterogeneities in the crystal structure which was detectable after martensite transformation. Widmanstätten austenite traces in the multipass weld were found only in the IT-HAZ and no traces have been found in HT-HAZ which shows that these microstructures were erased by allowing a complete transformation of the ferrite phase to take place.

Two types of inclusions have been found in the weld metal of current study: oxide inclusions which are round particles evenly distributed and un-molten alloying compounds coming from the electrode.

The oxide inclusions are circular inclusions which were found all over the weld metal (Figure 3.11(a)). Composition analysis showed that these particles consisted of aluminum, silicon, and zirconium oxides (Figure 3.11(b)). These oxides were formed by oxidizing chemical reactions in the weld pool. The image analysis showed that oxide inclusions have about a 0.01% volume fraction and 97% of their population have less than one micrometer in diameter. The oxide inclusions are helpful determining the weld fusion lines.

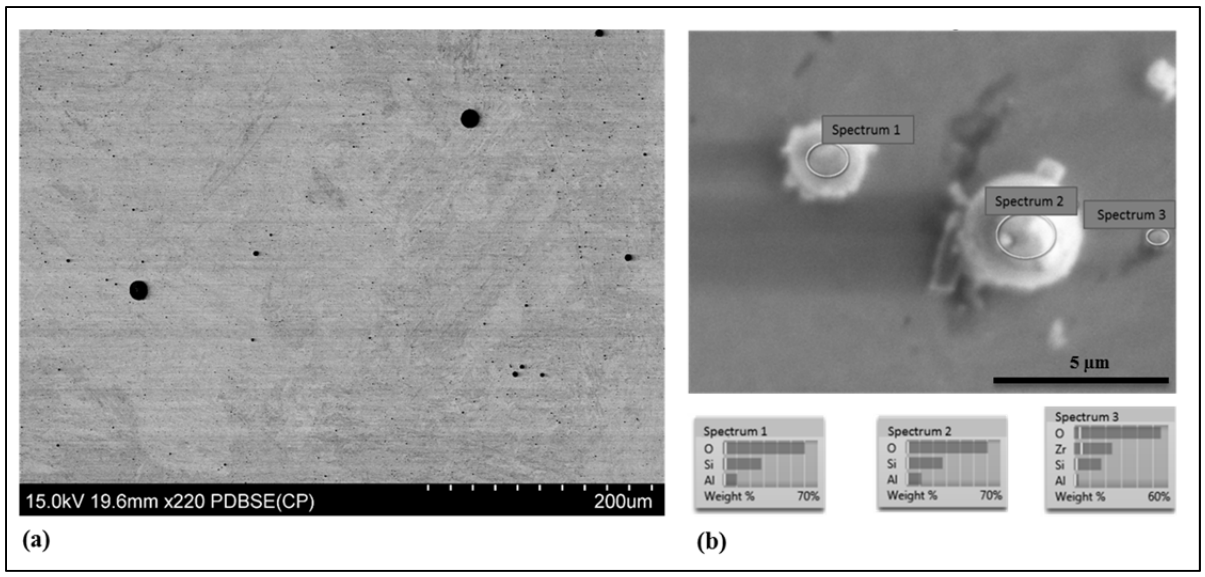

Figure 3.11 – (a) SEM image of etched multipass weld sample. Black circles are oxide cavities as they have been removed by mechanical polishing. (b) Example of EDX analysis of oxides found in the weld. Electropolishing method was used to preserve the oxides on the surface.

The second type of inclusions found in the weld was compounds enriched in chromium, nickel, or molybdenum. These particles were found in areas close to the boundaries between adjacent weld passes. They are un-dissolved particles coming from the filler materials. As the elements found in these particles are ferrite stabilizing elements, they promote the formation of δ-ferrite phase and dendritic ferrite microstructures around them during cooling. Figure 3.12(a, b, and c) shows a chromium particle in the weld metal. Although the particle was not melted, it produced δ-ferrite phase around it and traces of δ-ferrite solidification dendrites can be seen. Figure 3.12(d, e, and f) shows an incomplete melting of a ferromolybdenum particle which also formed solidification dendrites. No δ-ferrite phase was stable in this case.

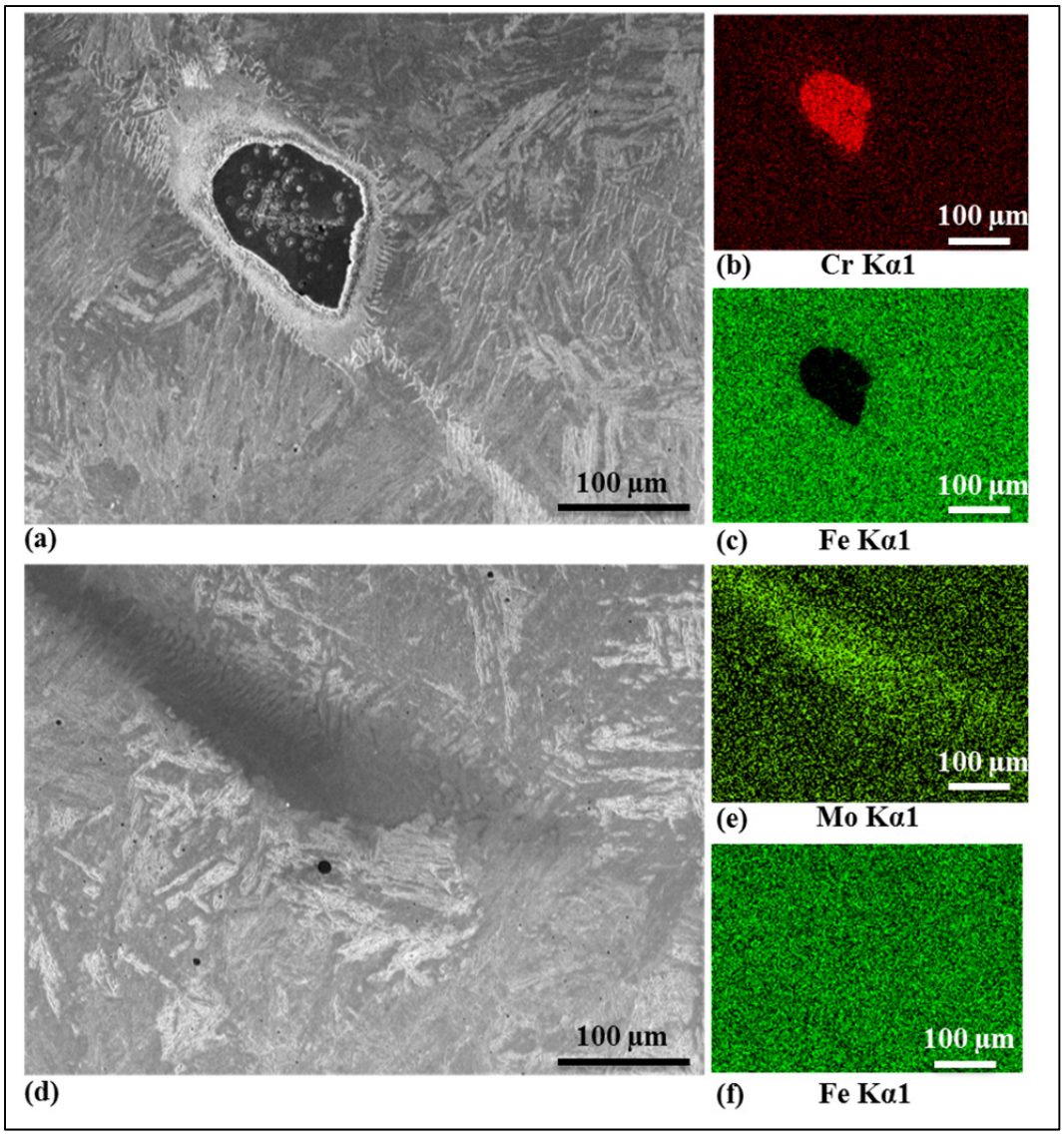

Figure 3.12 – (a) SEM image of a chromium particle in the weld metal. (b and c) EDX analysis of chromium and iron in area presented in (a) respectively. (d) SEM image of a molybdenum rich zone in the weld metal. (e and f) EDX analysis of molybdenum and iron in area presented in (d).

Cracks have also been found in δ-ferrite phases around chromium-nickel particles. The lower solidification temperature of stable δ-ferrite phase and its lower yield strength make it susceptible to cracking [51, 76]. Figure 3.13 shows an example of this type of cracks. These cracks may have been produced during austenite to martensite transformation as it has been reported recently [85]. Then the formation of stable δ-ferrite during solidification of the weld

metal is a major concern and can deteriorate ductility, toughness, and fatigue properties of the steel as it leaves a pre-crack in the welded joint [85].

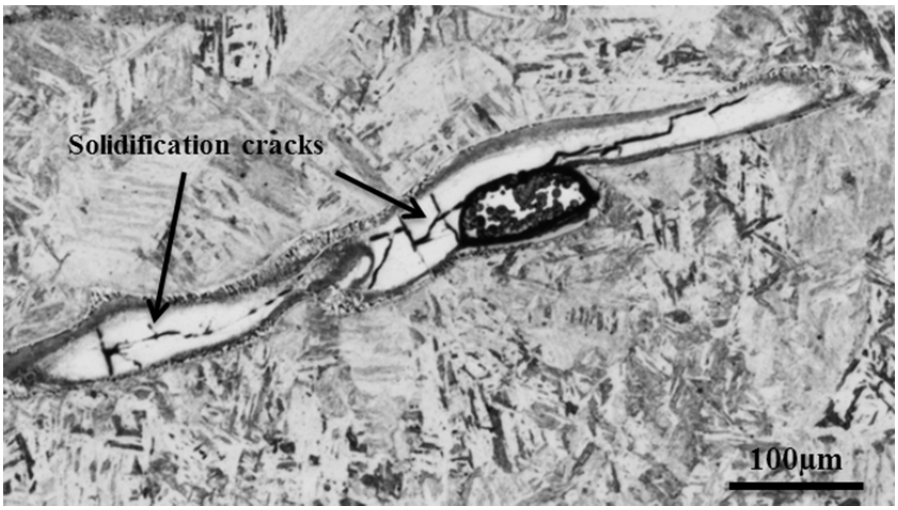

Figure 3.13 – Cracks in δ-ferrite phase produced by an uncompleted mixing of a chromium-nickel particle close to the weld line, revealed by Kalling's etchant.

Nanometer-size carbides were also found in the as-welded multipass samples (Figure 3.14). As it has been reported that there is no sign of carbides in a 13Cr4Ni single pass [82], their presence in a multipass weld suggests that thermal cycle of subsequent weld passes enhances their formation. Carbide particles were found mostly in HT-HAZ sub-block interfaces (See also Figure 3.9).

Austenite particles have also been found in the weld metal in IT-HAZ areas of multipass sample (Figure 3.14) and identified by EBSD analysis. These austenite particles were revealed using electropolishing techniques and they are always associated with the presence of chromium carbides in the neighborhoods. As there was no trace of austenite in an as-welded single pass sample [82], these austenite particles were formed from martensite reversed transformation to austenite and they are called reformed austenite. It has been reported that the reformed austenite remains stable at room temperature due to local

enrichment of chromium and nickel atoms and that their presence in the multipass weld is a favorable feature [14, 39, 40, 86].

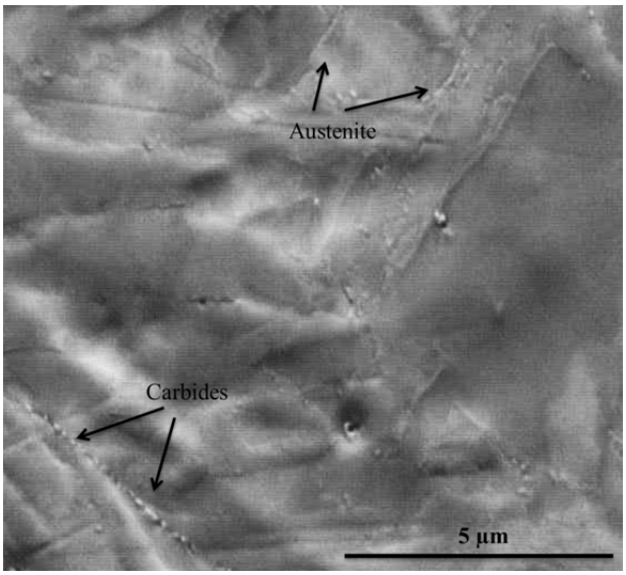

Figure 3.14 – SEM (SE) image of multipass weld showing carbide and austenite particles.

3.3.5. Hardness

In order to characterize the local properties of the weld and relate them to the microstructure variations identified in the previous section, hardness maps have been made on the multipass pass sample (Figure 3.15(a)). These maps present different hardness distribution layout inside beads compared to the results reported previously by the authors in a single and double weld pass beads [82]. A repetitive red pattern can be recognized surrounded by green bands. It is most likely that the green bands represent areas in which the collective heat of subsequent passes had a tempering effect and the red regions are the areas in which the subsequent passes produced fresh martensite. This hypothesis could be tested by studying the microstructures of each region.

Neither a green band nor a single red region belongs to a single bead. In fact, Figure 3.15(a) shows that by considering the approximative locations of the fusion lines, more regions can

be distinguished on a single bead. These regions could be explained by considering the accumulative heat effects of the exact subsequent weld pass and the 3 passes of the above layer.

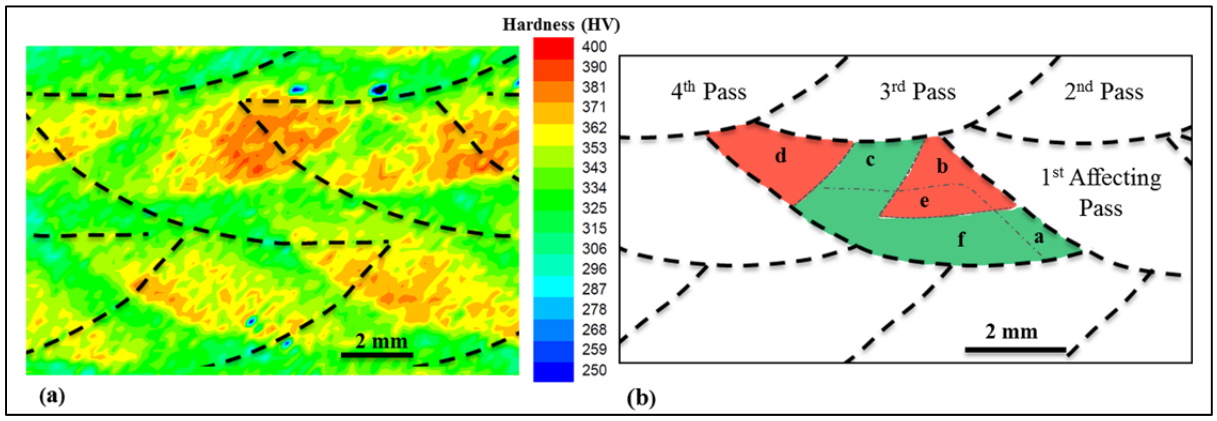

Figure 3.15 – (a) 2D Hardness maps of the multipass sample (30 points/mm^2) with dashed lines showing the approximative locations of weld lines. (b) Schematic presentation of regions in a single weld bead based on both microstructure and hardness.

The correlation between microstructure and hardness is schematically presented in Figure 3.15(b). Six regions can be recognized in each weld pass by projecting the microstructure (described in Figure 3.3) on the regions identified in the hardness map. These six regions are discussed in details as follows.

In region (a), the original columnar grains of the pass were replaced by a fine and fresh martensite due to the first subsequent pass. Later it receives some tempering heat from the second and the third passes, enough to temper the fresh martensite. Thus region (a) has a fine and tempered microstructure with hardness values of a tempered martensite.

In region (b) as in region (a), a fine and fresh martensite microstructure was produced by the first pass. This region is located in the HT-HAZ of the second and third passes but it is far from the 4th pass, then it stays a fine and fresh martensite. It has hardness values slightly higher than that of typical fresh martensite as a double-austenitization has taken place leading to a finer fresh martensite.

In region (c), the original columnar microstructure is transformed to a fine martensite microstructure by the third pass, but later it becomes tempered by the 4th pass. A fine and tempered microstructure and hardness values similar to region (a) are expected here.

In region (d), a fine and fresh martensite microstructure was produced by the third and the 4th passes. Hardness values of a fine and fresh martensite are expected similar to region (b).

The region (e) is located in the IT-HAZ of the second and the third passes having a double-quenching effect on microstructure of this region. Hardness values of double-quenched martensite is expected here which is as high as fresh martensite.

In region (f), the original columnar microstructure of the bead was located far from all of the surrounding passes and it received only tempering heats which led to the lowest hardness of all regions. This is the region in which the reformed austenite formation was observed.

The current study showed that a multipass weld microstructure has a complex microstructure consisting of various regions with different heat treatment histories altogether with micro-scale heterogeneities. Although the simplified HAZ consisting of three thermal cycle region (HT, IT and Tempered HAZ) can explain the overall microstructure and the hardness map, the actual microstructure is certainly more complicated if the precise HAZ locations are considered. These results confirm that any mechanical evaluation in the weld region should be done with great cautions.

3.4. Conclusions

This study showed that a multipass weld microstructure is much more complicated than a single pass weld. The microstructure of the 13Cr4Ni multipass weld consists of two main regions, one having a fine martensite microstructure and the other a column-shaped martensite packets. In the middle of the multilayer weld, each of these two regions can be divided in several regions affected in different ways by subsequent weld passes. It has been shown that with the current study's weld passes configuration, the heat effects of immediate

next pass and the three passes of the above layer can be used to explain the weld bead microstructure. The changes in hardness can be explained by variations in microstructure and local texture, based on the amount of heat received in different regions. Austenite parent grain partial recrystallization and carbides formation were observed. Solidification cracks[5] inside delta ferrite particles were reported which showed the importance of implementing proper welding parameters. The various regions of the multipass weld were detailed from the hardness map with the aid of a simplified three-layered heat affected zone configuration, consisting of a high, an intermediate, and a tempered zone. This study presented the multipass weld heterogeneous and complex microstructure which proves that any overall mechanical evaluation should be done with great cares.

Acknowledgements

The authors would like to acknowledge Natural Sciences and Engineering Research Council of Canada (NSERC), Institut de Recherche d'Hydro-Québec (IREQ), Alstom Power Co., and École de Technologie Supérieure (ÉTS) for the technical and financial supports.

[5] It has been an error mentioning it as solidification cracks. The "Solidification" word should be deleted.

CHAPTER 4

ARTICLE NO. 3
EFFECTS OF VARIOUS POST WELD HEAT TREATMENTS ON AUSTENITE AND CARBIDES FORMATION IN A 13CR4NI MULTIPASS WELD

Mohsen Mokhtabad Amrei[1], Hossein Monajati[1], Denis Thibault[2], Yves Verreman[3], Philippe Bocher[1]

[1]École de Technologie Supérieure, Montréal, Canada.
[2]Institut de recherche d'Hydro-Québec, Montréal, Canada.
[3]École Polytechnique de Montréal, Canada.

Keywords: 13Cr4NiMo; Multipass; Flux-Cored Arc Welding (FCAW); Post weld heat treatment (PWHT); Hardness; Reversed austenite; Carbides; Tempering;

Published in Metallography, Microstructure, and Analysis, Feb. 2016, Vol. 5, Issue 1, p. 50-61.

Abstract

Multipass welding procedures are common methods for 13Cr4Ni steels fabrication and repairs. Compared to a single-pass weld procedure, the weld microstructure in a multipass weld is more heterogeneous due to the complex local thermal cycles imposed by adjacent weld passes. Furthermore, the final microstructure and mechanical properties of these steels are very sensitive to their thermal history which increases the microstructure heterogeneities. Thus, post weld heat treatments are performed to reduce heterogeneities and produce a relatively homogenous weld. It has been found that the best option to improve mechanical properties of 13Cr4Ni steels is forming a "room temperature stable austenite" phase by heat treatments. This study focuses on the effects of these post weld heat treatments on the austenite phase and carbides formations and the related evolutions of microhardness distribution. The study shows that nanometer-size carbides form at martensite lath interfaces and sub-block boundaries, and then at higher temperatures austenite lamellae appear at these locations. Results also show that

the highest percentage of stable austenite achievable by a single-stage tempering obtained at 610 °C. When the heat treatments temperature is lower than 610 °C, longer holding time produces softer steel while longer heat treatments at temperatures higher than 610 °C, produces harder steel. Still, double-stage heat treatments are more effective and produce the highest percentages of austenite and the lowest hardness of all heat treatments.

4.1. Introduction

Low-carbon 13Cr4Ni martensitic steels are appreciated for their high strength, which make them the first choice in many industrial applications like hydraulic, offshore, and petrochemical industries [10, 12]. Moreover, the parts made out of these steels can be easily welded. Multipass welding processes are commonly used with a filler material of the same composition E410NiMo [10, 12].

13Cr4Ni steel solidifies to delta ferrite, then starts to transform to austenite at around 1300 ˚C and ends, in an equilibrium conditions, at around 1200 ˚C [10, 12]. From a thermodynamic equilibrium point of view, ferrite and carbides are expected to be the stable phases at temperatures below 720 ˚C, but in normal cooling conditions martensitic transformation affects the final microstructure. A martensitic microstructure is then expected after cooling to room temperature in industrial cooling conditions. Some ferrite and residual austenite are also expected due to elements segregation during solidification and incomplete transformations during cooling [10, 12].

Such a low carbon martensitic steel is known to present an ordered microstructure consisting of martensite packets, blocks, sub-blocks, and laths. The former parent austenite grains were divided into packets which consist of blocks of similar crystallographic orientations. Blocks are made up of smaller components called sub-blocks which are groups of laths with a single variant characterized by the Kurdjumov–Sachs (K–S) orientation relationship with that of the local former parent austenite grain [19, 20].

Many types of heterogeneities are common in weld microstructures and some of them are specific to the flux-cored arc welding (FCAW) process used in the current study. Many factors make the metallurgical characterization of a multipass weld particularly complicated. This includes, but is not limited to, directional solidification, solidification segregations, and porosities which have been studied in details [33, 51, 55, 82[6]]. More specifically, in a multipass weld, the thermal cycles imposed by adjacent passes act as a local heat treatment and increase the complexity of the weld microstructure. A detailed study of the weld microstructure and the effects of adjacent passes have been done by the authors [82]. Of particular interest, a column-shape grain zone can be found in the middle of each pass. In this area, a relatively uniform microstructure has been produced and used to document the heat treatment effects on the weld microstructure.

In an attempt to relieve the residual stress and homogenize the microstructure, post weld heat treatments are applied. These heat treatments help relieving the welding residual stresses caused by solidification, cooling, and phase transformations and also provide a tempering treatment to the fresh martensite region [80]. Carbides formation and reversed transformation of martensite to austenite can also take place [6, 21, 72, 74, 81]. Tempering temperatures between 560 ˚C and 620 ˚C are suggested for the steel of the current study [87]. Double tempering has also been introduced for this family of steel [51]. In the case of double tempering, the first stage consists of a heat treatment at temperatures (above 620 ˚C) which produces a mixture of fresh martensite and tempered martensite. The subsequent stage is a tempering heat treatment at lower temperatures to temper the fresh martensite and reform some stable austenite [3, 51]. Such heat treatments give the highest percentages of reformed austenite with a tempered martensite matrix. Values as high as 25% of reformed austenite can be formed after a double tempering heat [3].

---

[6] And [88].

In this context, the focus of this study is to document the effect of various heat treatments on the austenite and carbide formation and distributions in the column-shape region of a multipass weld made of E410NiMo steel.

4.2. Experimental Conditions

A flux-Cored Arc Welding (FCAW) procedure (AWS A.5.22) was used to produce a 50 mm thick weld metal layer on a CA6NM substrate using 13Cr4Ni flux-cored welding electrodes (E410NiMoT1-4) with a robotic welding machine [83]. Welding parameters are given in Table 4.1 and Figure 4.1 show the schematic cross-section of the welded part. The nominal compositions of the substrate and welding electrode are shown in Table 4.2.

Table 4.1 – Welding parameters.

Method	**Interpass Temp. (˚C)**	**Pre-heat temp. (˚C)**	**Voltage (V)**	**Current (A)**	**Torch Speed (mm/s)**	**Filler deposit rate (kg/h)**	**Heat Input (J/mm)**	**Welding Position**	**Gas**
FCAW	200	180	21.1	209	4.5	3.9	980	1G	Argon-25% CO_2

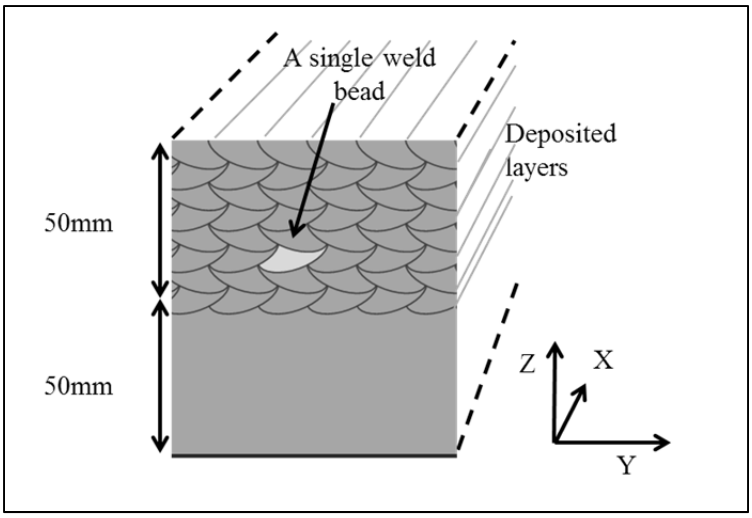

Figure 4.1 – Schematic cross-section of the welded layers.

Table 4.2 – Nominal composition of base metal and welding electrode (wt%).

Grade	Dimension	C	Mn	P	S	Si	Cr	Ni	Mo	Cu
CA6NM (Substrate plate)	50 cm (Thickness).	<0.06	<0.5	<0.04	<0.03	<0.1	11.5-14	3.5-4.5	0.4-1.0	<0.05
E410NiMoT1	1.6 mm Dia.	0.021	0.36	0.008	0.011	0.37	12.46	4.39	0.56	0.03

The actual chemical composition of the deposited weld metal was measured by the Glow Discharge Atomic Emission Spectrometers (except for C, N, O, and S that were measured by were measured by combustion/fusion determination methods) (Table 4.3). An Energy-dispersive X-ray spectrometer was used to perform chemical composition analysis of the weld phases.

Table 4.3 – Chemical compositions (wt%) of samples as measured on an average surface of 4 mm^2.

Name	Cr	Ni	Mo	Si	Mn	C	P	S	Al	N
Weld metal	11.6	4.5	0.529	0.44	0.38	0.023	0.01	0.01	0.014	0.003

Samples were prepared from the middle of the multipass weld (Figure 4.1), then heat treated, polished and etched to specify regions of each weld pass. It has been shown in a previous study that there are two distinctive microstructural regions inside each weld

pass defined as fine martensite and column-shape martensite regions [82]. Considering the heterogeneous nature inside a multipass weld, the columnar region is preferred for microstructure studies as it shows more uniform characteristics. This region is considered to be mainly martensitic in as-welded state and the austenite amount was negligible in the X-ray diffraction analysis of austenite phase [authors' article submitted for publication]. Areas of 20 mm^2 have been marked in columnar regions with the help of hardness indentations in order to produce a precise study of same specific regions as a function of tempering temperature or holding time.

Various heat treatments have been performed at temperatures below the austenite transformation temperature (<700 ˚C) to avoid any massive austenite formation during heating or cooling (Table 4.4). These temperatures are from 520 ˚C to 670 ˚C with different holding periods. To document the evolution of the microstructure after heat treatments, metallography studies have been performed and austenite measurements have been done. To reveal austenite and carbide particles, samples were polished mechanically and then electro-polished with a solution of 65 ml $HClO_4$, 550 ml ethanol, 70 ml butyl-cellusolve, and 70 ml H_2O with an electropolishing device at 25 °C, 25 V for 20 s. The chemical composition differences between phases helped to identify microstructural features in the martensitic matrix [71] and the observed contrast is due to chemical variations related to the presence of austenite-promoting elements. A Scanning Electron Microscope (SEM) operated at 5 kV to 20 kV was used to observe the microstructures of the samples. Electron backscatter diffraction (EBSD) analyses were carried out to study the crystal orientations of weld metal with Tango orientation map display and manipulation software. Image analyses were done by ImageJ software in order to measure the distance between austenite lamella and carbides distribution in heat treated samples. On SEM images, the carbides and austenite can be differentiated by the contrast as carbides appear as white glowing particles and austenite phases as light gray areas. Considering the heterogeneous nature of the weld, studying carbides and austenite distributions have been done by providing a minimum of 5 images to document the heat

treatments effects on microstructures. The volume fractions of the austenite in samples were measured by X-ray diffraction from a Rietveld analysis with a diffractometer device [75]. Hardness evaluations have been done in the as-welded and heat treated multipass samples by a micro-hardness testing machine with a load of 300 g and a loading time of 10.2 s and also after heat treatments.

Table 4.4 – Heat treatments performed in the current study.

First heat treatment		Second heat treatment	
Temp. (˚C)	Time (h)	Temp. (˚C)	Time (h)
520	1, 2	-	-
550	1, 2	-	-
580	1, 2	-	-
600	1, 2, 5, 23	-	-
610	1, 2, 5, 23	-	-
620	1, 2, 5, 23	-	-
650	1, 2	-	-
670	1, 2	-	-
670	1	600	1
670	1	610	1
670	1	620	1

4.3. Microstructure of the As-Welded Multipass Sample

Figure 4.2 shows a typical microstructure inside a sub-block of an as-welded sample at high magnification. This sub-block consists of a single variant, characterized by the red-pink color in EBSD map. Few nanometer-size carbides were observed here in laths and sub-blocks boundaries. Although some traces of reformed austenite were previously reported in as-welded multipass weld metal [82], no austenite phase has been detected in these specific as-welded samples using SEM image. While the SEM image reveals only oxides, some carbide particles, and blurred traces of martensite laths, several laths have been revealed in Band Contract image and EBSD maps of this area which is inside a block of 50 μm width [88]. These laths have variations in their crystal orientation which can be seen in areas with similar crystallographic orientations; slight variations exist up

to 10 degrees forming low (less than 3°) and high (3° to 10°) lath boundaries. The 60° orientation difference corresponds to the Kurdjumov–Sachs (K–S) variants (pink/blue laths in the figure). Such microstructure consisting of laths is reported to be a characteristic of martensitic transformation at this scale [19].

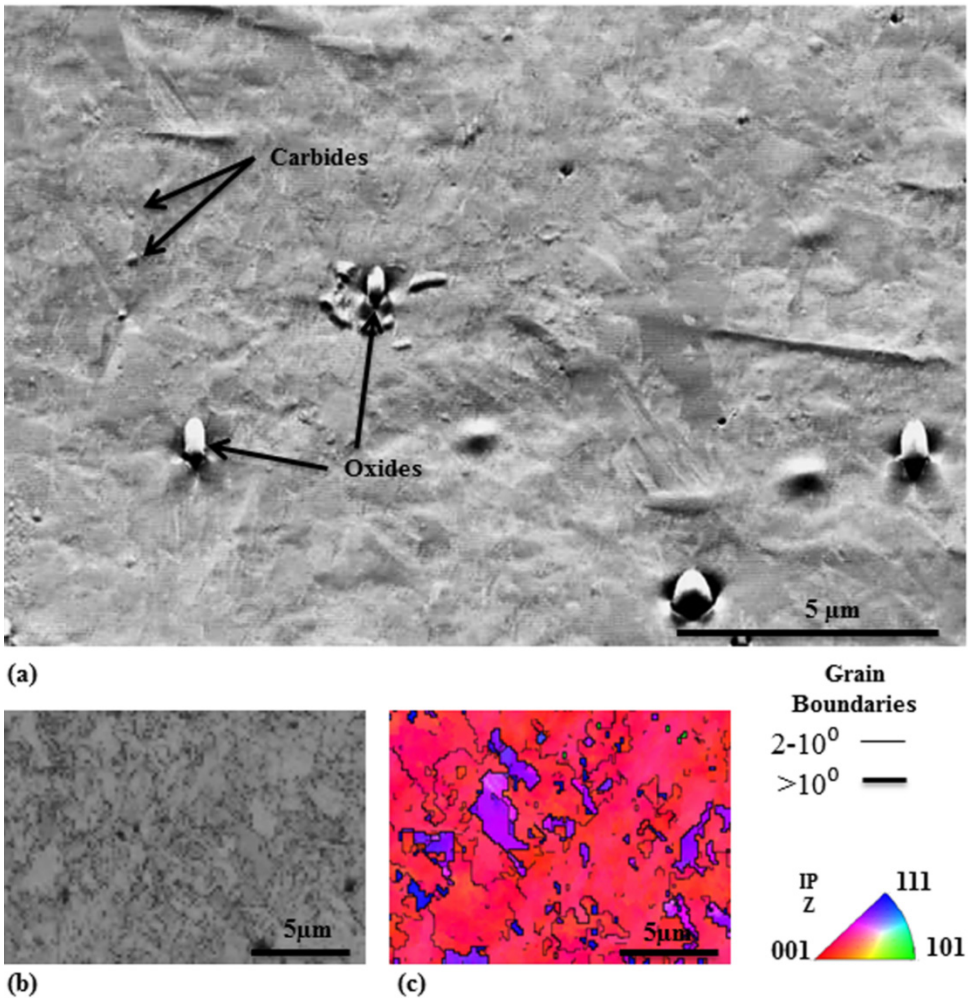

Figure 4.2 – (a) SEM (SE) image of a sub-block in the columnar type of an as-welded sample. (b, c) Band contrast and EBSD map of the same region are shown, illustrating martensite laths. Arrows are showing the locations of some carbide.

4.4. Carbides and Austenite Formations during Single Heat Treatments

The very first evidence of carbide formation was observed in samples tempered at 520 °C for 1hr. The carbides formed mostly on the laths boundaries and sub-blocks

interfaces. It can be seen in the Figure 4.3 that the carbides are heterogeneously distributed. Their diameters are about 25 ± 5 nanometers along specific lath interfaces. The carbides particles mean density was measured about 13.3 ± 3.5 per μm^2 but it can reach values as high as 30 in some specific groups of laths such as in region (A) in Figure 4.3.

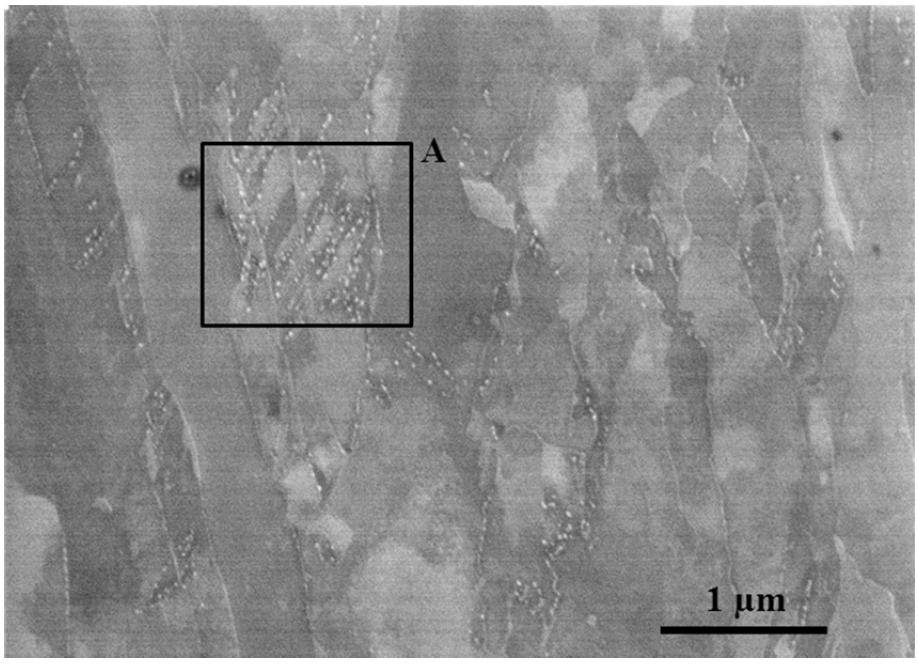

Figure 4.3 – SEM (SE) image of the sample heat treated at 520 °C for 1 hour. Nanometric carbides formed in laths boundaries.

By holding the sample at this temperature (520 °C) for 2 hours, some lath boundaries have been depleted from carbides while it seems that most of the carbides are now covering higher angle laths interfaces and only few of them remained on the low angle laths interfaces as seen in Figure 4.4. Meanwhile, coarsening of carbide particles to about 63 ± 17 nm with density of 12.5 ± 3.3 particles per μm^2 is measured.

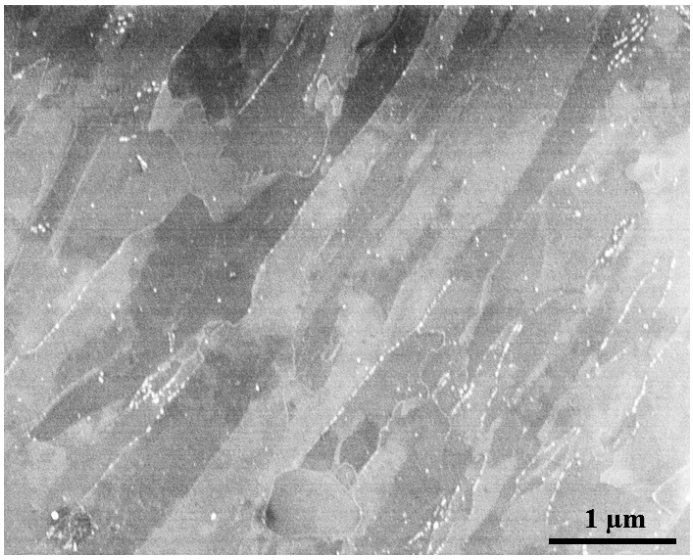

Figure 4.4 – SEM (SE) image of the sample heat treated at 520 °C for 2 hours. Nanometric carbides started to line up on lath boundaries.

For high temperature, at 550 °C for 1 hour, larger carbides were observed at about 55 ± 8 nanometers. Some traces of austenite particles were found around some of carbides at lath boundaries (Figure 4.5). Results are in agreement with the austenite percentages measured by XRD (about 4.7 ± 0.5%). It seems that austenite particles tend to grow in boundaries and close to carbides. Therefore, it is expected that by increasing the temperature, these austenite particles coalesced together and form elongated austenite particles at lath boundaries.

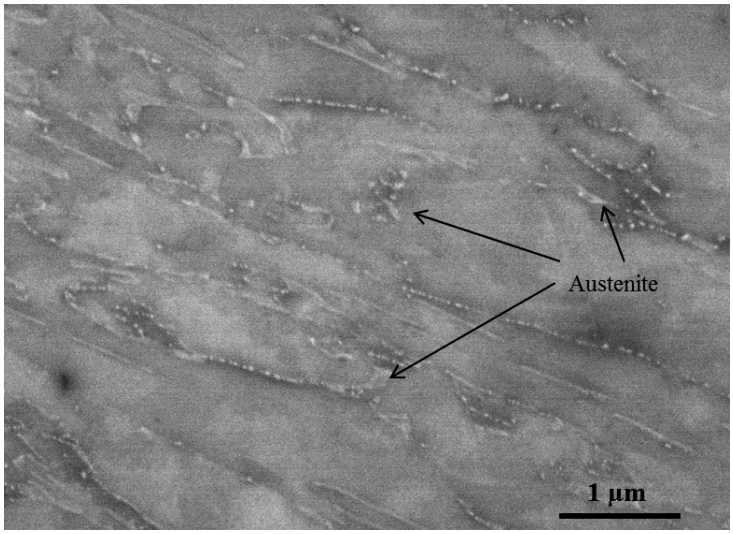

Figure 4.5 – SEM image of the sample heat treated at 550 °C for 1 hour. Carbide coarsening was observed together with formation of austenite particles on lath boundaries.

After 580 °C for 1hr, the carbides become even coarser (about 62 ± 20 nanometers) at lath boundaries. Meanwhile the carbides density decreases to about 3.2 ± 0.5 particles per μm^2 which probably shows carbide dissolution. Austenite particles could be found only at lath boundaries (Figure 4.6) and they were systematically associated with carbides. They could not be found as individual particles. A volume fraction of 5.9 ± 0.5% austenite was found even if no austenite particles can be clearly found on this specific image.

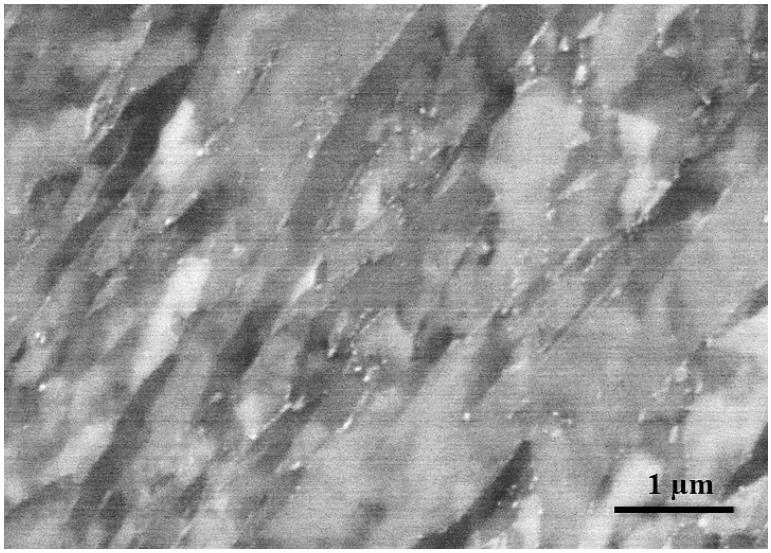

Figure 4.6 – SEM (SE) image of the sample heat treated at 580 °C for 1 hour. Carbides tend to form at higher angle lath interfaces (higher contrast corresponds to higher orientation differences).

After 2hr at 580 °C, the carbides size increases to about 70 ± 5 nanometers. Carbides density may decrease to 2.9 ± 0.8 particles per μm^2 but the measured variation is in the measurement error range (Figure 4.7). Similarly, the austenite volume fraction do not vary significantly between 1 hour and 2 hours at 580 °C and the small increase of 1.1% (to the total value of 7.1 ± 1.9%) observed is not significant.

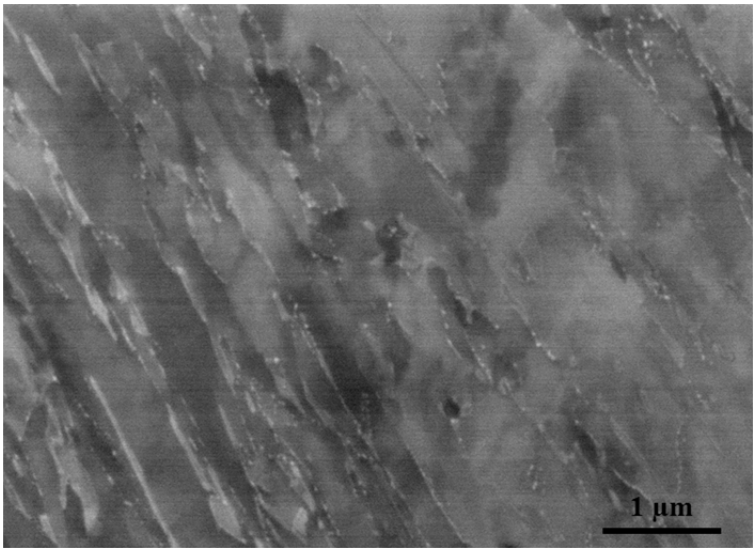

Figure 4.7 – SEM (SE) image of the sample microstructure heat treated at 580 °C for 2 hours. Carbide and austenite formations were observed.

Clearly, after tempering at 600 °C for 1hr, austenite particles appear larger and more elongated in laths boundaries (Figure 4.8). Austenite volume fraction was measured 7.6 ± 0.8% by X-ray diffraction (XRD) analysis. It can be observed that the shape and size of the austenite particles depends on the martensite characteristics of the region in which they form: if laths had been parallel in the region, austenite particles formed in parallel lamellae; if the laths have not been parallel in the region, which is not very common and it only happens at lath interfaces, the austenite particles formed flake-like particles. Again carbides coarsening to about 73 ± 22 nanometers and density of 2.1 ± 0.2 particles per μm^2 were measured under this tempering condition. Unlike lower tempering temperatures, many austenite particles were found to have no accompanying carbides. This could be explained by the carbide coarsening or the possible carbon dissolution in the austenite phase.

After 2 hours of tempering at 600 °C, austenite particles became even larger with volume fraction measured as 12.0 ± 1.8% by XRD (Figure 4.9). Carbides coarsening up to about 70 ± 35 nanometers were measured.

The enlargement of austenite particles was found to continue at higher tempering temperatures (Figure 4.10). The traces of austenite particles are more blurred compared to the ones displayed previously (produced by heat treatment with lower temperatures). As the observed contrast is due to chemical variations related to the presence of austenite-promoting elements, the blurred austenite particles were a sign that less amount of gammagene elements were present in the austenite phase at the heat treatment temperature. Therefore, some of the austenite phases formed above 620 °C were not stable at room temperature as the diffusion rate of other elements increases at higher temperatures and dilutes gammagene elements. They did eventually transform to fresh martensite upon cooling [55] (Figure 4.10 (c), (d), (e), and (f)). It can be suggested that at 650 °C, approximately 50% of the microstructure was austenite whereas the XRD analysis detects values less than 2 percent of austenite phase. The width of these regions is about the half of the laths (about 150 micrometers at Figure 4.10(c)).

Extending the holding time for one more hour (Figure 4.10(d)) or increasing the tempering temperature to 670 °C generate high percentage of austenite phase at heat treatment temperature. These austenite particles are still detectable at low temperature but nearly all of them transformed to fresh martensite (Figure 4.10(e), and (f)).

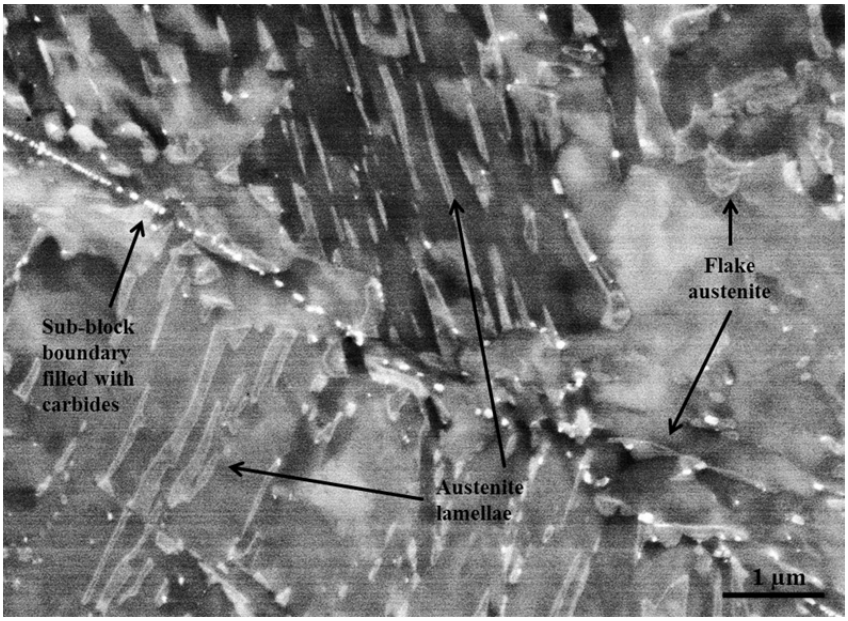

Figure 4.8 – SEM (SE) image of the sample heat treated at 600 °C for 1 hour. Austenite particles formed parallel lamellae in between laths and sub-block interfaces. Small white particles are carbides.

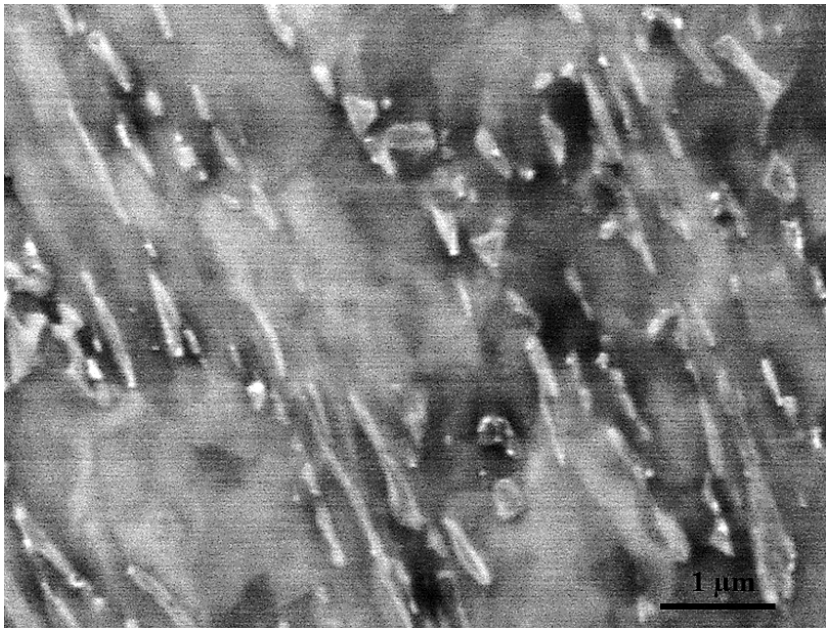

Figure 4.9 – SEM (SE) image of the sample heat treated at 600 °C for 2 hours showing bigger and thickened austenite particles compare to 600 °C for 1 hour heat treatment.

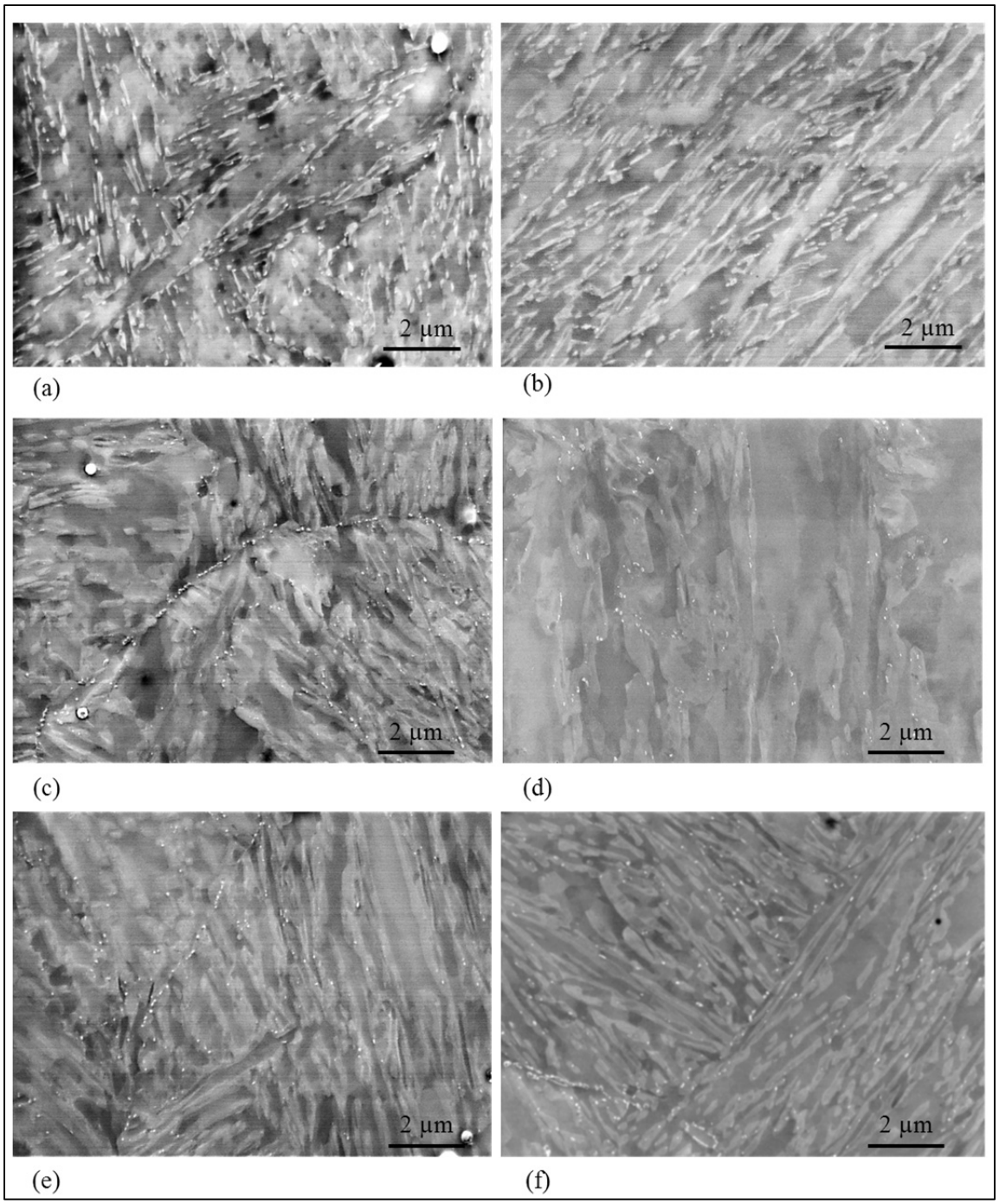

Figure 4.10 – SEM (SE) images of samples heat treated at (a) 620 °C for 1 hour, (b) 620 °C for 2 hours, (c) 650 °C for 1 hour, (d) 650 °C for 2 hours, (e) 670 °C for 1 hour, and (f) 670 °C for 2 hours. Austenite particles appearance in (a) and (b) is showing stable austenite but in (c), (d), (e) and (f), the austenite particles are mostly transformed to martensite and their traces remained because of chemical differences.

Figure 4.11 and Figure 4.12 summarize the carbides evolution previously discussed. Figure 4.11 shows the growth of carbide particles by increasing the holding time and a faster growth rate by increasing the heat treatment temperature up to 600 °C. Carbides reach smaller sizes between 600 °C to 650 °C followed by a possible size increase for temperatures higher than 650 °C. However, size distributions are wide and some of the results obtained may not be statistically significant.

While the carbide growth can be explained by faster diffusion and deposition of carbon and chromium atoms in laths boundaries, the drop in carbides size at 610 °C can be explained by dissolution of carbon atoms in the austenite phase. It is probable that higher percentages of austenite phase help to dissolve carbon atoms at temperatures above 610 °C.

Additionally, Figure 4.12 presents the carbides density in the microstructure of heat treated samples. At 580 °C, it shows a drop of about 10 particles per μm^2 (75% drop) in carbide density, documenting that the presence of austenite particles at higher temperatures decreases the chance of finding carbides in the microstructure. At higher temperatures a slight and nearly constant density of carbides is found.

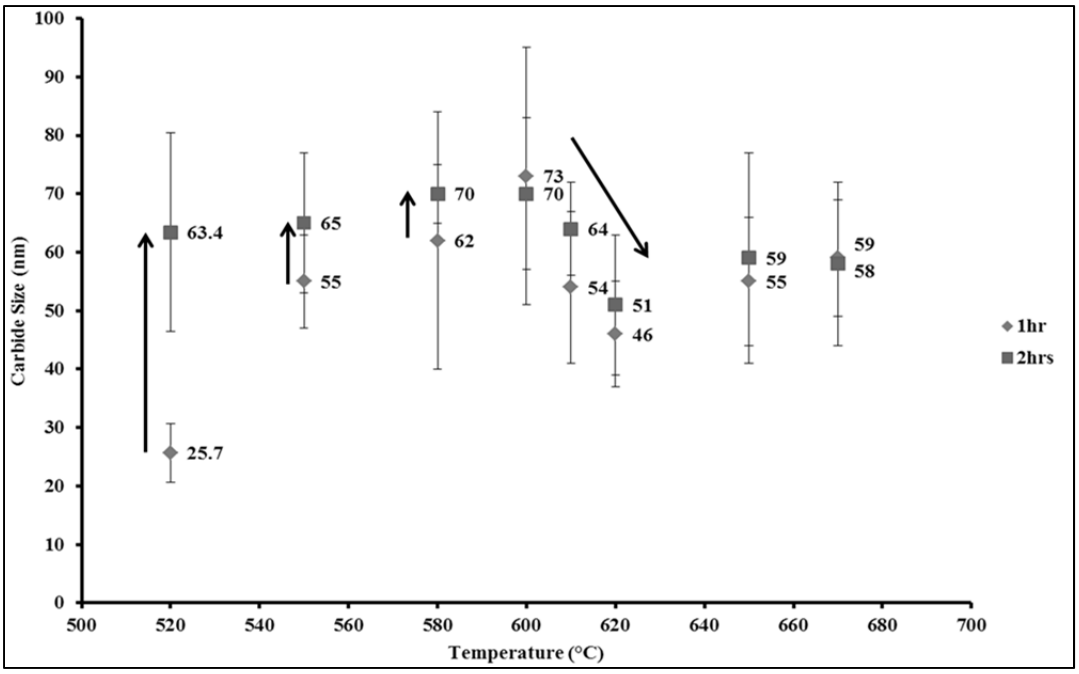

Figure 4.11 – The effect of tempering temperature and holding time on carbide particle size.

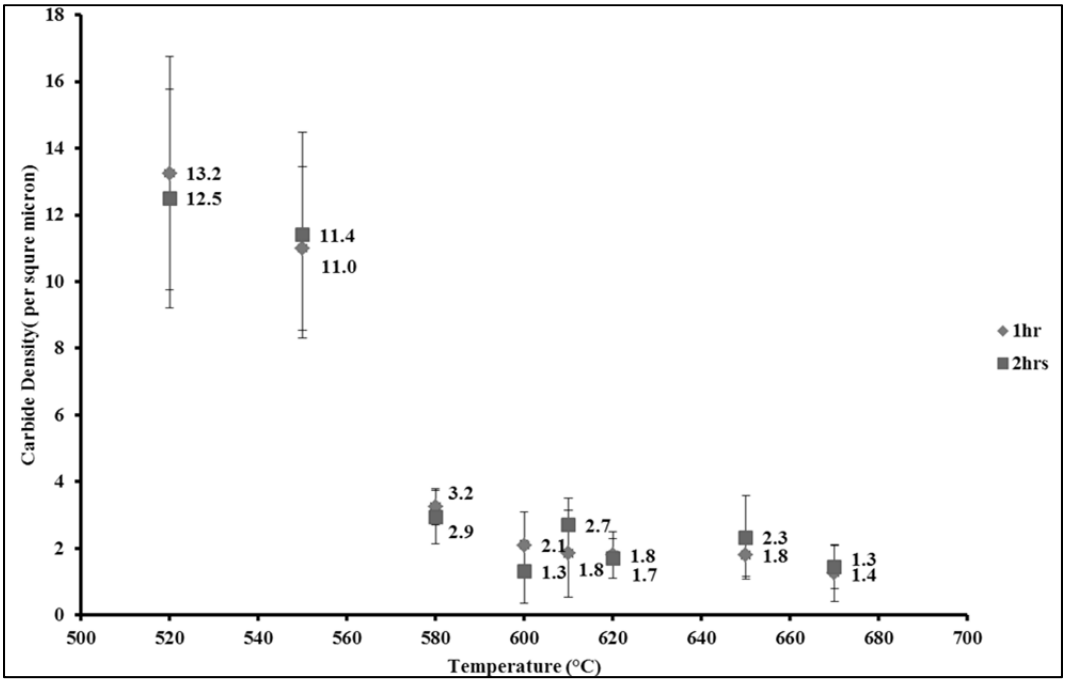

Figure 4.12 – The effect of tempering temperature and holding time on carbide particle density.

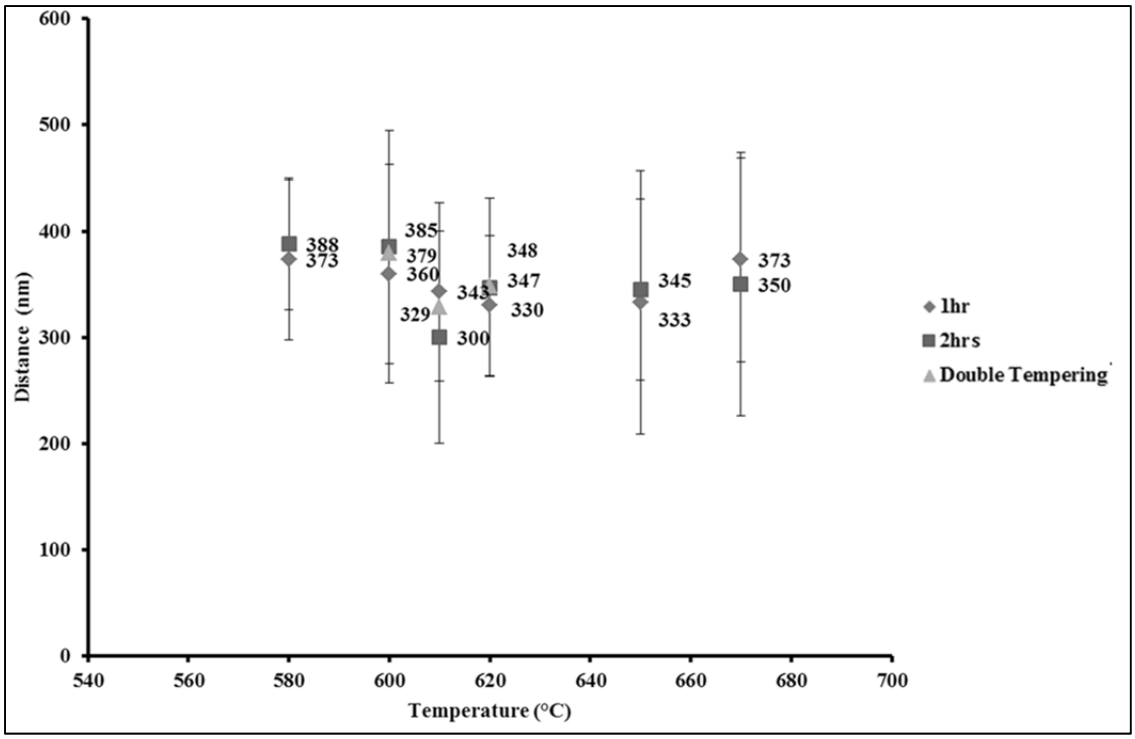

Figure 4.13 – The effect of tempering temperature and holding time on the distance between austenite lamella (center to center).

Figure 4.13 displays the effect of heat treatment on the mean distance between austenite lamellae which shows that this distance is not influenced by heat treatment temperature or holding time and it is most probably representing of the martensite microstructure characteristics. It can be concluded that any variation in austenite percentage during PWHT results in changes only in length and thickness of austenite lamellae, not by nucleation of new austenite particles on sites inside laths.

SEM image of a sample heat treated at 600 °C for 1 hour is provided in Figure 4.14 together with its Band Contrast and EBSD map. It can be seen that the austenite particles were formed in lath interfaces, supporting the results in Figure 4.13. In fact it can be seen that the mean distance between austenite lamellae represents the mean width of the laths and consequently it cannot be changed by tempering heat treatment unless high temperatures are reached and very large amounts of austenite are generated.

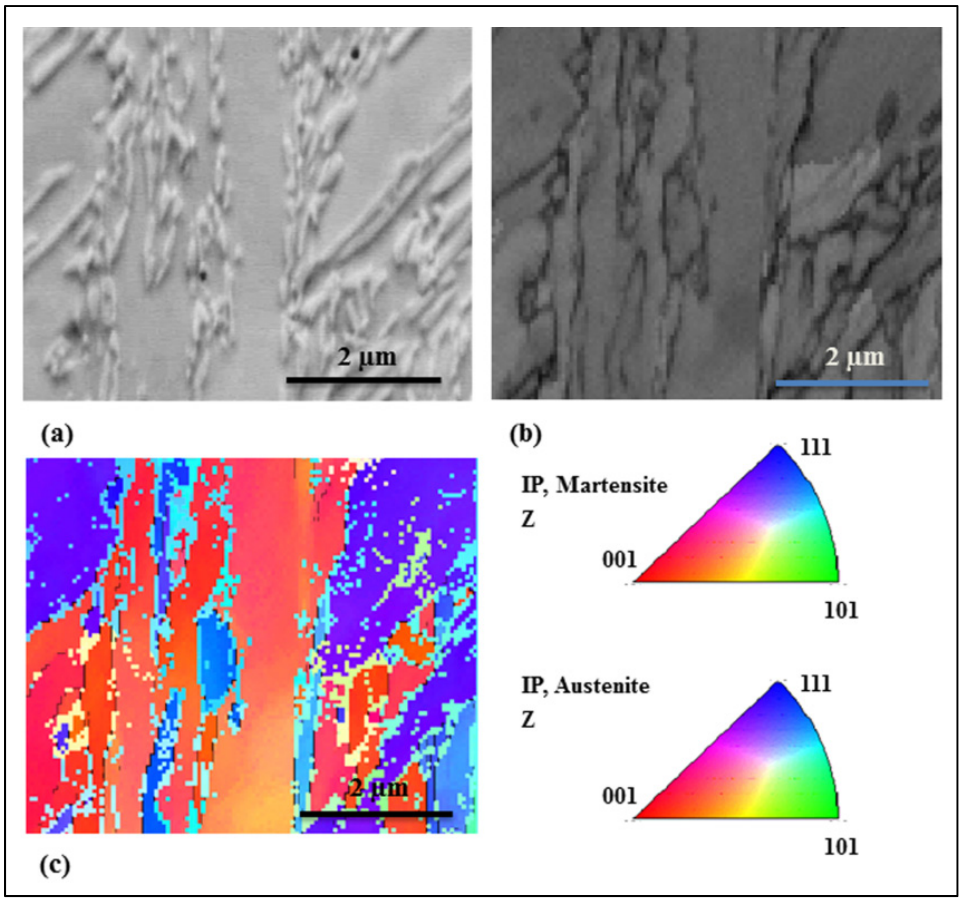

Figure 4.14 – (a) SEM image of a heat treated sample at 600 °C for 1 hour. (b) Band contrast and (c) EBSD map of the area shown on (a). Austenite particles were formed in lath boundaries and no austenite were found inside laths.

4.5. Effects of Double Tempering Heat Treatments

The double heat treatments effects could be studied by following up the microstructure evolution from the first heat treatment stage to the second tempering one. The first heat treatment temperature is high enough to ensure the formation of large amounts of austenite. In the present case, at 670 °C for 1 hour treatment results in a microstructure with about 25% of austenite (as seen in Figure 4.10(e)). The matrix becomes tempered martensite while the austenite produced on heating is not stable and mostly undergoes martensitic transformation on cooling as confirmed by XRD measurements (It is summarized in details on the discussion related to Figure 4.16). Thus the final

microstructure is a mixture of fresh martensite lamellae in between tempered matrix of martensite laths. These fresh martensites have higher percentages of gammagene elements (particularly nickel atoms) compared to the surrounding tempered martensite [55]. By the second heat treatment higher austenite percentages have been reached compared to the same single stage heat treatment. At the same time, the remaining fresh martensite particles also decompose into tempered martensite, producing softer matrix.

A comparison of single stage and double stage tempering could be made through Figure 4.15. A tempering stage at 670 °C for 1 hour is the difference between the first and the second row of images in this figure. Double tempering did not change the distance between austenite particles (about 350 nm for all heat treatments, see Figure 4.13), but higher austenite percentages were obtained for all three heat treatments when compared to their single stage heat treatments, mostly by the enlargement of austenite particles (Figure 4.16). In fact, the highest percentage of austenite (14.5 ± 1.8%) of all heat treatments was obtained by the double tempering of “670 °C for 1 hour + 620 °C for 1 hour”.

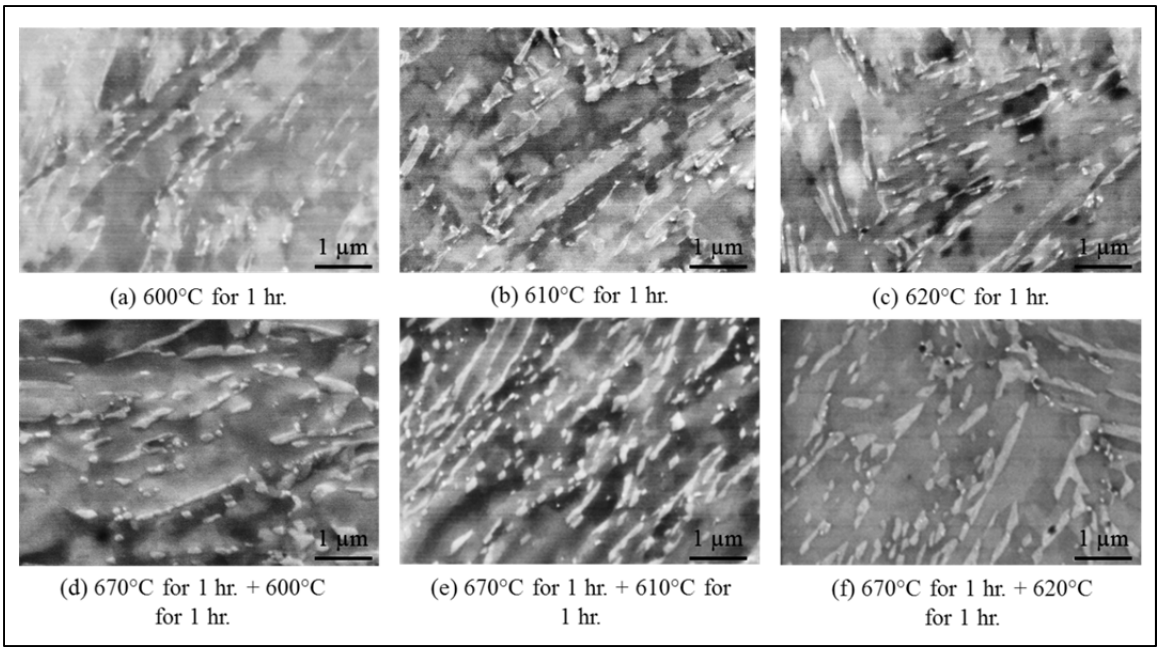

Figure 4.15 – SEM (SE) images of samples heat treated with single-stage and double tempering heat treatments. Samples heat treated at (a) 600 °C for 1 hour, (b) 610 °C for 1 hour, (c) 620 °C for 1 hour, (d) 670 °C for 1 hour + 600 °C for 1 hour, (e) 670 °C for 1 hour + 620 °C for 1 hour, and (f) 670 °C for 1 hour + 620 °C for 1 hour.

4.6. Effect of Heat Treatments on Hardness and Austenite Percentage

In order to evaluate the effect of tempering heat treatments beyond visual measurement, hardness measurement and austenite percentage evaluations have been documented on samples heat treated with various temperatures and holding times. These results are presented in Figure 4.16 and Figure 4.17.

Figure 4.16 shows the effects of tempering temperatures and holding durations on the austenite percentages. As the tempering temperature increases, the austenite percentage reaches a maximum at about 610 °C and decreases to about zero at 670 °C. For both holding durations, the peak in austenite percentage is found for the same heat treatment temperature of 610 °C. The percentages are higher for 2 hours of holding time in all single-stage cases.

The hardness results show an inverse trend; a decrease until 610 °C and then an increase. By increasing the holding durations from 1 hour to 2 hours, lower hardness values were reached while the minimum value shifted to a higher temperature for longer treatment time. Higher hardness values are obtained for 2 hours of holding time at high temperatures, which can be explained by higher percentages of fresh martensite produced by longer holding time due to larger percentages of produced austenite. The lowest hardness values correspond to the highest reformed austenite percentages and coincide with the drop in carbide size (seen in Figure 4.11). Similar results were observed by others [13].

Double tempering heat treatments have produced higher percentages of austenite compare to the related single-stage heat treatments (Figure 4.16) and lower hardness values than any other heat treatments. In fact the highest value of austenite was obtained by double tempering of 670 °C/1 hour + 620 °C/1 hour for a hardness value of only 283 HV.

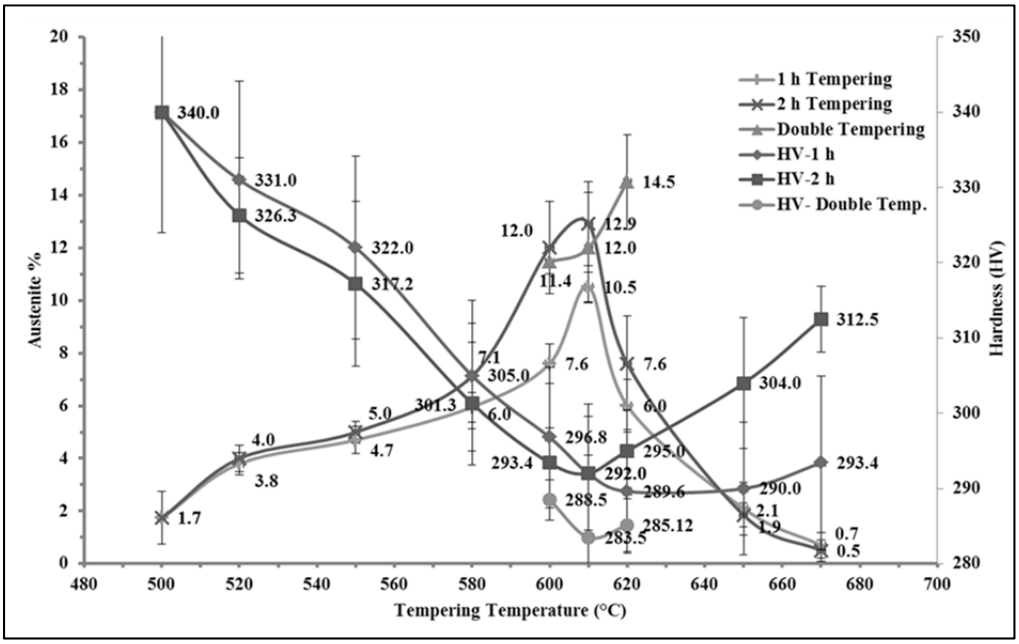

Figure 4.16 – The effect of tempering temperatures on austenite percentages and hardness values. Austenite volume fraction is measured by XRD analysis.

Although the results showed an increase in austenite percentage after 2 hours, longer holding periods did not increase austenite significantly. Some measurements have even suggested that much longer holding times could decrease the stability of austenite at room temperature (Figure 4.17) as it can be seen at 620 °C for holding time longer than 5 hours.

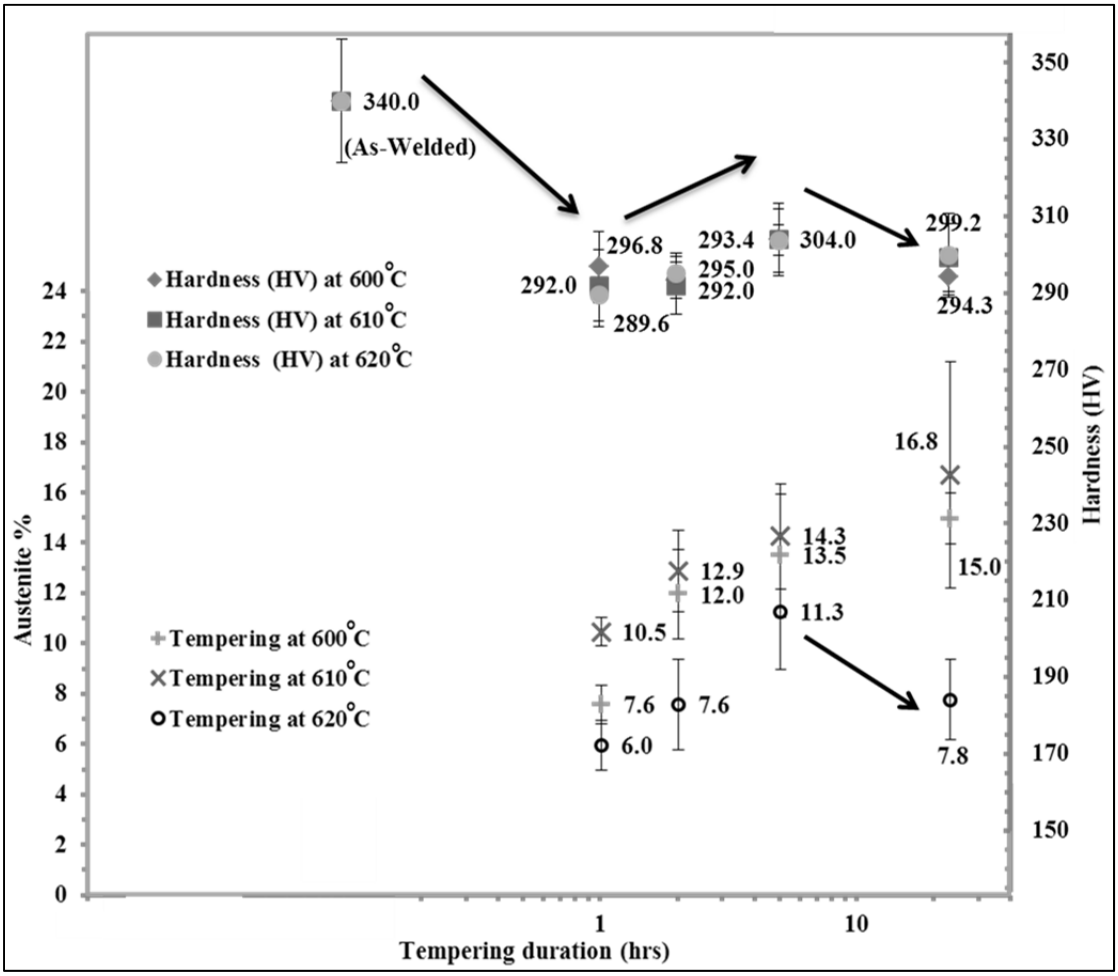

Figure 4.17 – The effect of tempering holding duration on austenite percentages and hardness values.

On the other hand, the hardness values in prolonged heat treatments showed that the hardness values decrease for short exposure times, and increases in all cases of tempering for more than 2 hours, and then decreases again after 5 hours of tempering. The initial softening can be explained by cumulative effect of increasing in austenite

percentages and the tempering of the martensite matrix (by reduction of dislocation density). The following increase of hardness can be explained by carbide coarsening (see Figure 4.11). The decrease of hardness after 5 hours of tempering suggests that the tempered martensite effect has outrun the other factors.

These results showed that the weld metal hardness is related to different factors such as austenite percentage, carbides features, and tempered martensite characteristics. Moreover, the focus of this study was only on a relatively homogeneous area inside a single bead of a multipass weld, it is sure that considering other regions will improve the overall understanding of actual case.

4.7. Conclusions

The main goal of the study was to characterize the microstructure of 13Cr4Ni multipass weld after various tempering heat treatments and record the carbides and austenite formations after tempering. It has been shown that heat treatment can significantly affect the microstructure by precipitation of carbides and reformation of austenite at lath and grain boundaries of samples heat treated at temperatures higher than 520 °C. Studying the evolution of microstructure showed that longer periods of tempering at temperatures lower than 600 °C, have produced higher amounts of reformed austenite and eventually led to a softer steel. Lower amounts of reformed austenite formed at temperatures higher than 600 °C presented an opposite effect of longer holding time. The highest percentages of reformed austenite, achievable by a single-stage tempering, were obtained by tempering at 610 °C. Eventually the amounts of reformed austenite produced by double-stage heat treatments were the highest compared to similar single-stage tempering heat treatments. The study showed that the anticipated increase in hardness by carbides formation cannot overcome the softening resulted by reformed austenite or tempered martensite. The coarsening of carbides was reported at temperatures between 520 °C and 600 °C. Dissolution of carbides observed at higher temperature which can be the result

of dissolution of carbon atoms in austenite phase. The results have shown that the mean distance between austenite lamella was not affected by any tempering heat treatment.

Acknowledgement

The authors would like to acknowledge Natural Sciences and Engineering Research Council of Canada (NSERC), Institut de Recherche d'Hydro-Québec (IREQ), Alstom Power Co., and École de Technologie Supérieure (ÉTS) for the technical and financial supports. The authors are grateful to ÉTS and IREQ metallography laboratory for austenite electropolishing and metallography studies.

CHAPTER 5

DISCUSSION

The purpose of this chapter is to discuss the results of the thesis as a whole. By relating aspects of the different parts of the project together, comprehensive conclusions will be drawn from the work presented in this dissertation.

5.1. Microstructure and Texture of a 13Cr4Ni Single-Pass Weld

The detailed study of a single-pass weld presented in the first article provided a comprehensive understanding of single-pass as-welded microstructures as the first building blocks for multi-pass welded joints. Column-shaped fresh martensite packets were observed in the single-pass microstructure, extending from the fusion line toward the surface of the weld. These columns constituted the remains of a columnar solidification mode that took place during the prior δ-ferrite phase formation. Observing these features revealed that subsequent transformations (including δ-ferrite-to-austenite and eventually austenite-to-martensite transformations) are affected by solidification characteristics; this means that even the martensite microstructure is altered by δ-ferrite solidification characteristics.

In an as-welded single-pass, the microstructure is expected to consist of quenched and fresh martensite; the weld is not affected by any exterior heat source and its internal heat is rapidly drained by the base metal. A relatively uniform hardness profile (mean value of about 350HV) of typical fresh martensite was observed throughout the weld pass in this study, confirming this prediction.

This study demonstrated that, although weld microstructure is known to be homogeneous, different types of inhomogeneity could be found within it. Segregations, oxides, Widmanstätten austenite traces, and inclusions are among the irregularities found in the microstructure in this study, amply illustrating the complex nature of the

weld. It can be concluded that, although treating welds as homogeneous entities can provide a close enough approximation of reality on a macro-scale, an assumption of homogeneity cannot be drawn on a micro-scale. This is particularly important for the case of 13Cr4Ni because of the profound influence of micro-scale features on mechanical properties.

The effect of the single-pass weld on the base metal was another part of this study. The study showed that according to the current case welding parameters, a single-pass weld can alter the microstructure of the base metal to a depth of 7 mm. In fact, the hardness profile shows that the base metal has been changed to a fresh martensite with a peak of hardness close to the fusion line, then decreasing to the hardness values even lower than that of the initial tempered base metal at the end. Ferrite reformation traces were observed at the first 500 μm of the weld fusion line assisted by the diffusion of chromium atoms into grain boundaries; High measured hardness in conjunction with the ferrite presence indicates that this region of HAZ is susceptible to loss of toughness and impact properties.

5.2. Microstructure and Texture of a 13Cr4Ni Double-Pass Weld

Similar to the effects of a single-pass on its base metal, the heat effects of a second pass were found to alter the first-pass microstructure to a depth of 6-7 mm. The study found that a second pass introduced new types of microstructure to the fresh martensite microstructure of the first pass. The second-pass heat cycle crumbled the formerly column-shaped packets of the first pass by heating adjacent areas up to the δ-ferrite stable region, with the result that finer martensite features were produced after cooling. The formerly column-shaped packets were no longer apparent in a 500 μm-wide band from the fusion line. The recalculation of austenite grains confirmed significant modification of the parent austenite grain in these areas.

Beyond the first 500-μm-wide band adjacent to the fusion line, the column-shaped packets remained unchanged, but higher hardness values were observed. The increase in hardness is attributed to the formation of new fresh martensite over the old martensite of the weld metal, although the heat was not high enough to change the austenite grains, and packets of martensite eventually formed again over the column-shaped structure. Further from the weld line, a tempering effect was reported, producing reformed austenite and carbide in the first pass.

As the size of the first pass was about 5 mm, the second pass heat cycle had the potential to alter the microstructure to a greater depth and affect the base metal. The second pass was found to smoothen the hardness profile peak produced by the first pass, resulting in a more uniform hardness. This effect can be beneficial as it can increase the toughness of the HAZ in the base metal.

5.3. Microstructure and Texture of a 13Cr4Ni Multi-Pass Weld

The results showed that the microstructure of a multi-pass weld is much more complex than that of a single-pass or double-pass weld; this increased complexity roots from the fact that the multi-pass structure receives heat from more than one subsequent pass. The microstructure of each single bead in the multi-pass study was found to be similar, on a superficial level, to the corresponding structure in the double-pass study case. The microstructure consists of two main regions, one having a fine martensite microstructure and the other, column-shaped martensite packets. However, an analysis of hardness maps showed that this classification failed to capture all the features and characteristics of the multi-pass microstructure.

In fact, each of these fine and column-shape regions can be divided in sub-regions that are differentially affected by subsequent weld passes. The four closer subsequent passes are responsible for the heat imposed on each weld bead microstructure, and changes in hardness were explained by variations in microstructure and local texture. Although the

immediate HAZ region exhibited the highest hardness in the single-pass case, the highest hardness in a multi-pass case was found in the middle of the weld, in a double-quenched column-shaped martensite. Conversely, the cumulative effects of the adjacent passes produced regions with hardness values comparable to tempered martensite.

Carbides and reformed austenite particles were observed frequently in different regions of the multi-pass weld, documenting its complex thermal history; while the single-pass weld lacked these particles. The results of this study suggest that any overall evaluation of future heat treatment should be done by taking into account the existence of these several sub-regions.

5.4. Effects of Tempering Heat Treatments on Microstructure

The effects of tempering heat treatments on the weld microstructure were documented by studying austenite and carbide formation as well as hardness evolution.

5.4.1. Reformed Austenite Formation

The first traces of austenite formation were found to occur at temperatures about 100 ^{o}C below the peak of austenite formation, accompanied with the formation of carbides at lath interfaces and grain boundaries. As noted in the literature review to this thesis, the faster diffusion rates of chromium and nickel atoms promote carbide and austenite phase formations. It is speculated that the rapid diffusion of chromium to lath interfaces and sub-block boundaries assists with carbide formation and increases nickel concentration in surrounding regions. This, in turn, promotes austenite formation on these lath interfaces. In most cases, the reformed austenite particles formed in parallel lamellae shapes; suggesting that their formation occurred over the parallel interfaces of the laths inside the martensite sub-blocks and blocks. Tempering heat treatments were not found to alter the mean distance between austenite lamellae, as these treatments do not affect the mean width of the martensite lath.

5.4.2. Effect of Tempering Temperature

Increasing the tempering temperature was generally found to increase the percentage of austenite in the microstructure, the highest percentages of reformed austenite were found at around 610 °C. Increasing the temperature past 610 °C, however, resulted in a decrease in the percentage of austenite, as the produced austenite at high temperature is not stable at low temperatures beyond this point. The increased homogenizing effects of high temperature tempering is responsible for the temperature effects observed in this study. Another way to explain this phenomenon is that as a greater amount of austenite is formed at high temperatures, the alloying elements compositions of the austenite phase (especially nickel which is thought to be the most influential element on promoting austenite reformation in this steel) are being less. This means more uniform dispersion of gammagene elements, therefore the majority of the austenite transforms to fresh martensite on cooling.

5.4.3. Effect of Tempering Holding Time

It has been shown that increasing the holding time promotes higher austenite percentages at temperatures lower than reformed austenite peak (610 °C in this case), while the contrary holds true for higher temperatures. At temperatures lower than the peak, the longer holding time provides more opportunity for alloying elements to diffuse into austenite phase. As the reformed austenite percentage is also little, the alloying composition of these austenite increases further. At high temperatures, longer holding time means a greater degree of homogenization, more reformed austenite at high temperatures, and consequently less accumulating of alloying elements on austenite phase. The resulting uniformity in compositions decreases the chemical stability of austenite at low temperatures, leading to even higher amount of fresh martensite than a short tempering.

The same argument as above can be used to explain the effects of holding time on hardness; longer holding at temperatures lower than austenite peak, results in higher austenite percentages and higher degrees of tempering. This produces a low hardness tempered martensite matrix with higher values of austenite compared to a short tempering. Longer holding at temperatures higher than the peak, means less reformed austenite and higher amount of fresh martensite compared to a short tempering at the same temperature. This results in higher hardness values with longer holding times.

5.4.4. Carbide Formation

Subjecting the alloy to a PWHT was found to produce a fast decrease in carbide density accompanying the appearance of austenite particles. However, as the carbon content of the steel was very low, carbide coarsening does not continue beyond the initial formation and carbides rapidly reach their final size. The initial carbide formation can be explained by fast diffusion and precipitation of carbon and chromium atoms at the lath boundaries. The drop observed in carbide size, immediately after the initial formation, can be explained by the dissolution of carbon atoms in the newly formed austenite phase. Thus, austenite particle formation appears to yield an increase in carbide solubility. At higher temperatures, a slight and nearly constant density of carbides is found which is believed to be the result of thermal stability of carbides.

5.4.5. Effect of Heat Treatment on Hardness

The hardness evolution can be understood by considering the effect of tempering on different features of steel microstructure, including the amount of reformed austenite, carbide, fresh martensite, and the tempering degree of the martensite matrix. Although the hardness values appear to be directly related to reformed austenite percentage, the conclusion of such relation cannot be made as hardness of the steel can be related to the effects of tempering on other features of the it as well. However, the study confirms that the lowest hardness is correlated to the highest reformed austenite values.

5.4.6. Double Tempering

Double tempering results in a higher percentage of austenite compared to single-stage tempering. It has been shown that prior austenite formation produced during the first tempering treatment facilitates additional austenite formation during the second stage and increases the total austenite percentage. The lowest hardness is also observed during this second stage, supporting this finding.

5.5. Contributions of the Study

The contributions of the current study can be summarized but not limited to the followings:

- The study has shown that the approach form a single-pass joint to multipass joint provides proper understanding of a multipass welded joint.
- The study confirmed suitability of some sample preparation methods for microhardness measurement and mapping and established modification to improve their results.
- Sample preparation methods for austenite, carbides and oxides revealing techniques have been modified for metallography, electron microscopy, and X-ray measurements.
- A comprehensive study of 13Cr4Ni weld joint has been performed resulting to a better understanding of weld heat cycles on microstructures of the steel.

5.6. Recommendations for Future Work

In order to increase the repeatability of the experiments and reliability of the results, the effects of tempering documented in this study was observed only on the most homogenous region of multipass weld beads which is the columnar-shape martensite in the middle of beads. However, a multi-pass weld bead consists of other regions with different thermal histories. These regions may experience thermal histories from double-quenching heat treatments to heat treatments similar to a tempering. Therefore, studying

the evolution of weld microstructure and particularly the development of reformed austenite in other regions is recommended, given the importance of PWHTs when no annealing heat treatment is possible.

This study also aimed to provide research grounds for future studies of the steel mechanical properties. The behavior of reformed austenite phase under mechanical loads is among these interesting and active topics of research. As the comprehensive study of microstructure has already been carried out in this project, it is feasible to conduct a short-term research project focused on mechanical behavior of austenite particles.

CONCLUSIONS

The weld microstructure is influenced by many fabrication process parameters. The welding process heat cycles and subsequent heat treatments can drastically modify the microstructure of 13Cr4Ni martensitic stainless steel.

The current study performed a comprehensive investigation into the effects of different tempering heat treatments on a 13Cr4Ni multi-pass weld. The major conclusions of this thesis are:

a) The thermal cycle of a single weld pass in the conditions used by this project affects regions of the base metal as deep as 6-7 mm, producing a multi-layer HAZ in the surrounding steel. The closest region to the weld fusion lines exhibits the highest hardness values, and the HAZ ends with a tempered-like region. The results show that the heat cycle produces a microstructure gradient in the base metal that starts from a fresh martensite close to the fusion line and ends as tempered martensite deep in the base metal.
b) In 13Cr4Ni multi-pass welds, the bead contains two main types of martensite microstructure: a column-shape martensite with martensite packets extended form the bottom of the bead up to the fusion line of subsequent pass and a fine martensite microstructure produced by the high temperature exposure of subsequent passes. This study found that the multi-pass weld procedure produces a relatively uniform hardness profile in the welded joint compared to the single-pass weld.
c) Each of these two main regions (column-shape and fine martensite regions) of a multi-pass weld can be divided into sub-regions, which are affected in different ways by subsequent weld passes.
d) Austenite parent grain modification, reformed austenite formation, and carbide formation were observed in various regions of the multi-pass weld.

e) Tempering heat treatments can significantly affect microstructure characteristics. Tempering of martensite, production of reformed austenite, and formation of carbide were all observed after heat treatments.
f) The highest percentages of reformed austenite were obtained by tempering at 610 °C for any holding time; double heat treatments produced higher percentages of austenite compared to similar single-stage tempering.
g) It has been shown that longer periods of tempering, at temperatures lower than 600 °C, produce larger amounts of reformed austenite and eventually softer martensite.
h) Carbide dissolution was observed in conjunction with the first formations of reversed austenite.
i) Reformed austenite particles were found along the lath interfaces, forming parallel lamellae.
j) Tempered martensite matrix with high percentages of austenite, no fresh martensite, and low carbide density exhibited the lowest hardness.

LIST OF REFERENCES

1. Thibault, D., Contribution a l'etude du comportement en fatigue des aciers inoxydables 13%Cr-4%Ni: Contraintes residuelles de soudage et transformation sous contrainte de l'austenite de reversion. 2010, Ecole de Technologie Superieure (Canada): Canada.

2. Bilmes, P.D., M. Solari, and C.L. Llorente, The Composition and Stability of Precipitated Austenite in Welded 13Cr4NiMo steels. 1999: p. 395-404.

3. Bilmes, P.D., C. Llorente, and J. Perez Ipina, Toughness and microstructure of 13Cr4NiMo high-strength steel welds. Journal of Materials Engineering and Performance, 2000. 9(6): p. 609-615.

4. Casas W. J. P., Henke S. L., and Novicki N., Fracture toughness of CA6NM alloy, quenched and tempered, and of its welded joint without PWHT. Welding International, 2009. 23(3): p. 166-72.

5. Bilmes, P.D., et al., Microstructure, heat treatment and pitting corrosion of 13CrNiMo plate and weld metals. Corrosion Science, 2009. 51(4): p. 876-81.

6. Thibault, D., et al., Reformed austenite transformation during fatigue crack propagation of 13%Cr-4%Ni stainless steel. Materials Science and Engineering: A, 2010. 528(21): p. 6519–6526.

7. Song, Y., et al., The influence of tempering temperature on the reversed austenite formation and tensile properties in Fe–13%Cr–4%Ni–Mo low carbon martensite stainless steels. Materials Science and Engineering: A, 2011. 528(12): p. 4075-4079.

8. M. Blair, Cast Stainless Steels, in ASM Handbook. 1990, ASM International. p. 908–929.

9. Nishiyama, Z., Martensitic transformation. 2012: Elsevier.

10. Folkhard, E., Welding Metallurgy of Stainless Steels. 1988, Berlin: Springer-Verlag.

11. Porter, D.A., Phase Transformations in Metals and Alloys. second ed. 1996: Chapman and Hall: p. 441.

12. Lippold, J.C. and D.J. Kotecki, Welding Metallurgy and Weldability of Stainless Steels. 2005: John Wiley & Sons.

13. Godin, S., Effet D'un Enrichissement en Nickel Sur La Stabilité Mécanique De L'austénite De Réversion Lorsque Soumise À De La Fatigue Oligocyclique. 2014.

14. Song, Y., et al., Formation of the reversed austenite during intercritical tempering in a Fe-13%Cr-4%Ni-Mo martensitic stainless steel. Materials Letters, 2010. 64(13): p. 1411-1414.

15. Zheng, H., et al., Effect of carbon content on microstructure and mechanical properties of hot-rolled low carbon 12Cr-Ni stainless steel. Materials Science and Engineering: A, 2010. 527(27-28): p. 7407-7412.

16. Gooch, T.G., Welding martensitic stainless steels. , Welding Institute Research Bulletin, 1977. 18(12): p. 343–349.

17. Thibault D., B.P., Thomas M.,Gharghouri M., Côté M., Residual stress characterization in low transformation temperature 13%Cr-4%Ni stainless steel weld by neutron diffraction and the contour method. Materials Science and Engineering: A, 2010. 527(23): p. 6205-6210.

18. Morito, S., et al., The morphology and crystallography of lath martensite in alloy steels. Acta Materialia, 2006. 54(19): p. 5323-5331.

19. Morito, S., et al., The morphology and crystallography of lath martensite in Fe-C alloys. Acta Materialia, 2003. 51(6): p. 1789-1799.

20. Morito, S., Y. Adachi, and T. Ohba, Morphology and Crystallography of Sub-Blocks in Ultra-Low Carbon Lath Martensite Steel. MATERIALS TRANSACTIONS, 2009. 50(8): p. 1919-1923.

21. Wu, W., et al., Relationship between alloying elements and retained austenite in martensitic stainless steel welds. Scripta Materialia, 2000. 42(Compendex): p. 1071-1076.

22. Wang, X.D., et al., Microstructures and stability of retained austenite in TRIP steels. Materials Science & Engineering A (Structural Materials: Properties, Microstructure and Processing), 2006. 438-440(Copyright 2007, The Institution of Engineering and Technology): p. 300-5.

23. Tjahjanto, D.D., et al., Micromechanical predictions of TRIP steel behavior as a function of microstructural parameters. Computational Materials Science, 2007. 41(1): p. 107-116.

24. Bilmes, P.D., C.L. Llorente, and M. Solari. Role of the Retained Austenite on the Mechanical Properties of 13Cr-4NiMo Weld Metals. 2000. St. Louis, MO, United states: ASM International.

25. Seong, B.S., et al. Effect of retained austenite and solute carbon on the mechanical properties in TRIP steels. 2004. Elsevier.

26. Caballero, F.G., et al., Effects of morphology and stability of retained austenite on the ductility of TRIP-aided bainitic steels. ISIJ International, 2008. 48(Compendex): p. 1256-1262.

27. Abareshi, M. and E. Emadoddin, Effect of retained austenite characteristics on fatigue behavior and tensile properties of transformation induced plasticity steel. Materials & Design, 2011. In Press, Corrected Proof.

28. Hertzberg, R.W., Deformation and fracture mechanics of engineering materials. 1996, New York: Wiley.

29. Balmforth, M.C. and J.C. Lippold, New ferritic-martensitic stainless steel constitution diagram. Welding Journal (Miami, Fla), 2000. 79(12): p. 339-s-345-s.

30. Marshall, A.W., J.C.M. Farrar, and T. Gooch, Welding of ferritic and martensitic 11-14% Cr steels. Welding Research Abroad, 2002. 48(10): p. 19-42.

31. Castro, R. and J.J. De Cadenet, Welding metallurgy of stainless and heat-resisting steels. 1975: CUP Archive.

32. Hara, T. and H. Asahi, Effect of. DELTA.-Ferrite on Sulfide Stress Cracking in a Low Carbon 13 mass% Chromium Steel. ISIJ international, 2000. 40(11): p. 1134-1141.

33. Ye. A. Sagalevich, Y.M.P., and V. V. Sachkov, The Effect of Delta-Ferrite on The Properties of Low-Carbon Martensite Stainless Steels. 1970.

34. Vasudevan, M., et al., Delta ferrite prediction in stainless steel welds using neural network analysis and comparison with other prediction methods. Journal of Materials Processing Technology, 2003. 142: p. 20-8.

35. Singh, J., G.R. Purdy, and G.C. Weatherly, Microstructural and microchemical aspects of the solid-state decomposition of delta ferrite in austenitic stainless steels. Metallurgical Transactions A, 1985. 16(8): p. 1363-1369.

36. Leone, G. and H. Kerr, The ferrite to austenite transformation in stainless steels. Welding Journal, 1982. 61(1): p. 13S-21S.

37. Carrouge, D., Phase transformations in welded supermartensitic stainless steels. 2002, University of Cambridge.

38. PAQUIN, M., Essais De Fissuration À Froid Appliqués Aux Métaux D'apport Inoxydables Martensitiques 410NiMo. 2014.

39. Thibault, D., P. Bocher, and M. Thomas, Residual stress and microstructure in welds of 13%Cr-4%Ni martensitic stainless steel. Journal of Materials Processing Technology, 2009. 209(4): p. 2195-2202.

40. Bilmes P. D., Llorente C., and Solari M. Effect of Post Weld Heat Treatments on the Microstructure and Mechanical Behaviour of 13Cr-4NiMoL and 13Cr-6NiMoL Weld Metals. 1998. Cincinatti, OH, United states: ASM International.

41. Akselsen, O., et al., Microstructure-property relationships in HAZ of new 13% Cr martensitic stainless steels. 2004.

42. Liu, Y.-r., et al., Effect of Heat Treatment on Microstructure and Property of Cr13 Super Martensitic Stainless Steel. Journal of Iron and Steel Research, International, 2011. 18(11): p. 60-66.

43. Iwabuchi, Y., Temper embrittlement of type l3Cr4Ni cast steel. Transactions of the Iron and Steel Institute of Japan, 1987. 27(3): p. 211-217.

44. Song, Y., et al., Anomalous Phase Transformation from Martensite to Austenite in Fe-13%Cr-4%Ni-Mo Martensitic Stainless Steel. Journal of Materials Science & Technology, 2010. 26(9): p. 823-826.

45. Pukasiewicz, A.G.M., S.L. Henke, and W.J.P. Casas, Effect of post-weld heat treatment on fatigue crack propagation in welded joints in CA6NM martensite stainless steel. Welding International, 2006. 20(12): p. 947-52.

46. Zappa, S., et al. Effect of PWHT on supermartensitic stainless steel all weld metal toughness. 2009. Pine Mountain, GA, United states: ASM International.

47. Divya, M., et al., Improving 410NiMo weld metal toughness by PWHT. Journal of Materials Processing Technology. In Press, Corrected Proof.

48. Rajasekhar, A., et al., Influence of post-weld heat treatments on microstructure and mechanical properties of AISI 431 martensitic stainless steel friction welds. Materials Science and Technology, 2008. 24(2): p. 201-12.

49. Das, C.R., et al., Repair welding of cracked turbine shroud using matching composition consumables. Science and Technology of Welding and Joining, 2005. 10(Copyright 2006, The Institution of Engineering and Technology): p. 110-12.

50. Gracioso, J.F.F.d.O., Carlos Augusto Silva, Effect Of Austenitization Temperature And Tempering Condition On The Microstructure and Mechanical Properties of a Casted Martensitic Stainless Steel - CA6NM. 60th Annual ABM International Congress, 2005.

51. Bilmes, P.D., M. Solari, and C.L. Llorente, Characteristics and effects of austenite resulting from tempering of 13Cr-NiMo martensitic steel weld metals. Materials Characterization, 2001. 46(4): p. 285-296.

52. Nakagawa, H. and T. Miyazaki, Effect of retained austenite on the microstructure and mechanical properties of martensitic precipitation hardening stainless steel. Journal of materials science, 1999. 34(16): p. 3901-3908.

53. Lee, Y.K., et al., Reverse transformation mechanism of martensite to austenite and amount of retained austenite after reverse transformation in Fe - 3Si - 13Cr - 7Ni (wt-%) martensitic stainless steel. Materials Science and Technology, 2003. 19(3): p. 393-398.

54. Zou, D. N., et al., Influence of Tempering Process on Mechanical Properties of 00Cr13Ni4Mo Supermartensitic Stainless Steel. Journal of Iron and Steel Research, International, 2010. 17(8): p. 50-54.

55. Song, Y.Y., et al., Microstructural evolution and low temperature impact toughness of a Fe-13%Cr-4%Ni-Mo martensitic stainless steel. Materials Science & Engineering: A (Structural Materials: Properties, Microstructure and Processing), 2010. 527(3): p. 614-18.

56. Robichaud, P., Stabilite de l'austenite residuelle de l'acier inoxydable 415 soumis a la fatigue oligocyclique. 2007, Ecole de Technologie Superieure (Canada): Canada. p. 171.

57. Iwabuchi, Y., Factors affecting on mechanical properties of soft martensitic stainless steel castings. 2003, JSME: Japan. p. 441-6.

58. Nakada, N., et al., Variant selection of reversed austenite in lath martensite. ISIJ international, 2007. 47(10): p. 1527-1532.

59. Fultz, B., et al., The chemical composition of precipitated austenite in 9Ni steel. Metallurgical Transactions A, 1986. 17(6): p. 967-972.

60. Lippold, J. and W. Savage, Solidification of Austenitic Stainless Steel Weldments. Proposed Mechanism. Welding Journal, 1979. 58(12): p. 362.

61. Ohmori, Y., et al., Mechanism of Widmanstätten Austenite Formation in a δ/γ Duplex Phase Stainless Steel. ISIJ International, 1995. 35(8): p. 969-975.

62. Yoo, C.-S., et al., Effect of grain size on transformation-induced plasticity in an ultrafine-grained metastable austenitic steel. Scripta Materialia, 2008. 59(1): p. 71-74.

63. Gey, N., et al. Restitution of the shapes and orientations of the prior austenitic grains from inherited alpha'orientation maps in steels. in Solid State Phenomena. 2011. Trans Tech Publ.

64. De Andrés, C.G., et al., Metallographic techniques for the determination of the austenite grain size in medium-carbon microalloyed steels. Materials characterization, 2001. 46(5): p. 389-398.

65. Lubin, S., Etude des mécanismes de transformation de phase de l'austénite en bainite dans les aciers bas carbone. 2009, Paris, ENMP.

66. Miyamoto, G., et al., Mapping the parent austenite orientation reconstructed from the orientation of martensite by EBSD and its application to ausformed martensite. Acta Materialia, 2010. 58(19): p. 6393-6403.

67. Blaineau, P., et al. A new approach to calculate the γ orientation maps in steels. in Solid State Phenomena. 2010. Trans Tech Publ.

68. Tari, V., A. Rollett, and H. Beladi, Back calculation of parent austenite orientation using a clustering approach. Journal of Applied Crystallography, 2013. 46(1): p. 210-215.

69. Weidmann, E., Electrolytic Polishing, Metallography and Microstructures, in ASM Handbook. 1985, American Society for Metals. p. 48–56.

70. G.F. Vander Voort, Metallography: Principles and Practice. 1999: McGraw-Hill, 1984, Reprinted ASM International. 785.

71. Chemical and Electrolytic Polishing, in Metallography and Microstructures, ASM Handbook. 2004, ASM International. p. 281–293.

72. Tsai, M.C., et al., Phase transformation in AISI 410 stainless steel. Materials Science & Engineering A (Structural Materials: Properties, Microstructure and Processing), 2002. A332(1-2): p. 1-10.

73. Syn, C., B. Fultz, and J. Morris, Mechanical stability of retained austenite in tempered 9Ni steel. Metallurgical and Materials Transactions A, 1978. 9(11): p. 1635-1640.
74. Voort, G.F.V., Martensite and retained austenite. Industrial Heating, 2009. 76(The Institution of Engineering and Technology): p. 51-4.

75. Rietveld, H.M., A profile refinement method for nuclear and magnetic structures. Journal of Applied Crystallography, 1969. 2(2): p. 65-71.

76. Wang, P., et al., Effect of delta ferrite on impact properties of low carbon 13Cr-4Ni martensitic stainless steel. Materials Science and Engineering A, 2010. 527(13-14): p. 3210-3216.

77. Rasband, W.S., ImageJ. 1997-2012, U. S. National Institutes of Health.
78. Totten, G.E., Steel Heat Treatment Metallurgy and Technologies. second ed. 2007, Portland: Taylor and Francis. 832.

79. Lancaster, J.F., Metallurgy of Welding (6th Edition). 1999, Woodhead Publishing. 339.

80. Thibault, D., et al., Residual stress characterization in low transformation temperature 13%Cr–4%Ni stainless steel weld by neutron diffraction and the contour method. Materials Science and Engineering: A, 2010. 527(23): p. 6205-6210.

81. Thibault, D., et al., Reformed austenite transformation during fatigue crack propagation of 13%Cr–4%Ni stainless steel. Materials Science and Engineering: A, 2011. 528(21): p. 6519-6526.

82. Mokhtabad Amrei, M., et al., Microstructure Characterization of Single and Multipass 13Cr4Ni Steel Welded Joints. Metallography, Microstructure, and Analysis, 2015: p. 1-12.

83. Hydro-Québec, I.d.r., Scompi Robot, Robotic System for Generating Station Work, U. patent, Editor. 2011: Canada.

84. Germain, L., et al., An advanced approach to reconstructing parent orientation maps in the case of approximate orientation relations: Application to steels. Acta Materialia, 2012. 60(11): p. 4551-4562.

85. Paquin, M., et al., Assessment of cold cracking tests for low transformation temperature martensitic stainless steel multipass welds. Welding in the World, 2015: p. 1-12.

86. Song, Y., et al., The influence of tempering temperature on the reversed austenite formation and tensile properties in Fe-13%Cr-4%Ni-Mo low carbon martensite stainless steels. Materials Science and Engineering: A, 2011. 528(12): p. 4075-4079.

87. ASTM International, ASTM A743/A743M-03 Standard Specification for Castings, Iron-Chromium, Iron-Chromium-Nickel, Corrosion Resistant, for General Application. 2003.

88. Amrei, M.M., et al., Microstructure characterization and hardness distribution of 13Cr4Ni multipass weld metal. Materials Characterization, 2016. 111: p. 128-136.